STUDIES IN INTERACTING GALAXIES

A Thesis

Submitted For The Degree Of

DOCTOR OF PHILOSOPHY

In The Faculty Of Science

BANGALORE UNIVERSITY

By

P.M.SANKARANARAYANAN NAMBOODIRI

INDIAN INSTITUTE OF ASTROPHYSICS
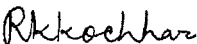
BANGALORE 560034

INDIA

NOVEMBER 1989

DECLARATION

I hereby declare that the matter embodied in this thesis is the result of the investigations carried out by me in the Indian Institute of Astrophysics Bangalore and the Department of Physics, Bangalore University, Bangalore under the supervision of Prof. R. K. Kochhar and Prof. B. C. Chandrasekhara and has not been submitted for the award of any degree, diploma, associateship, fellowship etc. of any university or institute.
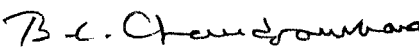
P.M.SANKARANARAYANAN NAMBOODIRI

Candidate

R. K. Kochhar

Supervisor

B. C. Chandrasekhara

Supervisor

Bangalore

Date: 20-11-1989.

CONTENTS

Acknowledgements

I am extremely grateful to Prof. R. K. Kochhar for suggesting the topic and for his valuable guidance during the course of this research work. I am also grateful to Prof. B. C. Chandrasekhara who took special interest and helped me in various ways for the successful completion of the thesis. I sincerely express my deep gratitude to Prof. J. C. Bhattacharyya for his constant encouragement and for allowing me to use the facilities at the institute. I also express my gratitude to Prof. P. Paramasivaiah and Prof. N. G. Puttaswamy for their keen interest in the progress this work.

It is with great pleasure that I express my gratitude to Prof. S. M. Alladin who was always a source of encouragement and inspiration. I thank Dr. S. J. Aarseth who kindly supplied the N-body 2 code. The computations reported in this thesis were performed with VAX 11/780 and Mighty Frame II computer of the institute. I thank Prof. A. Peraiah for allowing me unlimited access to the computer. I thankfully acknowledge the help rendered by my colleagues in the computer centre.

I sincerely thank Dr. T. P. Prabhu for carefully going through the entire manuscript and giving me several useful suggestions to improve the presentation.

The tracings of the diagrams were made by Mr. S. Muthukrishnan and I thank him. I thank the library staff for

their help: especially Mr.D.Venkatesh for the photocopying and Messers D.Kanagaraj, P.Pose and M.subramani for the binding work.

Finally I would like to thank my colleagues who were always ready to help in various ways during the course of this thesis.

SUMMARY

The discovery of peculiar galaxies from the
photographs of Palomar Sky Survey Programme conclusively
revealed that galaxies are not island universes evolving
slowly in isolation but they interact in various ways with
their environment which consists of satellites, neighbouring
galaxies and large intergalactic clouds. Many objects appeared
in pairs, groups and clusters. Binary galaxies represent an
important feature of the extra-galactic universe. The optical
observations of the powerful radio source Cygnus A showed that
it is an unusual system consisting of two galaxies. Numerical
simulations carried out by Toomre & Toomre (1972)
convincingly demonstrated that tidal forces play an important
role in the dynamics of interacting galaxies. They could
reproduce the features of four well-known interacting systems
Arp 295, M 51 + NGC 5195 NGC 4676 and NGC 4038/39.

Gravitational interaction between galaxies could
profoundly alter their morphological features. Sometimes the
outer parts of a galaxy pair are distorted into long bridges
and tails. The presence of multiple nuclei in irregular
galaxies enhances the importance of tidal interaction. Recent
observations using advanced techniques point out the
importance of star formation in interacting galaxies.
Observations also suggest that many compact elliptical
galaxies formed as a result of gravitational interaction. The

study of interacting galaxies is, therefore, vital in the sense that it may give clues to the origin and evolution of galaxies.

In the present work, we have used numerical simulations to study various processes associated with colliding galaxies. It is commonly assumed that tidal encounters produce most damage in the outer layers of a galaxy while leaving the inner part relatively unaffected. The material escaping from the outer parts may form intergalactic filaments and tails. The restricted three-body treatment has been found useful in this investigation. This method has been used to study the formation of bridges and tails in interacting galaxies. The important parameters in a pair of galaxies undergoing collision are the impact parameter, the velocity of the encounter and the mass of the galaxies. Various combinations of these collision parameters have been used to study the tidal distortions produced in the outer parts of a disk galaxy due the passage of point mass perturber. The perturber is moving in the plane of the test galaxy along a parabolic orbit. The sense of rotation of the disk is the same as the direction of motion of the perturber. It is shown that in grazing collisions, well-developed bridges and tails are formed when the two galaxies have comparable mass. The test galaxy remained unaffected when the perturber is significantly less massive than the test system while a massive perturber produced considerable damage to the test galaxy. It is also shown that similar types of bridges and

tails are formed if the masses and distances are chosen in a particular way.

The restricted three-body treatment gives a qualitative picture of the distortions caused in the outer parts of a galaxy. A quantitative study of the interactions require the use of self-consistent N-body simulations. The tidal effects on a spherical galaxy due to a massive companion is studied using Aarseth's N-body 2 code. It is flexible, makes no assumption about the geometry of the system and is easy to adapt to a variety of applications. The spherical galaxy consists of 250 particles and the perturber is a point mass. The distance of closest approach is chosen such that collisions does not lead to a merger. A wide range of density ratios and eccentricities of the relative orbit have been considered. The disruption of the test galaxy has been observed when the numerical value of the fractional change in the energy is greater than two and in this case the test galaxy loses more than 40 % of its mass. Considerable amount of orbital angular momentum is transferred to the test galaxy during the course of an encounter. A large fraction of the transferred angular momentum is carried away by the escaping particles. The changes in the energy and angular momentum show smooth variation with time in the case of unbound orbit encounters and irregular variation in bound orbit cases. The half-mass radius of the test galaxy remains almost the same as that of initial test galaxy. For a constant pericentric distance, increasing the density ratio decreases the tidal

effects. The dependence of tidal effects on eccentricity of the relative orbit has also been estimated. N-body simulation results are compared with those of earlier workers and also with estimates obtained from analytical computations.

Throughout the thesis, sections, figures, and tables are numbered sequentially. Equations within a chapter are also numbered sequentially. The references are given at the end of the thesis.

CHAPTER ONE

INTRODUCTION

1. Historical introduction

It was commonly believed until 1950 that galaxies were island universes evolving slowly in isolation. The existence of double and multiple systems was reported as early as 1920. Good photographs of interacting galaxies were probably first obtained by Pease (1917). Further observations of interacting galaxies and interpretation of the observations have been carred out by several astronomers (e.g., Curtis, 1921; Lundmark, 1926; Hubble, 1936 etc.). Holmberg (1940) was probably the first who demonstrated by use of statistics that most close pairs of galaxies are actually physical binaries. The determination of the masses of the galaxies is crucial to the study of their origin and evolution. As in the case of double stars the details of the motions of these physical pairs can be used to estimate their masses under the assumption that binary galaxies are stable in orbits and the Newtonian gravitation is the only dominant force. Holmberg demonstrated how the average mass of a galaxy in a pair can be obtained by measuring the separation between them and the minimum speed related to one another. By this method he derived the average mass of a galaxy as one hundred times the Sun's mass from a sample of 16 galaxies in eight pairs. Even

1

though this figure has been refined since then, the estimate seems to have been pretty good.

The study of interacting galaxies was neglected for quite some time since their discovery mainly due to the fact that these objects were very faint and the available telescopes were quite *'slow '* making them ill-suited for the observations of these objects. Investigators concentrated their efforts to study simpler normal isolated galaxies. Many investigators believed collision between galaxies to be an impossible event. It was in 1951 that F. G. Smith carried out radio observations of the faint objects far out beyond the stars of our Milky Way. He could detect a strong source of radio emission called Cygnus A. The object photographed with 200 inch telescope by Walter Baade turned out to be an unusual system composed of two galaxies one superposed on the other. The nuclei of these objects were strongly distorted which was interpreted as due to gravitational interaction. The optical and radio emissions were so intense that the collision was considered to be one of interpenetrating with high speed. Intensive search for collisions in other radio sources detected a few more but none of them were as intense as Cyg A.

Much stimulus to the study of interacting galaxies came from the discovery of peculiar galaxies from the Palomar Sky Survey programme. From this survey, Vorontsev-Velyaminov (1959) compiled a catalogue of 355 interacting galaxies called *The Atlas of Interacting Galaxies.* A collection of 300 photographs of interacting galaxies had been published in the *Atlas of Peculiar Galaxies* by Arp in 1966. Thus it became

2

clear that galaxies could interact with their environment which consists of satellites, neighbour galaxies and large intergalactic clouds.

Binary galaxies occur over a wide range from well separated pairs to closely interacting pairs. In closely interacting pairs, the average separation between one galaxy and its nearest neighbour is not greater than a galactic diameter. The mass distribution surrounding many galaxies extends far beyond their optical boundaries implying the presence of dark halos. Spherical halos in close binaries must interpenetrate such that the frequency of effective gravitational encounters may be greater than one would expect from appearance alone (White,1982).

Interacting galaxies often produce striking morphological features such as bridges, tails, and counterarms of various sizes and shapes. Zwicky (1959) believed that tides could in fact explain the bridges and tails. The tidal theory was opposed by Vorontsev-Velyaminov (1961) who believed that all galaxies possessed certain unknown macroscopic properties distinct from the properties of gravitation. The tidal theory was proved to be right by Toomre & Toomre (1972) a decade later.

2.Analytic calculations

Theoreticians have long suggested that galaxy collisions are inevitable in clusters of galaxies. Collisions between galaxies will generally be hyperbolic regardless of

3

the impact parameter and deviations from rectilinear motion of the galaxy centres will be small (Ostriker,1977). Such high velocity encounters often leave the galaxies unaffected. For fast encounters, the tidal effects between galaxies can be estimated to a first approximation by the impulse approximation (IA). In this approximation, the motion of the stars is neglected in comparison with the motion of the galaxy. This was first used by Spitzer (1958) to study the disruption of galactic clusters by passing interstellar clouds. Several investigators used IA to obtain energy exchange and mass loss in colliding galaxies (Alladin,1965; Sastry & Alladin, 1970; Gallagher & Ostriker, 1972; Richstone, 1975; Biermann, 1976; etc.). Analytic expression for the energy change during the course of an encounter has been obtained by Alladin & Narasimhan (1982) for different relative orbits of the colliding galaxies.

The second method generally used to study interacting galaxies is the adiabatic approximation (AA) in which the orbital motion of the pair is neglected in comparison with the motion of the stars in the system. This approximation is mostly useful in studying slow bound orbit encounters. Avner & King (1967) used this method to study the secular change in the angular momentum of stars in the galaxy due to the influence of the Magellanic Clouds. Alladin et al. (1985) used AA to estimate the merger rates of binary stellar systems.

4

3. Test particle method

The response of a stellar system to external influences can be studied to a first approximation by neglecting the self-gravity of the particles representing the stellar system. In this method, a galaxy is represented by a massive central core surrounded by mass less test particles. Stars orbiting in the outer most regions will be experiencing the gravitational force of the perturber significantly. The motion of these stars is influenced by the two rigid mass centres and thus the problem reduces to a restricted three-body problem for each star. The computation time is considerably less than that for a full N-body code and large time-steps can be used for each star since close encounters between them are avoided. The usefulness of this method was demonstrated by Toomre & Toomre (1972) in a comprehensive study of several well-known interacting stellar systems. In particular, by carefully choosing the initial conditions, they could convincingly reproduce the orbits and outer shapes of four real interacting systems. Several investigators used this method to study the morphological features produced in the outer parts of a galaxy due to the passage of a companion of comparable size (e. g., Wright,1972; Clutton-Brock,1972; Eneev et al.,1973; Gutowski & Larson, 1976 etc.). The above works showed the fact that tidal forces do play an important role in the dynamics of interacting galaxies.

A modified version of the restricted three-body treatment was used by Lin & Tremaine (1983) to study the

effect of dynamical friction on a satellite galaxy as it orbits around a massive companion. Borne (1984) developed a numerical method called multiple three-body algorithm which essentially involves the integration of N three body equations. He studied the collisions of two equal spherical galaxies and obtained merger times that turned out to be larger than the previously estimated values.

4. N-body method

The impulse approximation and the restricted three-body approach are not suitable in slow galactic encounters during which the structure of the galaxy changes appreciably. The above methods neglect the self-gravity of the stars and hence does not calculate the orbits accurately. Self-consistent simulations are required to study the tidal effects in colliding galaxies of comparable mass by directly integrating the N-body equations of motion with appropriate time step for each particle. Collisions of spherical galaxies have been simulated by direct N-body technique by Holmberg (1940) with 37 particles per galaxy and showed that the orbital energy is transferred to the internal energy (the motion of the stars) of the individual galaxies. He also pointed out that in nearly head-on collision, two spiral galaxies could merge and form an elliptical galaxy.

Lauberts (1974) considered collisions of two spherical stellar systems of equal size and mass and showed that the internal energy increase by up to 25 % at the cost of

orbital energy. In slow orbit encounter, a fraction of 0.1 of the total mass is exchanged between the systems. He also noted that the IA is valid in the case of fast encounters. White (1978, 1979) considered the merger of two similar spherical galaxies by taking 250 particles in each galaxy and showed that rapid merging occurs when the two galaxies overlap significantly at closest approach and the merger remnant resembled like observed elliptical galaxies. Roos & Norman (1979) modeled each galaxy with approximately 30 particles and used a wide range of values for the impact parameter. He discussed the loss of orbital kinetic energy, merger criteria and the mass loss. Aarseth & Fall (1980) performed N-body experiments to see whether ellipticals are formed out of mergers. They found that merging occurs from marginally bound two body orbits of low angular momentum and the results did not support the idea that many ellipticals were merger remnants.

Dekel et al. (1980) studied in detail slow hyperbolic collisions of spherical galaxies of comparable mass. The test galaxy was modeled by 250 particles with $\rho \propto r^{-3}$ and the perturber by a point mass. They obtained net gain in the internal energy and mass loss. They compared the energy exchange with IA estimates and found agreement in slow hyperbolic encounters.

Gerhard (1981) simulated disk galaxy collisions in which each galaxy consisted of a flat disk, an extended halo and a core. Each galaxy contained 250 particle. He observed that a few percent of the particles escape but they

7

carry away substantial fraction of angular momentum. Further the galaxy spins decreased and the disk and halo angular momentum vectors were not aligned after an encounter. Farouki & Shapiro (1982) studied by N-body simulations the conditions under which two identical disk-halo galaxies could merge for a variety of orbits and orientations of the galaxies. Negroponte & White (1983) carried out N-body simulations of merging disk-halo galaxies by treating a fraction of the disk particles as gas clouds undergoing inelastic collisions. They found that the clouds are lost to the tails of the galaxies along with stars but those clouds that remain dissipate the energy rapidly and fall to the centre of the remnant thereby enhancing its central density, its velocity dispersion and presumably its metallicity.

Aguilar & White (1985) used N-body simulations to investigate the effects of gravitational encounters between spherical galaxies of comparable mass and showed that their N-body results agree well with IA estimates. Rao et al. (1987) performed simulations spherical galaxies of unequal masses and found fairly good agreement between their numerical results and IA estimates even for elliptic encounters.

Collisions of disk-halo galaxies have been carried out by Barnes (1988) in which each galaxy is modelled by 10^4 particles. He could reproduce the tidal tail of NGC 4038/9 and in merging simulations, the remnant system showed properties similar to the observed elliptical galaxies.

Head-on collisions of spherical galaxies were simulated by Navarro & Masconi (1989). They compared their

8

results with IA estimates and found good agreement for large collision velocities.

The second type of N-body simulation is to use a fixed time step and determine the gravitational potential by Fast Fourier Transform (FFT) techniques. This method has been employed by the following workers.

Van Albada & van Gorkom (1977) studied the head-on collision of two spherically symmetric galaxies with density distribution that of a polytrope of index n = 3. This method can only be used to study head-on collisions because of the assumption of axial symmetry. An Eulerian Fast-Fourier code was used by Miller & Smith (1980) to study the merging process of two spherical galaxies. Stewart (1981) studied, by Fast-Fourier transform technique, head-on collision of two equal mass galaxies each galaxy comprising 10^4 particles.

Villumsen (1982) has used tesseral harmonics to study the merger of two spherical galaxies each containing 1200 particles and observed that equal mass mergers are more flattened than unequal mass mergers. Miller (1986) performed computations to study the dynamical effects of a galaxy orbiting within a cluster of galaxies. The galaxy was modelled by 100352 particles and obtained a disruption criterion based on the ratio of tidal stress to the internal stress within the galaxy.

Lee & Ostriker (1987) used an orbit averaged Fokker-Planck code to study the evolution and final disintegration of spherical stellar systems in a steady galactic tidal field.

It seems relevant at this point to mention the analytic work of Palmer & Papaloizou (1982) wherein they have contented that under certain circumstances, encounters between disk galaxies can lead to an acceleration of their relative motion rather than the decay of the satellite orbit due to dynamical friction. It may also be pointed out that Byrd et al. (1986) studied the effect of dynamical friction on a satellite of a disk galaxy and their results for cold disks are opposite to those calculated by Palmer & Papaloizou.

5. The outline of present work

The N-body simulations so far described concentrated either on the merger aspect or the tidal effect in slow hyperbolic encounters. These computations are useful for determining the properties of merger remnants at the centre of rich clusters. In most of these simulations, the masses of the component galaxies have generally been taken of the same order. The disruption aspect in colliding galaxies has not been studied in a systematic manner. Tidal disruption and merger are two important processes in the dynamical evolution of binary stellar systems. The rates of disruption and merger can be given as

$$\frac{t_d}{t_c} = \frac{6}{5 - n} \frac{a}{R} \frac{M}{M_1} \tag{1}$$

where t_d and t_c are the disruption and merger times, a is

the orbital radius, R is the radius of the satellite, M and M_1 are respectively the masses of the satellite and the perturber and n is the polytropic index describing the density distribution of the satellite (see Alladin & Narasimhan, 1982). It can be seen that if the galaxies are centrally concentrated and have similar masses, merger occurs more rapidly than disruption. On the other hand a massive perturber is likely to cause considerable disruption of the satellite and in this case the disruption time could be shorter than the merger time. Alladin et al. (1985) made a comparative study of the disruption and merger rates of galaxies under IA and AA and showed that there is a sudden transition in the rate of disruption at $\rho = \rho_R$ where ρ is the mean density of the satellite and ρ_R the Roche density. If $\rho < \rho_R$, the disruption is quite rapid and if $\rho > \rho_R$, the rate of disruption is considered negligible. In this case the tidal effects on the small galaxy would be much larger than on the big galaxy. In some cases the disruptive effects of a giant galaxy on a small companion are directly visible - the Magellanic Stream is the best known example of this kind.

The aim of the present study is to investigate the tidal effects on a galaxy due to the passage of a perturber. The difference between our simulations and earlier ones is the use of a massive perturber which is set to move in initial relative orbits of various eccentricities. The introduction of the concept of Roche density helps us to verify results obtained previously by theoretical investigators. A detailed comparison of our numerical results

11

appears to be new.

The present study involves restricted three-body treatment and N-body simulations of interacting galaxies. The restricted three-body approach uses various collision parameters to study the formation of bridges and tails in the outer parts of a disk galaxy. To supplement this study, a series of N-body simulations have been performed to investigate the criterion under which a satellite galaxy disrupts due to the influence of a massive perturber. Collisions are simulated in such a way that mergers are excluded. A wide range of density ratio and eccentricity of the relative orbit have been considered in the simulation of non-penetrating stellar systems. The dependence of tidal effects on masses of the galaxy pair and the velocity of the orbit has been investigated.

In Chapter Two the restricted three-body approach is used to study the dependence of mass ratio in producing morphological features in interacting galaxies. Chapter Three gives a brief explanation of the N-body code we have used. N-body simulation results are described in Chapter Four. The numerical results are compared with results of earlier investigators in Chapter Five. The concluding remarks are given in Chapter Six.

CHAPTER TWO

FORMATION OF BRIDGES AND TAILS

6. Morphological features of interacting galaxies.

Most of the galaxies have regular shapes and symmetry. A small fraction of them however show distorted structure and they are generally associated with close companions. Collisions of galaxies are, therefore, a rather frequent phenomena. Zwicky's (1952) systematic investigations of luminous intergalactic formations in widely separated galaxies could not show evidence that these formations contained gases and dust. He, therefore, concluded that these intergalactic formations could be jets of stars ejected from galaxies which are undergoing collision. As a small galaxy orbits around a giant companion, the time dependent tidal field can have significant effect on their outer regions. For distant encounters, the galaxies may pass around each other without causing much damage. In close encounters, the tidal field removes orbital energy of the pair and transfers it to the internal energy of the galaxies. The tidal effects cause significant rearrangement of the structure of the galaxies in their outer parts in the form of bridges, tails and counterarms of various sizes and shapes. If the encounter is very close or even head-on, either considerable disruption of

both systems results or the pair may merge to form a single system. The restricted three-body treatment has been found useful in studying the formation of various features on the outer parts of a galaxy during an encounter.

The change of form of a galaxy due to the gravitational force of a by passing galaxy has been investigated by Pfleiderer (1963) using restricted three-body treatment, who could produce the spiral structure in the orbital plane of the pair. He noted, however, that the probability of two galaxies meeting under conditions favourable to the development of spirals is very small.

The outflow of material from the vertex of a homogeneous prolate galaxy due to the close approach of another galaxy was hydrodynamically investigated by Tashpulatov (1970). He showed that nearly straight and short bridges between the galaxies could be produced if the distance of closest approach is sufficiently small. Yabushita (1977) investigated the possibility of formation of binary galaxies by tidal encounters and showed that if the galaxies have a relative velocity of 30 - 40 kms^{-1} or less they formed gravitationally bound system after the encounter. Clutton-Brock's (1972) computer simulations of a disk of stars and gas perturbed by a point mass galaxy produced remarkably long narrow filaments from the gaseous component.

Wright (1972) using restricted three-body treatment concluded that the tails and bridges frequently observed in majority of the cases could be explained solely in

terms of the gravitational interactions within the system.

Toomre & Toomre (1972) performed computer simulations of interacting galaxies and convincingly reproduced the orbits and outer shapes of four well known interacting systems; Arp 295; M 51 + NGC 5195; NGC 4676; and NGC 4038/39. They also discussed many related issues like eccentric bound orbit, orbital decay, accretion and forced spiral waves.

Eneev et al. (1973) studied the tidal effects when a massive body moves in a hyperbolic orbit of different inclinations and showed that the interactions should lead to formation of similar spiral arms in the outer parts of a disk galaxy. Gutowski & Larson (1976) considered the encounter between a spherical galaxy and a smaller companion and obtained the energy change and mass loss.

Stockton (1974a,b) observationally verified the existence of long narrow tail in the peculiar double galaxy NGC 4676 and showed that the radial velocity and the mass ratio of the interacting system Arp 295 agree well with the tidal model proposed by Toomre & Toomre. Schweizer (1978) also invoked the tidal theory to describe the tail of NGC 4038/39.

The computer experiments described so far show that gravitational interaction between galaxies can really produce the peculiar features observed in them. According to Toomre & Toomre (1972), to produce good bridges and tails, the collisions must be slow; the galaxies must penetrate each other, but not too deeply; the sense of motion of the

15

perturber and the galactic rotation should roughly be the same. They also noted that the formation of bridge is favoured if the perturber's mass is smaller and of the tail if it is larger or equal. The present investigation attempts to study the effect of collision parameters of the galaxies on the formation of bridges and tails over a wide range of values in mass ratio, eccentricity, and separation.

7. Numerical method and initial conditions

The test galaxy is assumed to be a point mass which is fixed at the origin. It is surrounded by non-interacting test particles distributed in a thin disk containing the test galaxy. The perturber, also assumed to be a point mass, approaches the test galaxy along a parabolic orbit. This assumption enables one to analytically evaluate the position of the perturber at any time; and the problem reduces to a restricted three-body problem for each star.

The initial positions of the stars are determined using pseudo-random number generator in such a way that the density of the stars in the disk decreases inversely as their distance from the centre. No stars were placed at a distance of less than 0.3 units of the disk radius since these stars are assumed to remain unaffected during the encounter. Time was reckoned from positive to negative values with zero being the time of pericentric passage. The initial positions and velocities are given by

$$x = a \cos \theta \quad ; \qquad y = a \sin \theta \quad , \tag{1}$$

$$V_x = a^{-1/2} \sin \theta \quad ; \qquad V_y = - a^{-1/2} \cos \theta, \tag{2}$$

where a and θ are chosen such that

$$0.3 < a \leq 1 \quad ; \quad 0 \leq \theta \leq 2\pi \quad . \tag{3}$$

The equations of motion of a particular star can be written as

$$\frac{d^2 R}{d t^2} = - \frac{G M}{R^3} R - \frac{G M_1}{R_1^3} R_1 - \frac{G M_1}{R_0^3} R_0 \quad , \tag{4}$$

where $R = (x,y)$ is the position vector of a star; $R_0 = (X_0,Y_0)$ is the position vector of the perturber; R_1 the position vector of the perturber with respect to the star; M the mass of the test galaxy; M_1 the mass of the perturber; G the gravitational constant; and t the time. The unit of mass is $M = 10^{11} M_\odot$, the unit of distance is the pericentric distance of the perturbing galaxy (20 kpc). Time is measured in units of $\left(Q^3 / G (M + M_1) \right)^{1/2}$ where Q is the pericentric distance; the unit corresponds to nearly 10^8 yr when $M = M_1$.

The equations of motion (4) are numerically

integrated for each star, using Adam- Moulton's predictor corrector method. The formulae used are

$$x_{n+1}^{p} = x_n + \frac{\Delta t}{24} (55\dot{x}_n - 59\dot{x}_{n-1} + 37\dot{x}_{n-2} - 9\dot{x}_{n-3}),$$

$$\ldots\ldots(5)$$

$$x_{n+1}^{c} = x_n + \frac{\Delta t}{24} (9\dot{x}_{n+1} + 19\dot{x}_n - 5\dot{x}_{n-1} + \dot{x}_{n-2}),$$

$$\ldots\ldots(6)$$

$$y_{n+1}^{p} = y_n + \frac{\Delta t}{24} (55\dot{y}_n - 59\dot{y}_{n-1} + 37\dot{y}_{n-2} - 9\dot{y}_{n-3}),$$

$$\ldots\ldots(7)$$

$$y_{n+1}^{c} = x_n + \frac{\Delta t}{24} (9\dot{y}_{n+1} + 19\dot{y}_n - 5\dot{y}_{n-1} + \dot{y}_{n-2}).$$

$$\ldots\ldots(8)$$

Here $\dot{x}_n$ and $\dot{y}_n$ are respectively the components of the velocity in the x and y directions at time $t = t_n$. To start the integration, one should know the positions and velocities at three time steps and these are obtained by using a fourth order Runge-Kutta method. The time step for each star is determined in such a way that two iterations produced an error in its position of less than one percent. The test system contained 150 particles and the integration starts at $t = -2$ and proceeds up to $t = 5$.

8. Dependence on mass ratio

A series of experiments were performed in which the mass ratio $\mu = M_1/M$ ranges from 10 to 0.001 and the perturber moves in parabolic orbit. In all cases, the stars rotate in a clockwise direction which is also the direction of motion of the perturber. Consequently tails are observed to be formed in a direction opposite to the motion of the perturber. The initial configuration of the test galaxy is shown in figure 1.

In the cases when $\mu = 0.001$ and 0.01, no bridge or tail is observed and all the stars essentially remain bound to the test system. Even though the positions of the stars are disturbed, the overall structure of the test galaxy remains the same. The results of computations for $\mu = 0.001$, 0.01 and 0.1 are shown in figure 2.

A series of computations were performed for the mass ratio range 0.1 to 1. In each case, tail appeared to form shortly after the perturber has passed the pericentric point. When $\mu = 0.1$, the tail is short and thin. A bridge connects the test with the perturber at t = 2 but it ceases to exist at t = 5. Nearly 68 % of the stars remain bound to the test galaxy; 25 % form a tail while the remaining stars escape by the end of the computation.

When $\mu = 0.5$, the formation of bridge and tail is observed at t = 2. The tail develops further by t = 5 whereas the bridge has almost disappeared by this time. A
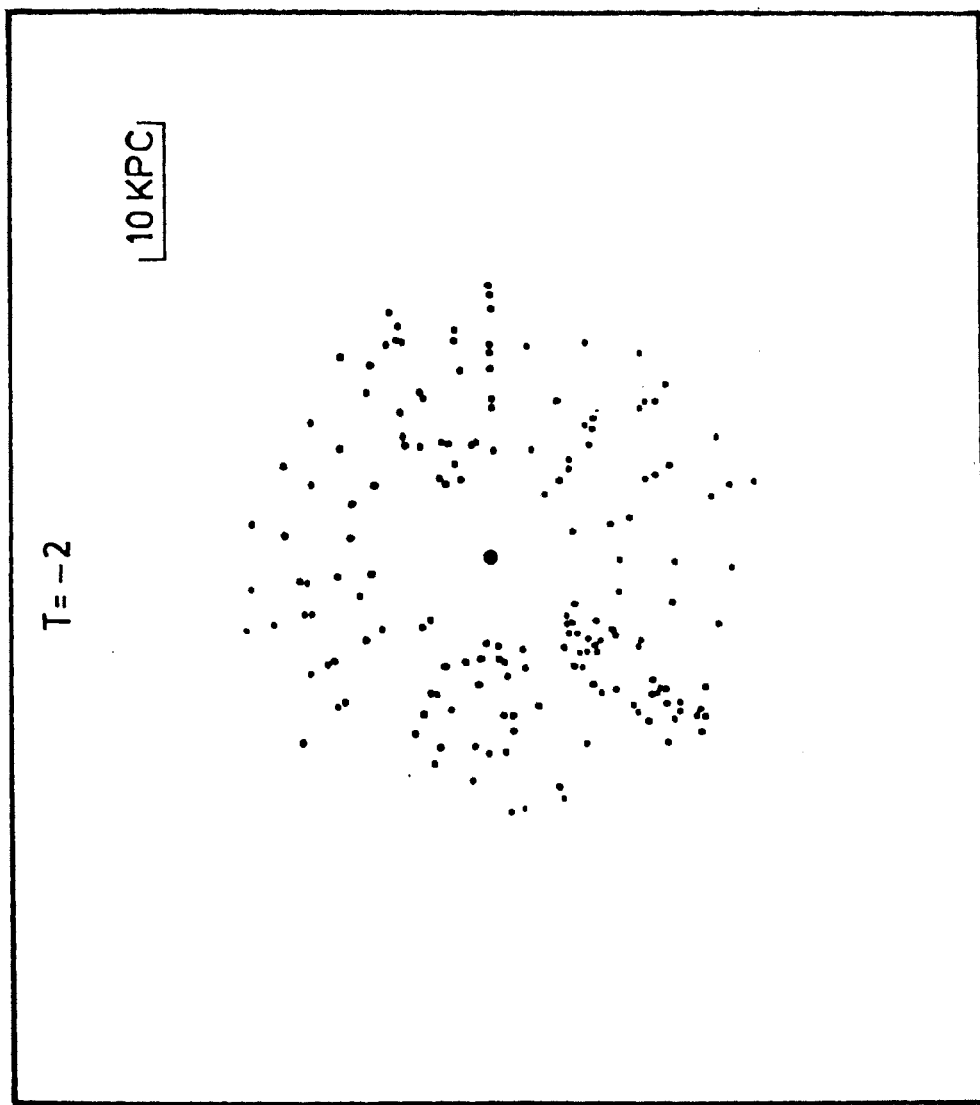
19

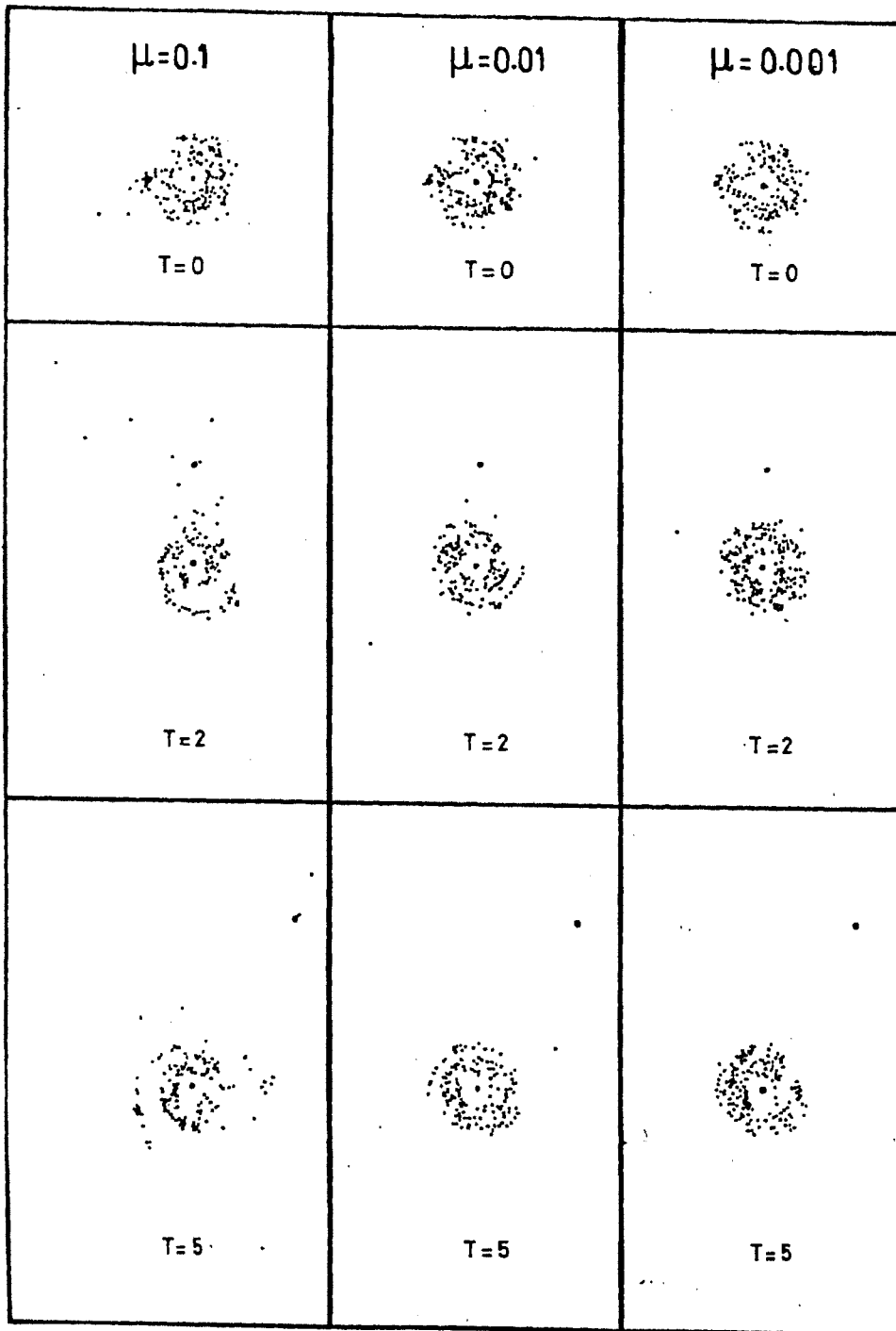Figure 1. Initial configuration of the test galaxy (i. e., at time T = -2).

Figure 2. Configuration of the test galaxy for μ = 0.1, 0.01 and 0.001 at different times during the encounter.

total of 34 % of the stars remain bound to the system, whereas 45 % form the tail. When $\mu = 1$, the tail is well developed at time $t = 2$ and extends to double the distance at $t = 5$ as compared to its size at $t = 2$. A total of 21 % of the stars remain bound to the system, 48 % forming tail, and 31 % escape from the system. The configurations of the system for $\mu = 0.5$ and 1 are shown in figure 3. When $\mu = 2$, very few stars remain bound to the test galaxy and for $\mu = 10$, most of the stars escape and few of them are captured by the perturber. The configurations for $\mu = 2$ and 10 are shown in figure 4.

Certain authors have considered isolated cases of mass ratio (Wright, 1972; Toomre & Toomre, 1972) . The present work takes into account a wide range of values for the mass ratio and therefore enables one to study the effect of mass ratio on the formation of bridges and tails in interacting galaxies. Figure 5 is a histogram showing the fraction of the stars remaining bound to the system after an encounter plotted as a function of μ . This figure shows that as mass ratio increases, the fraction of the stars remaining bound to the test system decreases. The variation appears to be smooth in the mass ratio range considered in the present work.

Figure 6 shows the fraction of the stars forming the tail as a function of mass ratio at the end of computation. The number of stars forming tail increases as the mass ratio increases and remains almost constant in the range $0.5 \leq \mu \leq 1$. When $\mu < 0.5$, the tail appears to be thinner and shorter
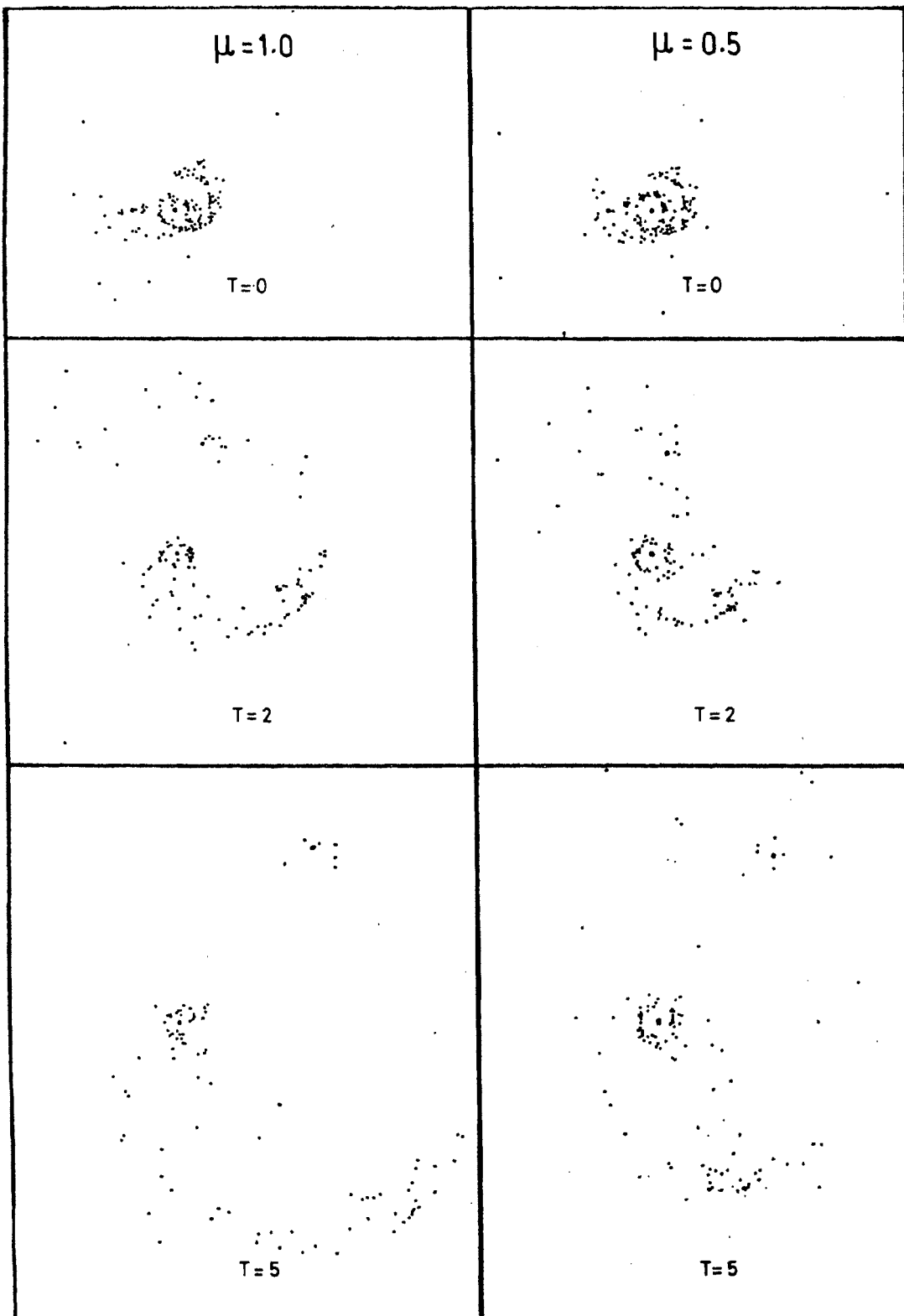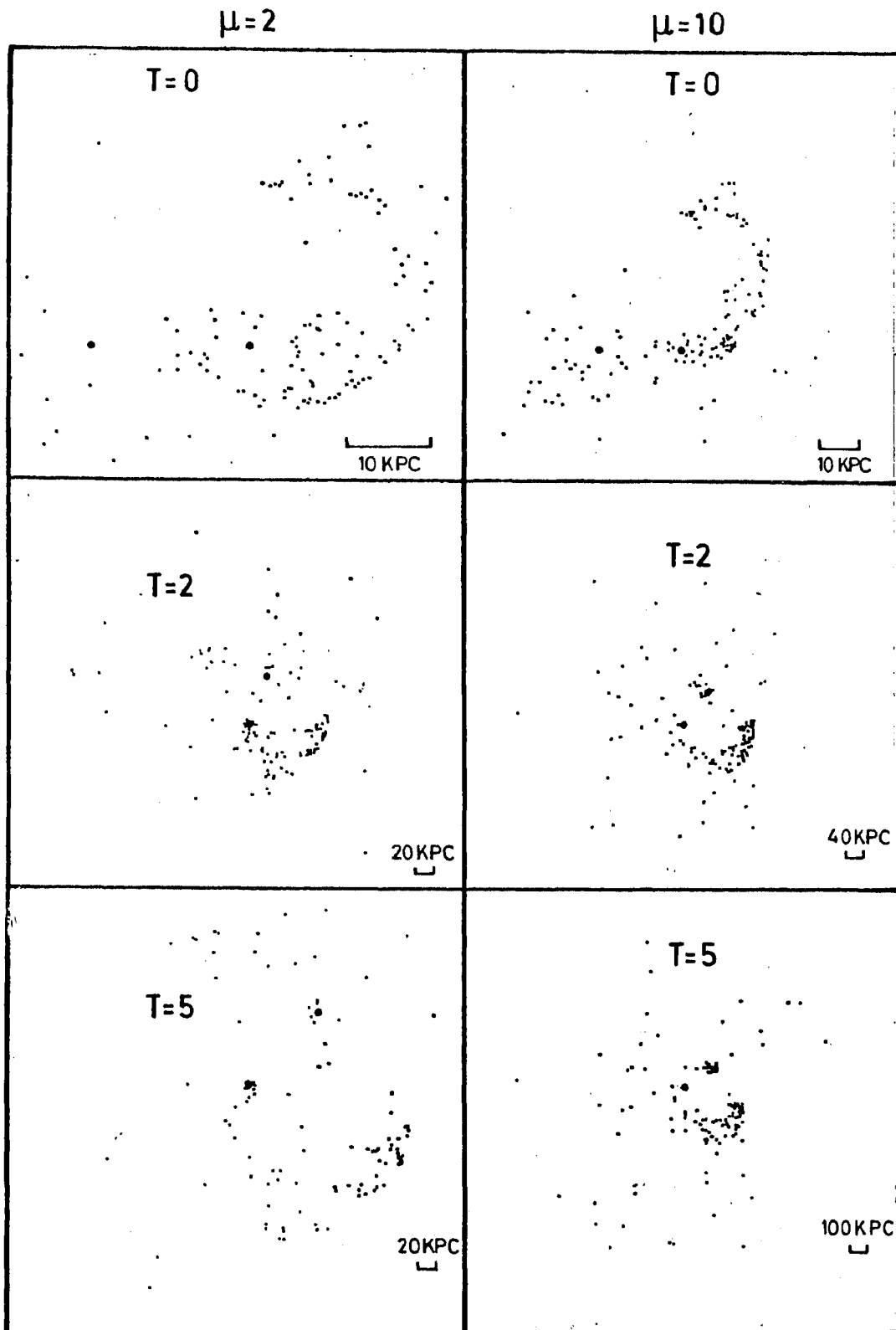
Figure 3. Same as figure 2, but for $\mu = 0.5$ and 1.

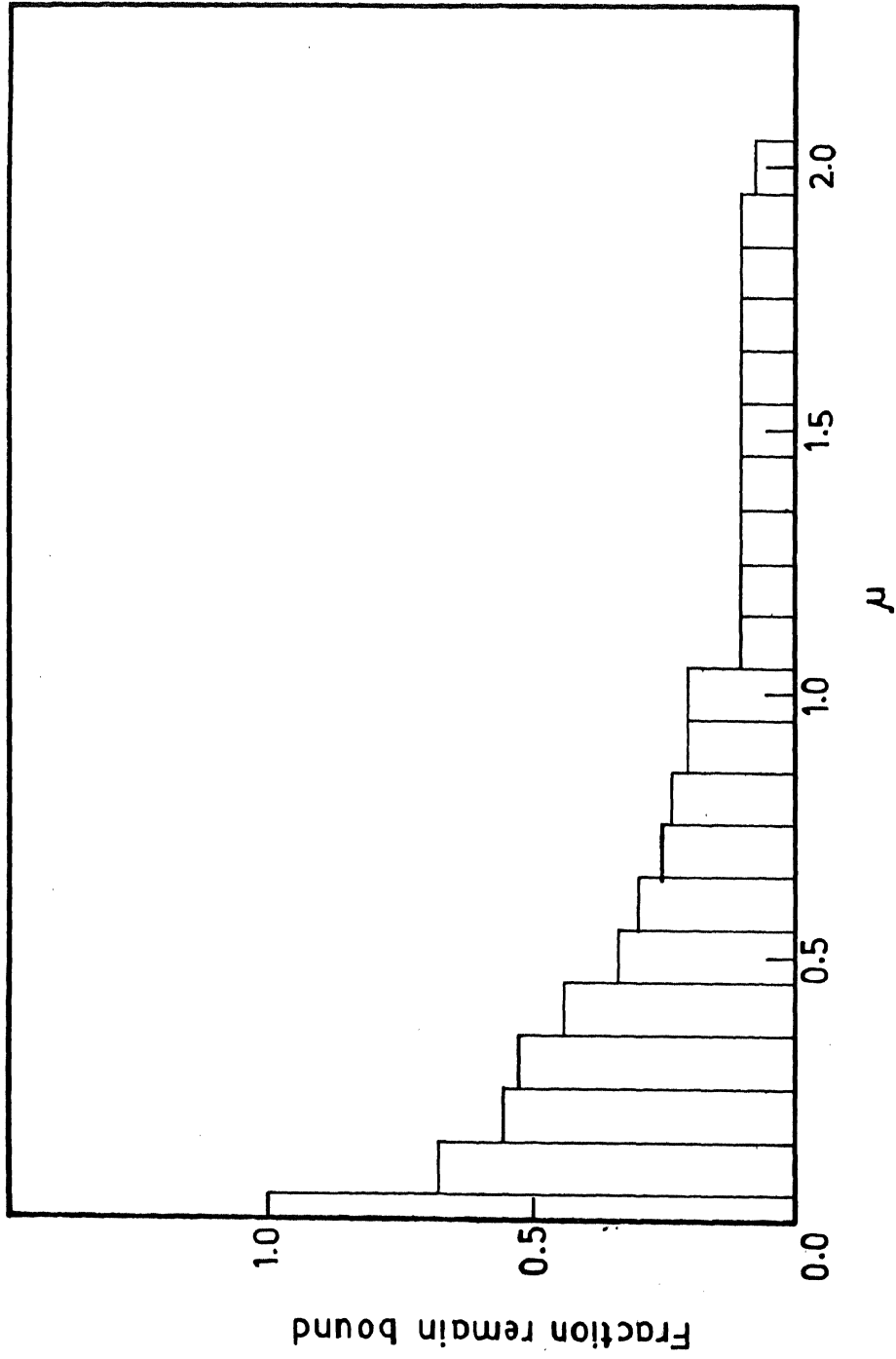Figure 4. Same as figure 2, but for μ = 2 and 10.

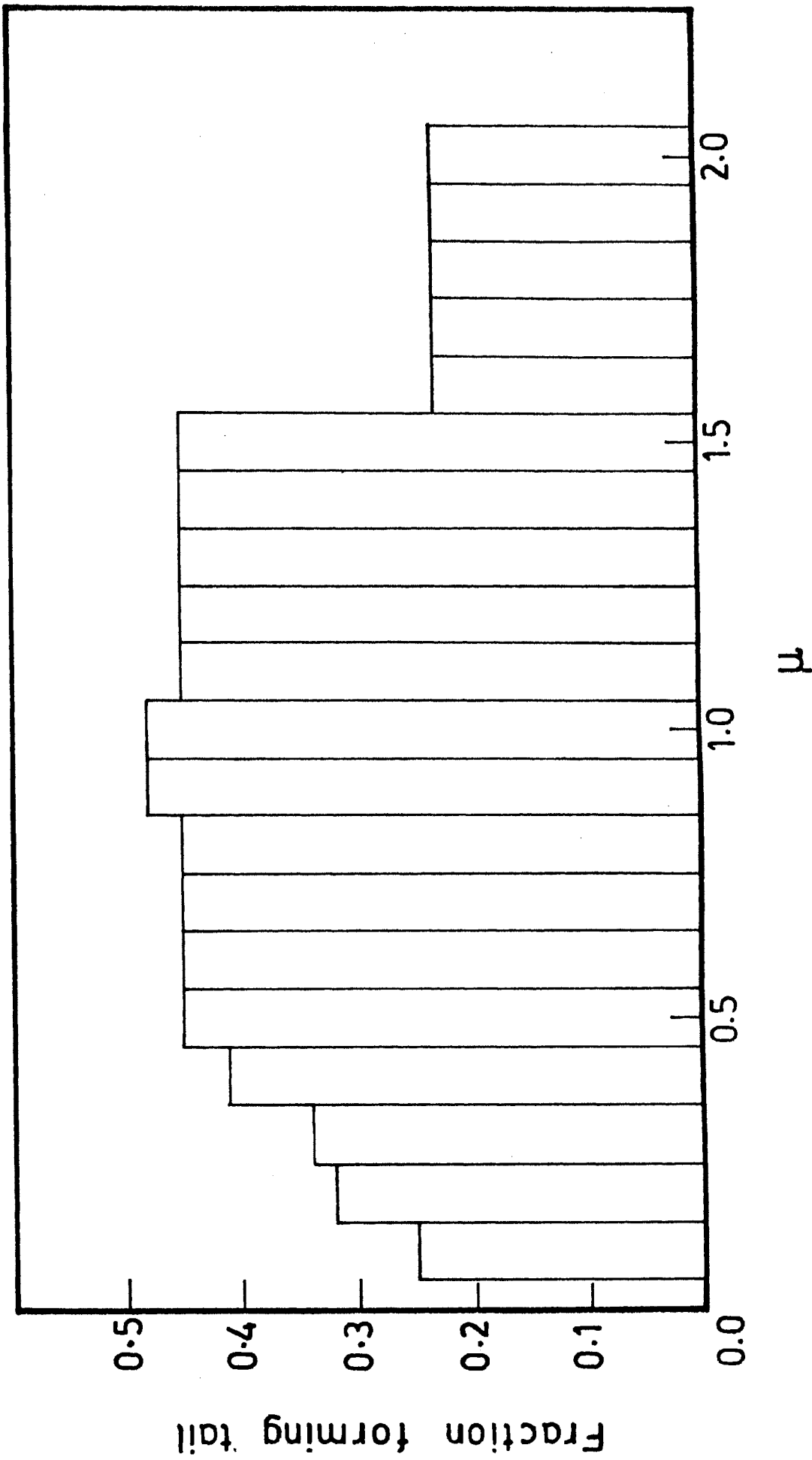Figure 5. Histogram showing the fraction of the stars remaining bound to the test galaxy at τ = 5.

Figure 6. Histogram showing fraction of the stars forming tail at $T = 5$.

than in the case when μ is about unity indicating that the tail formation is favoured when the mass ratio is close to unity (Namboodiri & Kochhar, 1985).

9. Dependence on collision parameter ν

The structural changes produced in the outer parts of a test galaxy as evidenced by bridges and tails due to the passage of a perturber moving in a coplanar,corotating orbit are shown here to depend on a parameter ν which is a function of the mass ratio, the separation of the pair and the eccentricity of the orbit. Let S (x,y,z) be a star in a test galaxy. Let the perturber move in a conic section of eccentricity $e \leq 1$. The components of the velocity perturbations of S, ΔV_x, ΔV_y, ΔV_z , under the impulse approximation (Alladin & Narasimhan, 1982) are

$$\Delta V_x = \frac{\pi \, G \, M_1 \, x}{(1 + e) \, p^2 \, V_p} \quad , \tag{9}$$

$$\Delta V_y = \frac{\pi \, G \, M_1 \, y}{(1 + e) \, p^2 \, V_p} \quad , \tag{10}$$

$$\Delta V_z = - \frac{2 \, \pi \, G \, M_1 \, z}{(1 + e) \, p^2 \, V_p} \quad , \tag{11}$$

where p is the distance of closest approach and V_p is the speed at closest approach given by

$$V_p = \left(\frac{G (M + M_1)}{p} (1 + e) \right)^{1/2}.$$ (12)

Since the stars in the test galaxy are moving in the X-Y plane, $\Delta V_z = 0$. For a star situated at the periphery of the test galaxy whose distance from the centre is equal to the radius R of the disk, the velocity increment $\Delta V(R)$ and circular velocity $V_c(R)$ are given by

$$\Delta V^2(R) = \Delta V_x^2 + \Delta V_y^2$$ (13)

$$= \frac{\Pi^2 G^2 M_1^2 R^2}{(1 + e)^2 p^4 V_p^2}$$ (14)

and

$$V_c^2(R) = \frac{G M}{R} .$$ (15)

We define dimensionless parameter ν

28

$$\nu^2 = \frac{\Delta V^2(R)}{V_c^2(R)}$$

$$= \left(\frac{\Pi^2}{(1+e)^3} \right) \left(\frac{M_1^2}{M(M_1+M)} \right) \left(\frac{R}{p} \right)^3 . \quad (16)$$

It can be seen from equation (16) that the important parameters in a galaxy-galaxy collision are p/R , M_1/M, and e. The impulse approximation suggests that if ν is kept constant, the peripheral morphological effects would be similar. A series of numerical experiments have been performed in which the value of ν varies in the range 0.05 - 0.9. Each value of υ is arrived at by two different sets of values of p/R and $\mu = M_1/M$. The collision parameters for these experiments are given in table 1.

Table 1. Collision parameters.

Model	p/R	μ	ν
1 a	6.27	1	0.05
1 b	36.56	100	0.05
2 a	4.00	1	0.10
2 b	10.00	10	0.10
3 a	1.57	1	0.40
3 b	9.14	100	0.40
4 a	2.50	10	0.70
4 b	125.00	10	0.70
5 a	2.40	10	0.90
5 b	5.32	100	0.90

The structure of the galaxy for ν = 0.05 shows no trace of bridge or tail as is evident from figures 7a,b. As
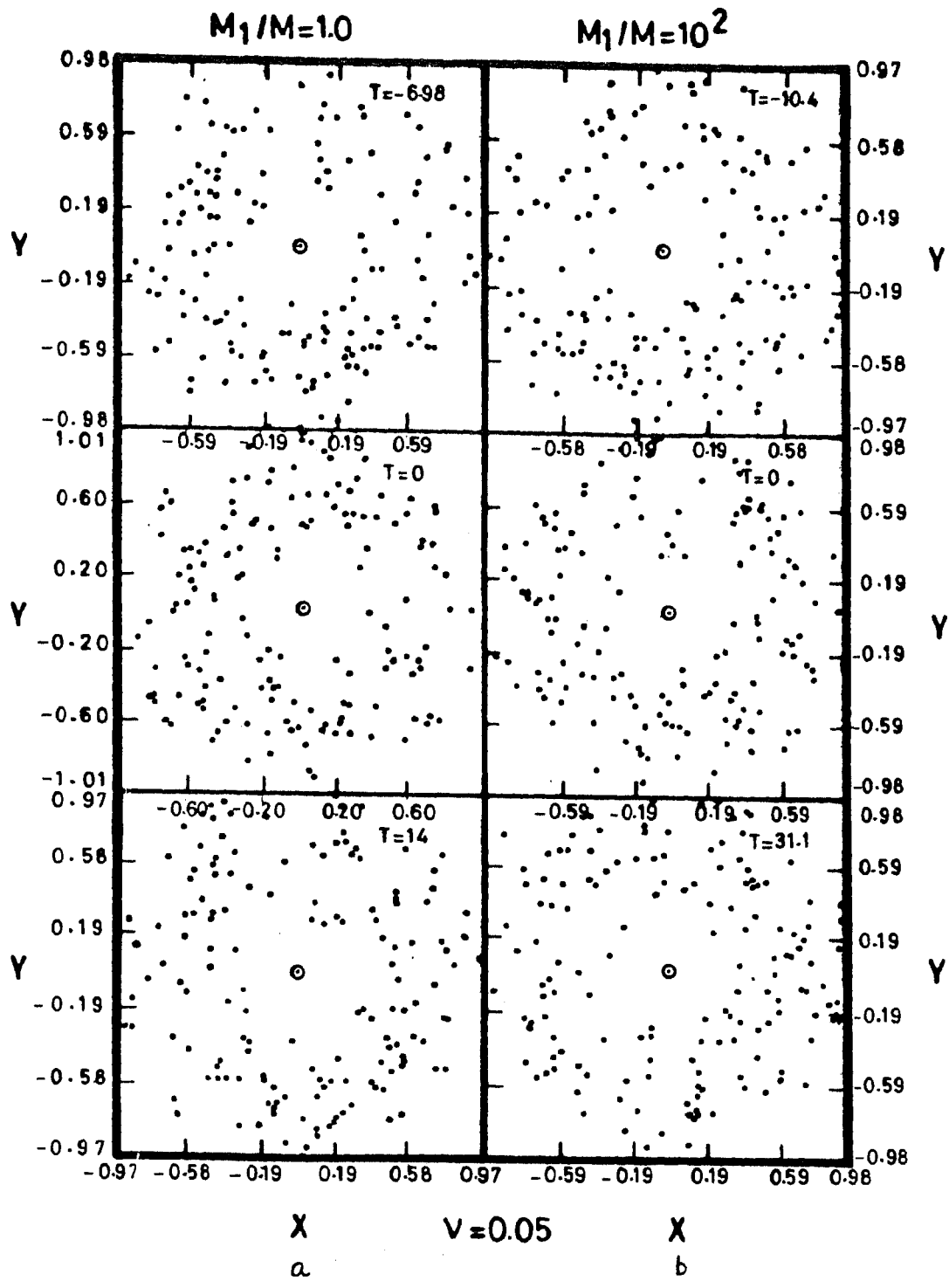
Figure 7. Configuration of the test galaxy at different times for $V = 0.05$. Figures 7a and b correspond to $p/R = 6.27$ and 36.56 respectively.

one increases the value of the parameter ν, the tendency for the formation of tail emerges (see figures 8a,b). Although the values of μ and p/R are different, the structure determined by $\nu = 0.1$ is the same in both the cases.

Figures 9a,b show the case in which bridges and tails are developed. The tail gets developed after the pericentric passage of the perturber. Expansion in the size of the system is observed after an encounter. Structural changes produced for $\nu = 0.7$ are shown in figures 10a and b. Bridges and tails are developed in both the cases. In case 4b, even though the perturber is much more massive than the test galaxy compared to case 4a, the changes produced in the test galaxy are almost identical. Figures 11a,b show the case for $\nu = 0.9$. In these cases, the bridges and tails form but do not last long. The galaxy suffers considerable damage due to the encounter although identical structures are produced in both the cases.

10. Discussion

The formation of similar bridges and tails in interacting galaxies can be understood in terms of a simple scaling of masses and distances. The development of bridges and tails depends on the parameter υ in the range $0.1 \leq \nu \leq 0.7$. If $\nu < 0.1$, practically no damage is done to the test galaxy while for $\nu > 0.7$, the test galaxy suffers
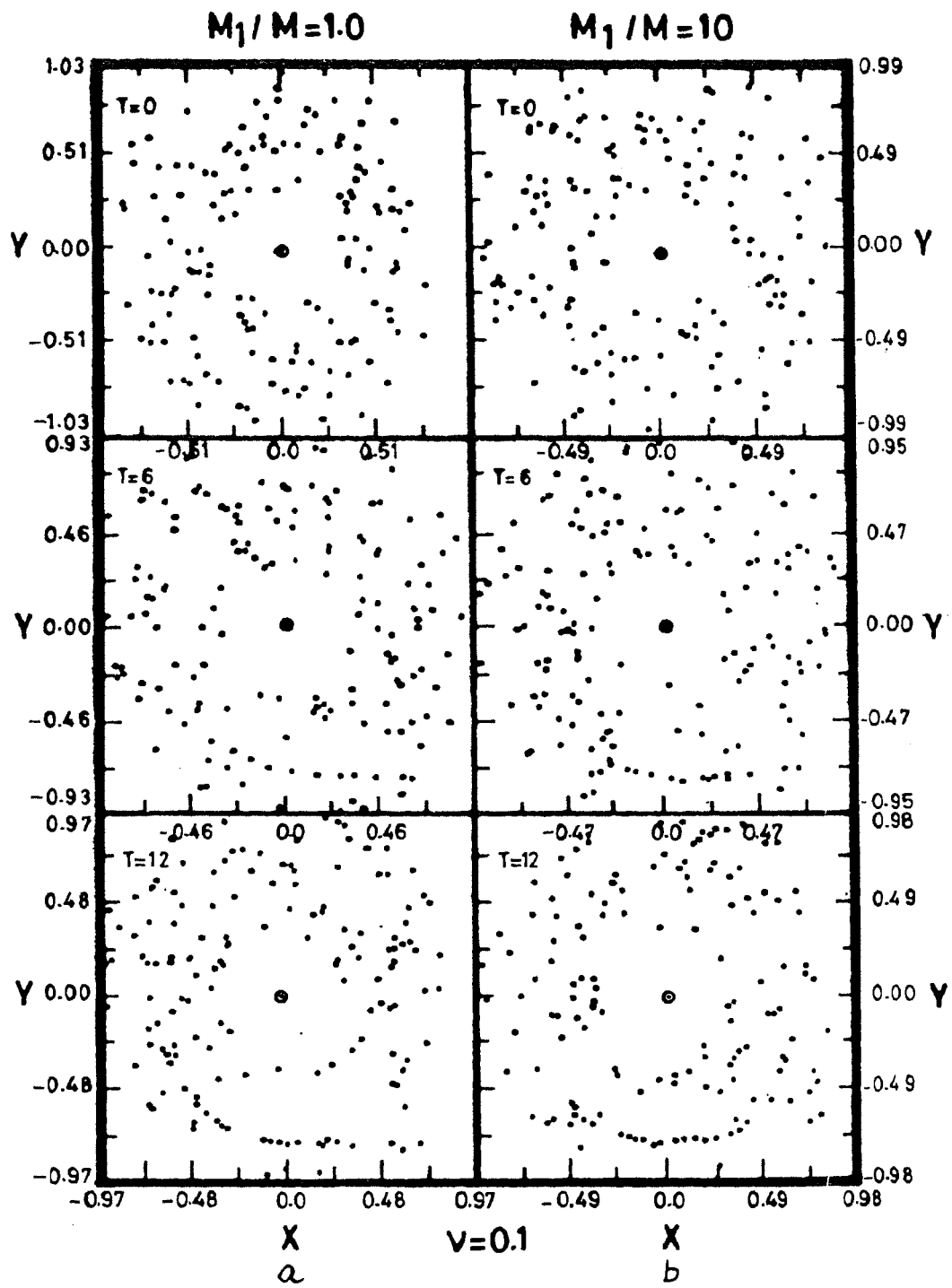
31

Figure 8. Same as figure 7, but for ν = 0.1. Figures 8a and b correspond to p/R = 4 and 10 respectively.

32

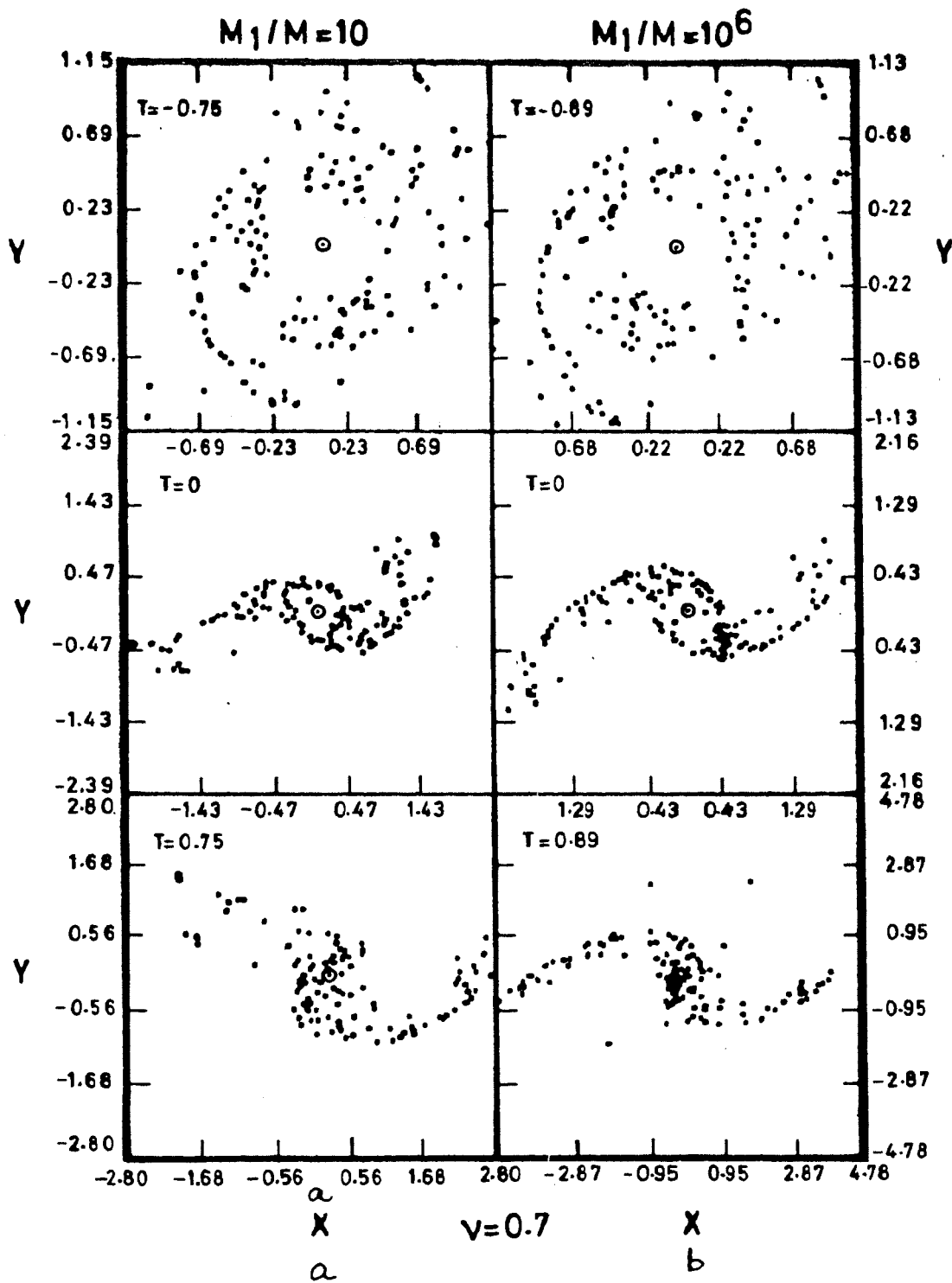Figure 9. Same as figure 7, but for $V = 0.4$. Figures 9a and b correspond to p/R = 1.57 and 9.14 respectively.

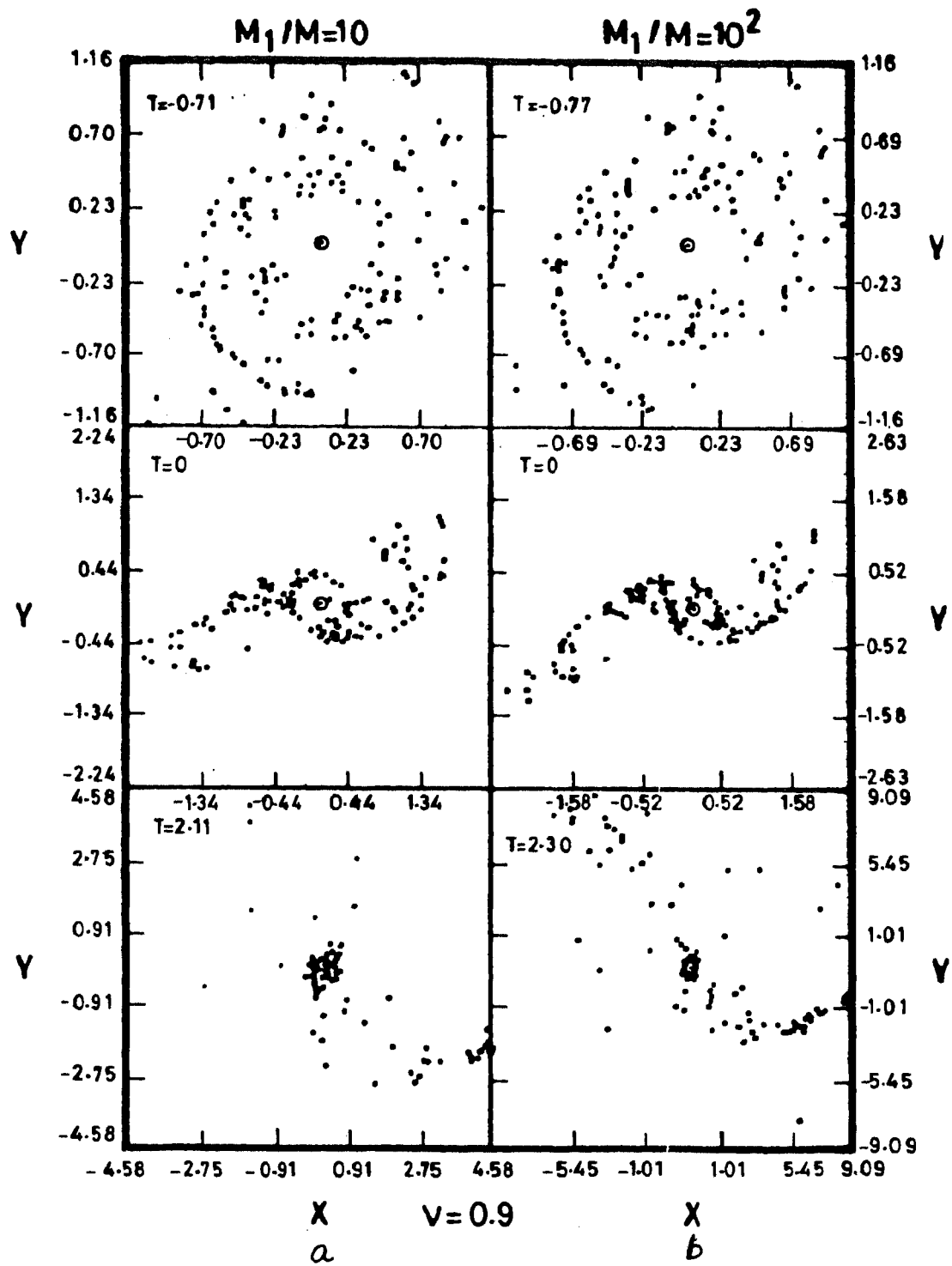Figure 10. Same as figure 7, but for ν = 0.7. Figures 10a and b correspond to p/R = 2.5 and 125 respectively.

Figure 11. Same as figure 7, but for $V = 0.9$. Figures 11a and b correspond to p/R = 2.4 and 5.32 respectively.

appreciable disruption during the course of an encounter (Namboodiri et al. , 1987a & 1987b).

Since a massive galaxy will also generally be large in size, the values of p considered in the present work are of the order of $R_1 + R_2$ where R_1 and R_2 are the radii of the two interacting galaxies. Grazing or slightly penetrating collisions are effective in producing bridges and tails. However, if the massive galaxy happens to be compact, distant collisions can also lead to the formation of these morphological features since in this case the separation would be much greater than the sum of the radii of the individual galaxies.

The computations give a qualitative picture of the tidal effects which depend on the parameters of collision. The tidal effects depend strongly on the separation and weakly on the ratio of the masses. The amount of material which escapes from closely interacting systems can be a substantial fraction (10 - 30 %) of each galaxy's initial mass. Mass may be lost from the system through repeated encounters and the remaining mass is widely dispersed over a large volume thereby decreasing the detected luminosity of the system. This, then, poses a question whether binary galaxies will remain bound or not. The possibility that the perturber will escape can account for isolated galaxies showing tail structure without any visible companion.

Observational evidence, which supports that the filaments should contain large amount of gas, is not very

promising. If the luminosity of the filaments is due to gas excited by OB stars, the spectra should contain emission lines. On the other hand, if the luminosity is mainly due to stars, the spectra should contain absorption lines. However, Arp (1962) found that the light from A295 is strongly polarized which indicates the presence of energetic particles embedded in a magnetic field. No satisfactory explanation for the presence of energetic particles in the filaments is available. Emission lines are not seen in the bridge and tail of A174 whereas H and K absorption lines have been detected in them. Thus the luminosity of the filaments of A174 is mainly due to stars. Evidence from observations thus suggests, even though weakly, that the bridges and tails are produced from the stellqr component rather than the gaseous component.

CHAPTER THREE

N-BODY SIMULATIONS : METHOD

11. N-body simulations

Numerical simulations of the evolution of two or more interacting galaxies require a fine spatial resolution to resolve details in individual systems. Self-consistent N-body simulations are usually umployed for modelling real stellar systems, for investigating the detailed dynamical processes as well as for checking theoretical predictions. There are mainly two procedures for the self-consistent modelling of a stellar system. One is the direct method which uses appropriate individual time steps for each particle to update its position and velocity. The advantage of this method is that it is flexible, makes no assumptions about the geometry of the system and is easy to adapt to a variety of applications. The main drawback of this scheme is that the simulations become prohibitively expensive for systems containing large number of particles. The second method uses a fixed time step for all particles and determines the gravitational potential at each time step by an algorithm based on the Fast Fourier Tranform technique. This technique is less flexible than the former but can handle a large number of particles.

12. Direct method

The evolution of a stellar system consisting of N particles is governed by the equations

$$\frac{d^2 r_i}{d t^2} = - G \sum_{\substack{j=1 \\ i \neq j}}^{N} \frac{m_j\, r_{ij}}{r_{ij}^{\,3}} \qquad i = 1,2,3,\ldots\ldots,N, \qquad (1)$$

$$r_{ij} = r_i - r_j \qquad\qquad\qquad (2)$$

where r_i and m_i are the position and mass of the ith particle respectively; G is the gravitational constant; and t the time. The problem involves the solution of N second order differential equations, one corresponding to each particle of the system. Basically there are two difficulties in directly integrating the system of equations.

First, the force on each particle becomes unbounded when another particle comes close to it. Although actual collisions are rare events, the formation of tight binaries is quite common. One has to use a very small time step to calculate the forces in such circumstances and hence the conventional integration schemes, which use a fixed time step, become inefficient and slow down the computations considerably. Von Horner (1960) tried to evolve clusters containing up to 16 stars using single time step for each star. The time step is chosen small enough to be appropriate

for the pair of stars undergoing strongest interaction at the time. This method is inefficient and time consuming when there is a pair of particles forming a tight binary. Aarseth (1963) introduced individual time steps for each star in order to overcome this difficulty. The assignment of an individual time step for each particle means that particles are no longer synchronized during integration. The synchronization is achieved while the force on a star is being calculated. This takes less computing time than the recalculation of the forces of the whole system at each time step. This refinement considerably reduces the computing time, thus permitting a inclusion of a larger number of particles in the model stellar system.

The second difficulty in directly integrating the system of equations (1) is that the force on each of the N particle depends on the positions of all other particles and hence the time needed in calculating the force increases as N^2. This restricts the study of systems with large N. Ahmed & Cohen (1973) have devised a scheme which avoids recalculation of the force at frequent intervals. This method makes use of the fact that the force on a star can be divided into two parts: a slowly varying part due to the distant stars, called the regular force; and another component, the rapidly varying part due to stars in the immediate neighbourhood, called the irregular force. The irregular force arises due to the cumulative effects of a few close encounters in a stellar system. Its calculation involves enclosing each particle

within a sphere of given radius and computing the force due to the particles within that sphere. The size of the sphere and the number of neighbours depend on the local density. The efficiency of the scheme arises from the fact that the regular force changes much more slowly than the irregular force and thus need be calculated at longer time intervals. In systems containing large number of particles, the number of neighbours a star has is small thus considerably reducing the computing time. To study the evolution of the interacting galaxies, Aarseth's N-body 2 code is used which is described briefly in the next section.

13. Aarseth's N-body 2 code

The N-body 2 code developed by Aarseth employs individual time steps for each particle and divides the force acting on a particle into regular and irregular forces. It has successfully been used to simulate the collision of two galaxies. Since the force on a particle is divided into two parts, each particle will have two time steps. The regular time step ΔT_1 is taken to be the smaller value of the two time steps determined by

$$\Delta T_i = \beta \frac{K_i}{|\dot{K}_i|} \quad , \quad \text{(3)}$$

and

$$\Delta T_i = \beta \frac{|r_i|}{< v^2 >^{1/2}} \quad . \quad \text{(4)}$$

Here K_i and $\dot{K}_i$ are the regular force and its time derivative; β is a constant used to control the accuracy of the integration; and $<v^2>^{1/2}$ is the root mean square velocity of the system. The irregular time step is determined from

$$\delta T_i = \alpha \left(\min (r_{ij}) \right)^{3/2} \quad , \quad \text{(5)}$$

where $\min (r_{ij})$ is the distance between the ith particle and its closest neighbour, j. The constant α is again an error control parameter. If this time step happens to be very large, it is again computed using the formula

$$\delta T_i = \frac{\eta \alpha}{m^{1/2}} \min \left(\frac{r_{ij}}{v_{ij}} \right) \quad , \quad \text{(6)}$$

where η is a constant and equal to 3.3.

The position and velocity of the ith particle are updated using a Taylor series of the form

$$r_i(T) = r_i(T_0) + v_i(T_0) \Delta T + \frac{1}{2} \frac{F_i(T_0)}{m_i} \Delta T^2 +$$

$$+ \sum_{k=1}^{l} \frac{F_i^{(k)}(T_0) \Delta T^{k+2}}{m_i (k+2)!} \quad , \quad (7)$$

$$v_i(T) = v_i(T_0) + \frac{F_i(T_0)}{m_i} \Delta T + \sum_{k=1}^{l} \frac{F_i^{(k)}(T_0) \Delta T^{k+1}}{m_i (k+1)!} \quad .$$

$$(8)$$

Here T_0 and T are the old and new times; F_i is the total force on the particle; $F_i^{(k)}$ is the kth derivative of the force evaluated at time T_0; and $\Delta T = T - T_0$. In equation (7), retaining the first four terms in the summation gives fairly accurate results (Weilen 1967). The total force and its derivatives are obtained from

$$F_i^{(k)} = K_i^{(k)} + S_i^{(k)} \quad , \quad k = 1,2,3,4 \quad , \quad (9)$$

where K_i and S_i are the regular and irregular forces evaluated at time T_0. The regular and irregular forces are evaluated using a divided difference scheme which is the most suitable method for a system having variable time step. A fourth order force polynomial is defined as

43

$$F(T) = F(T_0) + D \, [T_0, T_1](T - T_0) + D^2 \, [T_0, T_2](T - T_0)(T - T_1) +$$

$$+ \; D^3 \, [T_0, T_3](T - T_0)(T - T_1)(T - T_2) \; +$$

$$+ \; D^4 \, [T, T_3](T - T_0)(T - T_1)(T - T_2)(T - T_3) \; , \quad (10)$$

where T_0 , T_1 , T_2 , T_3 are four previous times with T_0 being the most recent one. The divided differences are given by

$$D^k[T_0, T_k] \; = \; \frac{1}{T_k'} \left(\; D^{k-1}[T_0, T_{k-1}] \; - \; D^{k-1}[T_1, T_k] \; \right) \qquad (11)$$

$$T_k' \; = \; T_0 \; - \; T_k \; , \qquad k = 1, 2, 3. \qquad (12)$$

Here D^0 represents F. A fourth order Taylor series expansion of the force can be written as

$$F(T) \; = \; F(T_0) + \sum_{k=1}^{4} \frac{F^{(k)}(T - T_0)^k}{k \, !} \; . \qquad (13)$$

Equating the coefficients $(T - T_0)^k$, $k = 1, 2, 3, 4$ from equations (10) and (13), we obtain the following expressions for the force derivatives

44

$$F^{(1)} = D\,[T_0,T_1] + T_1'\,D^2[T_0,T_2] + T_1'\,T_2'\,D^3[T_0,T_3] +$$

$$+ T_1'\,T_2'\,T_3'\,D^4[T,T_3] \quad ,$$

$$F^{(2)} = 2\,!\,\left\{ D^2\,[T_0,T_2] + (T_1' + T_2')\,D^3\,[T_0,T_3] + \right.$$

$$\left. + (T_1'\,T_2' + T_2'\,T_3' + T_3'\,T_1')\,D^4\,[T,T_3] \right\} \quad , \qquad (14)$$

$$F^{(3)} = 3\,!\,\left\{ D^3[T_0,T_3] + (T_1' + T_2' + T_3')\,D^4\,[T,T_3] \right\} \quad ,$$

$$F^{(4)} = 4\,!\,D^4\,[T,T_3] \quad .$$

The calculation of D^4 requires a knowledge at time T of the force which is unknown at time T_0. The position and velocity are updated first using equation (7) up to $F^{(3)}$ terms by evaluating differences up to D^3. The new position is used to find the force on the star at time T from which D^4 can be evaluated. The correct position is then determined by adding $F^{(4)}$ term and also adding contributions to lower order derivatives due to D^4 term. This semi-iteration procedure gives increased accuracy at little cost and no extra computer memory.

Ideally, the N-body simulations should use very large value for N to represent a stellar system. The availability of computer time and other facilities restrict the value of N to a manageable size. The present simulations use N = 250. Due to the small value of N chosen to represent

45

a stellar system, the relaxation time would be much shorter than what it is for a real galaxy. The reference relaxation time T_r for a spherical stellar system in which particles have equal mass is approximately given by

$$T_r = \frac{T_c \, N}{26 \, \log(0.4 \, N)} \tag{15}$$

where T_c is the and crossing time (Spitzer & Hart, 1971). The relaxation effects can be substantially reduced by using a soft potential for each particle of the form

$$\phi_{ij} = - \frac{G \, m_i \, m_j}{(\, r_{ij}^2 + \varepsilon^2 \,)^{1/2}} \quad , \tag{16}$$

where ε is called the softening parameter which may be considered as the size of the particles. A stellar system with a softened potential of the form given by equation (16) represents a Plummer model galaxy. The softening of the potential, which has generally been exploited in N-body simulations, eliminates close binaries and somewhat reduces the importance of relaxation effects for the overall evolution of the systems. Real galaxies contain so many stars that two-body effects are completely negligible over the time-scales for which simulations are generally carried out.

It should however be noted that a softened potential of the form given by equation (16) modifies the

46

standard equilibrium virial theorem as

$$2 \, T \; = \; \sum_{i=1}^{N} m_i v_i^2 \; = \; \sum_{i,j=1}^{N} \frac{G \, m_i \, m_j \, r_{ij}^2}{(\, r_{ij}^2 + \varepsilon^2 \,)^{3/2}}$$

$$= W + F(\varepsilon) \qquad\qquad\qquad (17)$$

where T and W are the total kinetic and potential energy. The value of the virial coefficient

$$Q \; = \; T \, / \, | \, W \, | \quad , \qquad\qquad\qquad (18)$$

will now be slightly different from 0.5 as is expected from a potential of the form $1 \, / \, r$. For the present simulations a value of $\varepsilon = 0.1$ R is chosen where R is the radius of the stellar system.

14. Initial conditions

The model galaxy consists of 250 particles each having unit mass so that its total mass M = 250 units. The particles are distributed uniformly in 10 concentric spheres of radius two units so that the total radius R is 20 units. The initial mass distribution can be approximately represented by $M(r) \; \alpha \; r$. Each particle is initially given a velocity equal to the circular velocity appropriate to its position and the directions of the velocity vectors are chosen randomly. The

47

units are defined in such a way that $G = 1$. If $R = 20$ kpc and $M = 10^{11} M_{\odot}$, one unit of time is nearly equal to 1.3×10^{8} yr. and the unit of velocity is 147 kms^{-1}. The cluster so formed is very close to virial equilibrium with root mean square velocity $V_{rms} = 2.6$, half-mass radius $R_h = 10.3$ and crossing time $T_c = 2 R_h / V_{rms} \approx 8$. The cluster is not rotating in an inertial frame although it usually has some amount of orbital angular momentum.

The test galaxy is evolved for eight crossing times to obtain a dynamically stable system. The evolved system shows higher concentration toward the centre and an expansion in the outer region. Its half-mass radius is 6.55 units. 90 % of its mass is within about $3R_h$ (denoted by $R_{0.9}$) and the radius of the total system (denoted by R_B) extends to about $6R_h$. The ratio v_{rrms} / v_{trms}, where v_{rrms} and v_{trms} are the root mean square radial and tangential velocity, shows that some particles in the system move in elongated orbits. The parameters of the initial model and the evolved one (standard model) are given in table 2.

Table 2. Model parameters

Model	R	$R_{0.9}$	R_h	R_{rms}	V_{rms}	V_{Disp}	$\dfrac{V_{rrms}}{V_{trms}}$
INITIAL	19.75	18.03	10.25	11.73	2.60	0.97	0.66
STANDARD	36.62	18.62	6.55	10.81	3.42	1.45	0.74

The standard model is used as the test galaxy for subsequent encounters with another galaxy.

48

It is well known that a stellar system with sufficiently high density is stable against disruption due to the tidal force of an external galaxy. Considerable tidal disruption occurs if the satellite density ρ is less than a critical density – the Roche density ρ_R . Alladin et al. (1985) have shown from a comparative study of impulse approximation and adiabatic approximation that a satellite galaxy disrupts if its density at half-mass radius $\rho_h < \rho_R$ whereas for $\rho_h > \rho_R$, the disruption is considered negligible. In this latter case the tidal effects of the satellite on the outer parts of the primary generally turn out to be quite important and may lead to the decay of the orbit of the satellite. It is therefore necessary to carefully choose the densities of the galaxies so that the circumstances under which tidal disruption takes place can be studied.

The perturber is considered to be a point mass with mass M_1. The mean density of the satellite within a sphere of radius R_h is defined as

$$\rho_h = \frac{M / 2}{4/3 \; \Pi \; R_h^{\;3}} \; .$$

(19)

The Roche density ρ_R is defined as

$$\rho_R = 2\rho_1 = 2\left[\frac{M_1}{4/3 \; \Pi \; p^3}\right]$$

(20)

so that

$$\frac{\rho_h}{\rho_R} = \frac{1}{4} \left(\frac{M}{M_1} \right) \left(\frac{p}{R_h} \right)^3 , \qquad (21)$$

where p is the distance of closest approach associated with the initial Kepler orbit. A wide range of values for the density ratios have been considered including the case $\rho_h = \rho_R$.

A necessary condition for a merger to occur in a head-on collision is that the relative velocity at closest approach be less than 1.16 times the escape velocity there (van Albada & van Gorkom, 1977). This velocity should be even slower for collisions with larger impact parameters. Whenever two galaxies overlap substantially such that $p < 2.5\ R_h$, the encounter results in a merger (White, 1978). Mergers are not considered in the present simulations; we set p = 100 to avoid mergers. This value of p is almost equal to three times the radius of the test galaxy and the encounters are therefore weak and non-penetrating. The relative velocity of the perturber at the start of the simulations is chosen such that mergers are excluded.

Initially the galaxies are positioned on the two-body orbit that point-mass particles would execute. This orbit is an excellent approximation when the mass distributions do not overlap. The relative orbit of M_1 around M is a conic given by

50

$$\frac{1}{r} = 1 + e \cos\theta \quad , \quad (22)$$

with M at the focus; l is the semi-latus rectum; and e is the eccentricity of the relative orbit. The orbital plane of M_1 is chosen as the X-Y plane with the X-axis pointing in the direction of closest approach. For a given value of p and e, the value of l can be readily obtained from

$$l = p(1 + e) \quad . \quad (23)$$

The simulation of tidal interaction between two galaxies must commence with an initial galaxy separation appreciably larger than the size of the test galaxy. The initial separation r_0 between the galaxies is determined from

$$r_0 = k p \quad , \quad (24)$$

where k is a constant depending on the relative orbit of the perturber. For bound orbits, the galaxies are placed initially at the apocentre. Once the initial separation r_0 is known the corresponding angle θ_0 can be found from equation (22). The cordinates of M_1 are given by

$$x_0 = r_0 \cos\theta_0 \ , \qquad y_0 = r_0 \sin\theta_0 \ , \qquad z_0 = 0 \ . \qquad (25)$$

The magnitude of the relative velocity V_0 of M_1 is given by

$$V_0^2 = \mu \left[\frac{2}{r_0} - \frac{1-e}{p} \right] \quad , \quad e < 1$$

$$V_0^2 = \frac{2\mu}{r_0} \quad , \quad e = 1 \quad\quad\quad (26)$$

$$V_0^2 = \mu \left[\frac{2}{r_0} + \frac{e-1}{p} \right] \quad , \quad e > 1$$

where $\mu = G (M + M_1)$. To obtain the direction of the velocity, the law of conservation of angular momentum is used:

$$r_0 \times V_0 = p \times V_p \quad , \quad\quad\quad (27)$$

where V_p is the velocity at closest approach and

$$V_p^2 = \frac{\mu}{p} (1 + e) \quad . \quad\quad\quad (28)$$

If α is the angle between r_0 and V_0 :

$$\sin \alpha = \frac{p \, V_p}{|r_0| \, |V_0|} \quad . \quad\quad\quad (29)$$

The components of the initial relative velocity are given by

$$V_{x0} = V_0 \cos (\alpha - \theta_0) \quad,$$

$$V_{y0} = V_0 \sin (\alpha - \theta_0) \quad, \tag{30}$$

$$V_{z0} = 0 \qquad .$$

For the N-body simulations it is recommended to use a co-ordinate system with origin at the centre of mass of the total system. Accordingly, the positions and velocities of the particles in the test galaxy and the perturber are recalculated with respect to the centre of mass of the total system. The evolution of the test galaxy has been followed till the perturber reached a distance $r > 2 p$. In some bound orbit encounters, the integration was performed for two orbital periods.

We have considered four specific models in which the perturber is allowed to move initially in relative orbits that are hyperbolic (model H), parabolic (model P), elliptic (model E), and circular (model C). These models are designated by the letters followed by the numbers 1, 2, 3, 4, 5, 6, 7, 8, and 10 which respectively corresponding to density ratios 0.75, 1.50, 2.67, 5.34, 10.68, 21.36, 42.71, 85.41, and 341.63. For example H1 means that the relative orbit is hyperbolic and density ratio is 0.75 (Namboodiri & Kochhar, 1990). For H-models the initial eccentricity of the relative orbit of the perturber is $e = 2$, whereas in the elliptic case $e = 0.5$. For model ES , $p = 72$, $e = 0.8$ and $\rho_h/\rho_R = 33.21$. The

53

other collision parameters for various models are given in table 3.

The values of p and e for all these models are meaningful only if the galaxies are assumed to be point masses moving in Keplerian orbits. It should however be noted that soft potential orbits are not exactly conical orbits, and the use of p and e is therefore valid only to a good approximation but not strictly (Gerhard,1981).

The data obtained from the simulations are stored at selected time intervals for later analysis which is described in the next chapter.

Table 3. Parameters of collision

MODEL	ρ_h/ρ_R	M_1/M	r_0/p	v_p/v_{rms}
H1	0.75	1186.2	3.0	27.591
H2	1.50	593.1	3.0	19.518
H3	2.67	333.3	3.0	14.641
H4	5.34	166.7	3.0	10.370
P1	0.75	1186.2	2.0	22.528
P2	1.50	593.1	2.0	15.936
P3	2.67	333.3	2.0	11.594
P4	5.34	166.7	2.0	8.467
P5	10.68	83.3	2.0	6.003
P6	21.36	41.7	2.0	4.272
P7	42.71	20.8	2.0	3.053
P8	85.41	10.4	2.0	2.209
P10	341.63	2.6	2.0	1.241
E1	0.75	1186.2	1.5	19.510
E2	1.50	593.1	1.5	13.801
E3	2.67	333.3	1.5	10.353
E4	5.34	166.7	1.5	7.333
E5	10.68	83.3	1.5	5.199
E6	21.36	41.7	3.0	3.700
E7	42.71	20.8	3.0	2.644
E8	85.41	10.4	3.0	1.910
E10	341.63	2.6	3.0	1.070
ES	33.21	10.0	9.0	2.424
C6	21.36	41.7	1.0	3.021
C7	42.71	20.8	1.0	2.159
C8	85.41	10.4	1.0	1.561
C10	341.63	2.6	1.0	0.878

CHAPTER FOUR

N-BODY SIMULATIONS : RESULTS

15. Data analysis

The data obtained from the N-body simulations at
selected intervals essentially contain the positions and
velocities of all the particles in the test galaxy and of the
perturber in the centre of mass reference frame of the total
system. These data have to be analysed with respect to a
reference frame appropriate to the test system. It is,
therefore, necessary to formulate a criterion to determine the
centre of mass of the test system.

The centre of mass of all the stars originally
residing in the test galaxy does not give a reasonable
indication of its true position at subsequent stages because
of the escape of stars and the formation of extensive tidal
tails. Further if the mass distribution is not spherically
symmetric - as is the case after an encounter - the origin
chosen as above may lie outside the most dense region in the
system. It seems reasonable to identify the most dense region
of the system and to take the origin at the centre of mass of
the particles in this region for the purpose of describing the
mass distribution. Von Horner (1963) suggested that a more

accurate estimate of the centre of the highest density region
in the galaxy is provided by

$$r_c = \sum_i \rho_i r_i / \sum_i \rho_i \qquad (1)$$

where $\rho_i = r_{13}^{-3}$, r_{13} being the distance between the ith star
and its third nearest neighbour. However the present analysis
uses an iterative method to determine the centre of mass of
the test galaxy (see Dekel et al. , 1980).

At each time interval during the course of an
encounter, the centre of mass (CM) of N particles is computed.
The energy of each particle

$$U_i = 0.5 \, m_i v_i^2 + \sum_{j \neq i} \phi_{ij} \qquad (2)$$

is computed with respect to this CM. All particles with
positive energy, i. e., $U_i > 0$ relative to this CM are
identified as escapers and the CM of the remaining bound
particles ($U_i < 0$) is evaluated. This procedure is continued
till the number of escapers becomes zero. The iterative
process generally converges in three or four passes. The CM of
the final bound system is chosen as the true centre of test
system. The X-Y plane corresponding to this CM coincides
fairly well with the orbital plane of the galaxy pair. The
positions and velocities of all the particles in the test

57

galaxy are computed with respect to this CM and particles with $U_i > 0$ are identified as escapers and their number noted. The total energy U, magnitude of the angular momentum J, and other relevant quantities are computed with respect to this new CM. The corresponding values for the bound system U_B and J_B are also obtained after removing the escapers. The values of these quantities at the end of the simulations are given in table 4.

16. General features

The structural changes produced in the test galaxy due to the passage of a perturber are displayed in figures 12-39. These figures represent the projections of the particles on the X-Y plane at various time intervals for all the models. The test galaxy becomes flattened and its major axis become elongated in models where the disruptive effects are significant. This can be seen in figures 12, 13, 19 - 21, and 25 - 28. Disrupted galaxies appear amorphous with no well-defined centre. In non-disrupting models, there is less flattening. Elongation of the major axis is evident in figures 15, 22 - 24, 29 - 33, and 37 - 39. In these figures we can identify a compact central region surrounded by a spray of particles. In each of these figures, the third one in the upper panel generally represents the configuration near the closest approach time. Tidal damage is seen to occur after the perturber has passed the closest approach point.

Table 4. N-body simulation results for various models

Model	$\Delta u/|u|$	$\Delta u_B/|u_B|$	$\Delta M/M$	$\dfrac{J_T}{J_{orb}}$	$\dfrac{J_B}{J_{orb}}$
H1	2.080	0.716	0.420	0.001	3.69E-4
H2	1.260	0.576	0.316	0.001	5.83E-4
H3	0.986	0.450	0.260	0.011	4.33E-4
H4	0.514	0.265	0.148	0.011	9.54E-4
P1	6.203	0.956	0.812	0.106	1.96E-4
P2	5.357	0.771	0.548	0.160	2.16E-4
P3	4.100	0.594	0.388	0.205	7.12E-4
P4	2.297	0.403	0.272	0.142	9.43E-4
P5	0.970	0.209	0.124	0.115	1.09E-3
P6	0.449	0.131	0.068	0.058	2.64E-3
P7	0.066	0.037	0.024	0.014	1.05E-3
P8	0.051	0.024	0.008	0.024	2.32E-3
P10	0.003	0.003	0.000	0.003	2.86E-3
E1	14.095		1.000		
E2	13.222		1.000		
E3	10.236		1.000		
E4	8.711	0.514	0.396	0.582	7.48E-4
E5	3.774	0.290	0.236	0.381	1.08E-3
E6a	1.035	0.168	0.140	0.205	1.13E-3
E6b	1.754	0.227	0.196	0.419	1.30E-3
E7a	0.396	0.089	0.076	0.122	1.66E-3
E7b	0.838	0.152	0.156	0.363	8.68E-4
ESa	0.248	0.111	0.080	0.239	8.01E-3
ESb	0.574	0.185	0.188	0.582	3.33E-3
E8	0.167	0.059	0.044	0.060	5.02E-3
E10	0.026	0.018	0.016	0.070	9.53E-3
C6	11.470		1.000		
C7	1.610	0.196	0.172	0.297	2.36E-3
C8a	0.553	0.093	0.084	0.163	5.44E-3
C8b	0.539	0.159	0.128	0.199	1.91E-3
C10a	0.032	0.024	0.016	0.029	7.41E-3
C10b	0.062	0.050	0.036	0.087	0.011
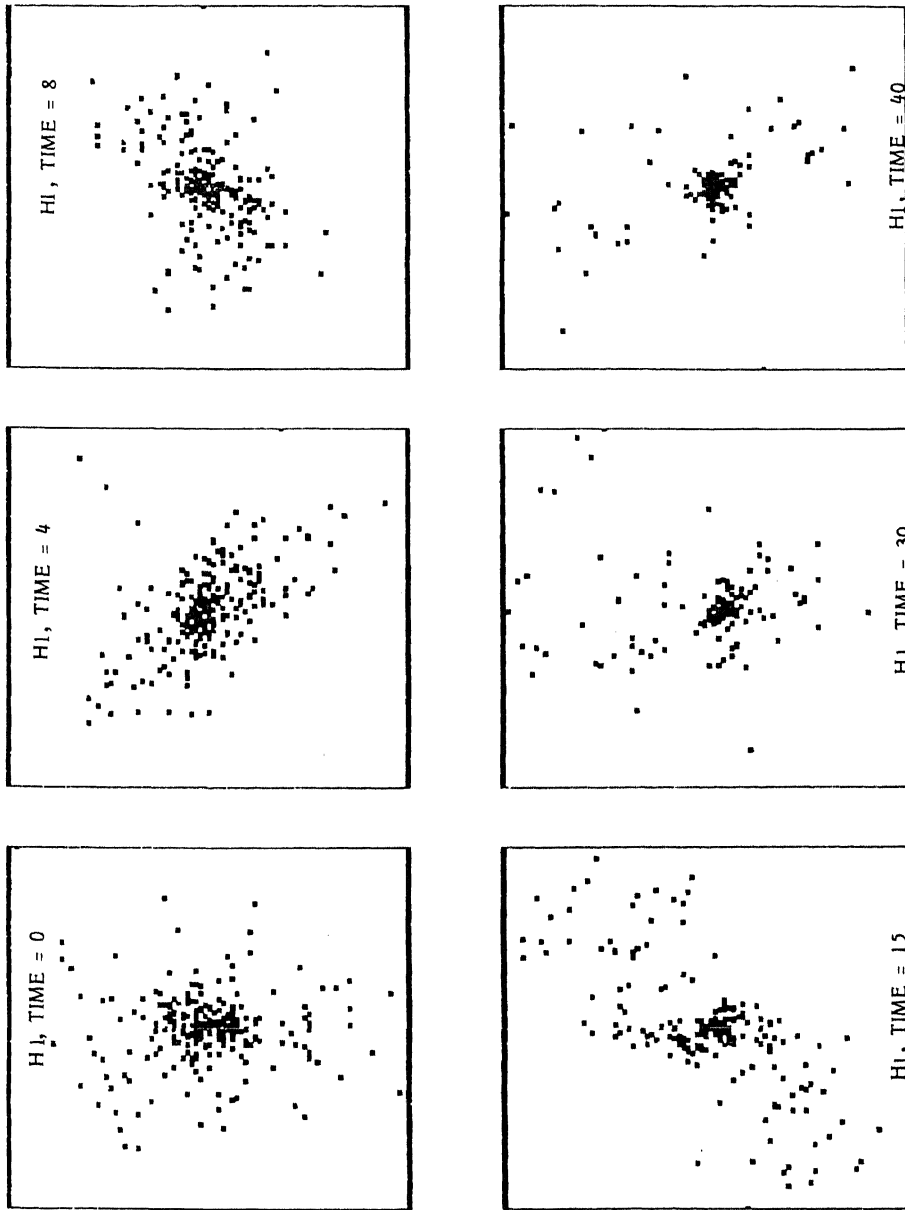
Figure 12. Projections of the particles of the 'hyperbolic model H1 on to the X-Y plane at six different times during the course of the encounter. The two galaxies are orbiting in a counter clock clockwise direction. The third figure in the upper panel gives the configuration near the closest distance. The rotation of the major axis can be seen at time = 4.

60
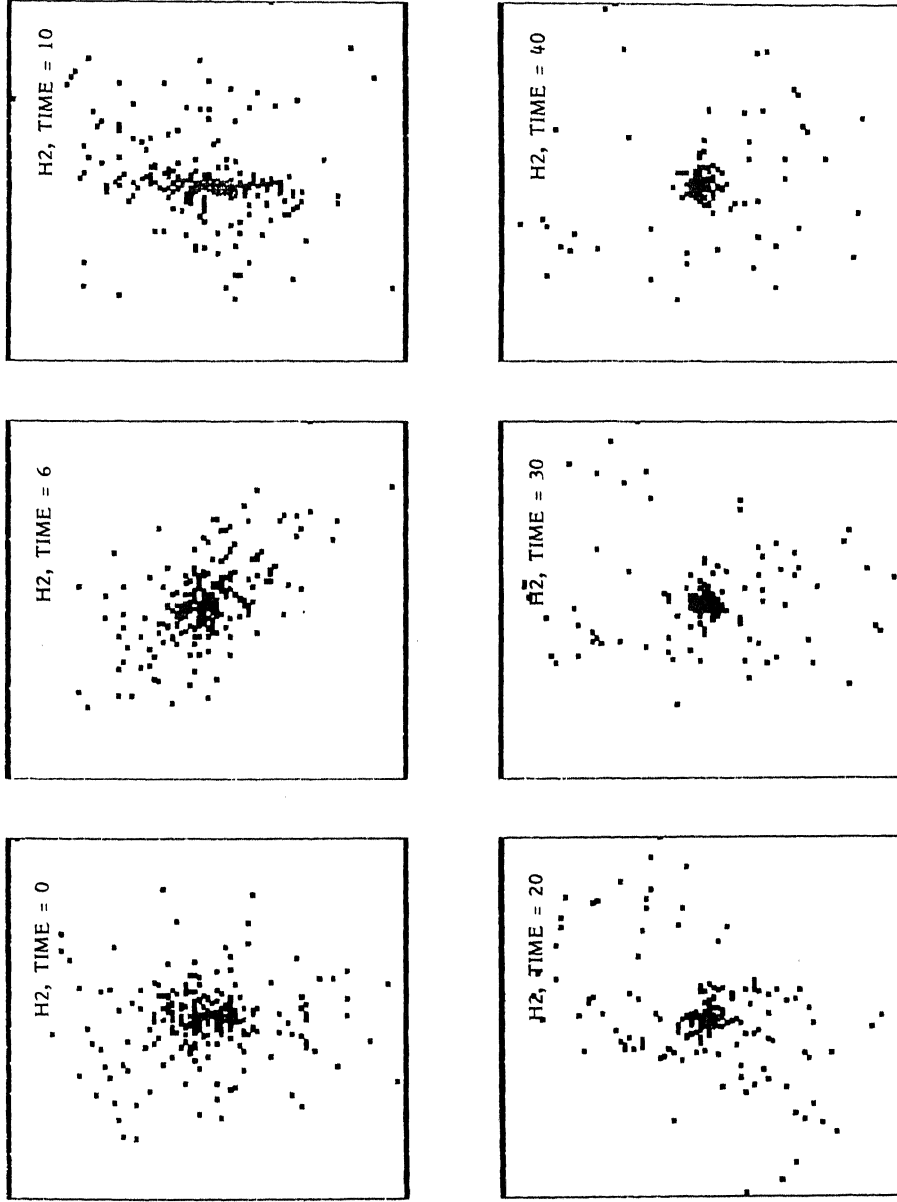
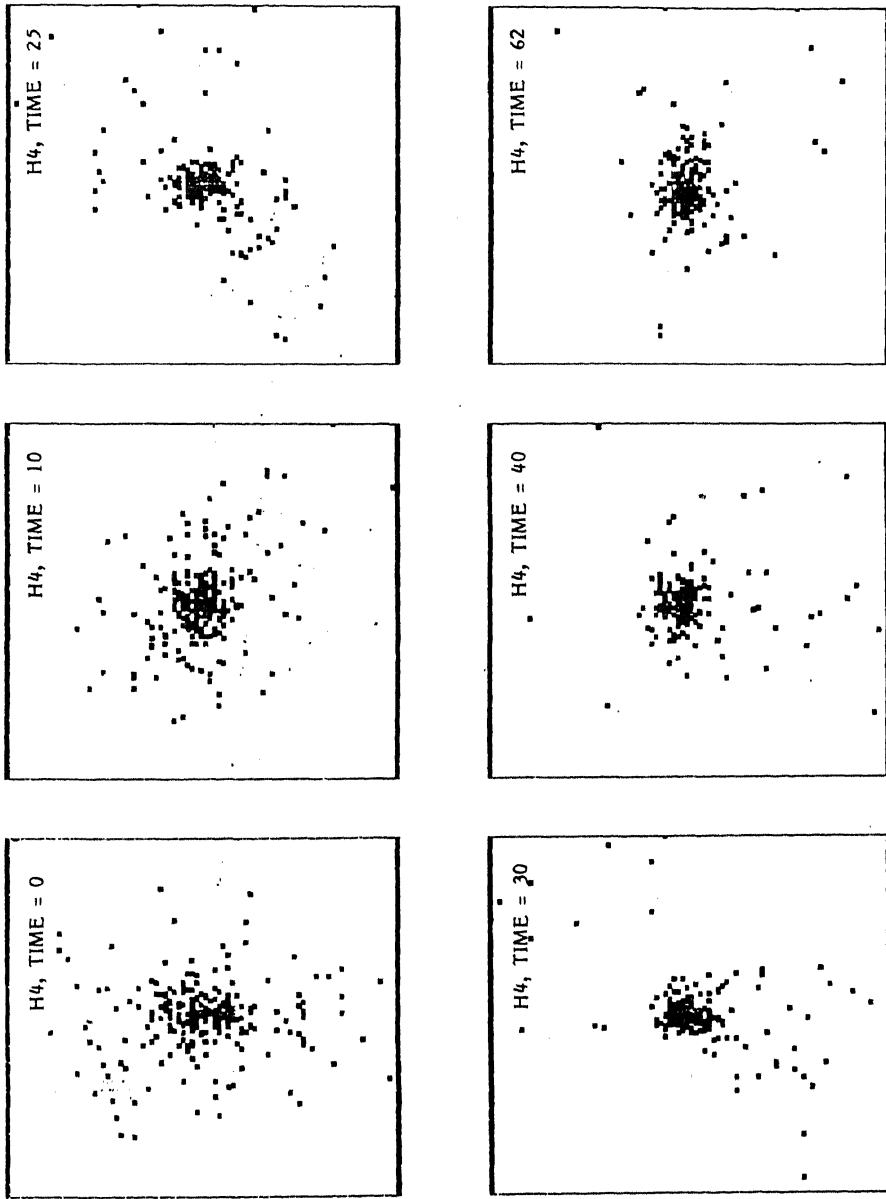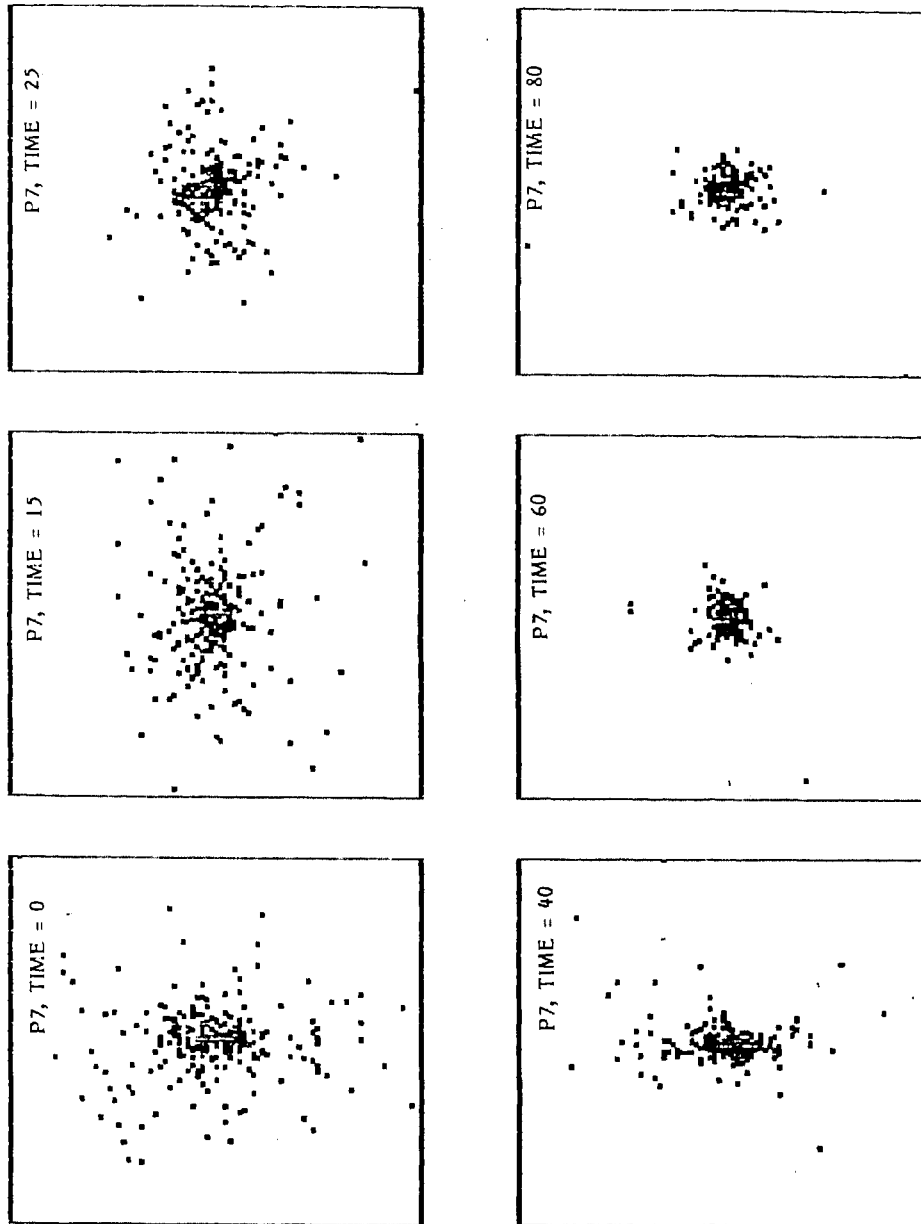Figure 13. Same as figure 12, but for model H2. The rotation of the major axis can be seen at time = 6.

61
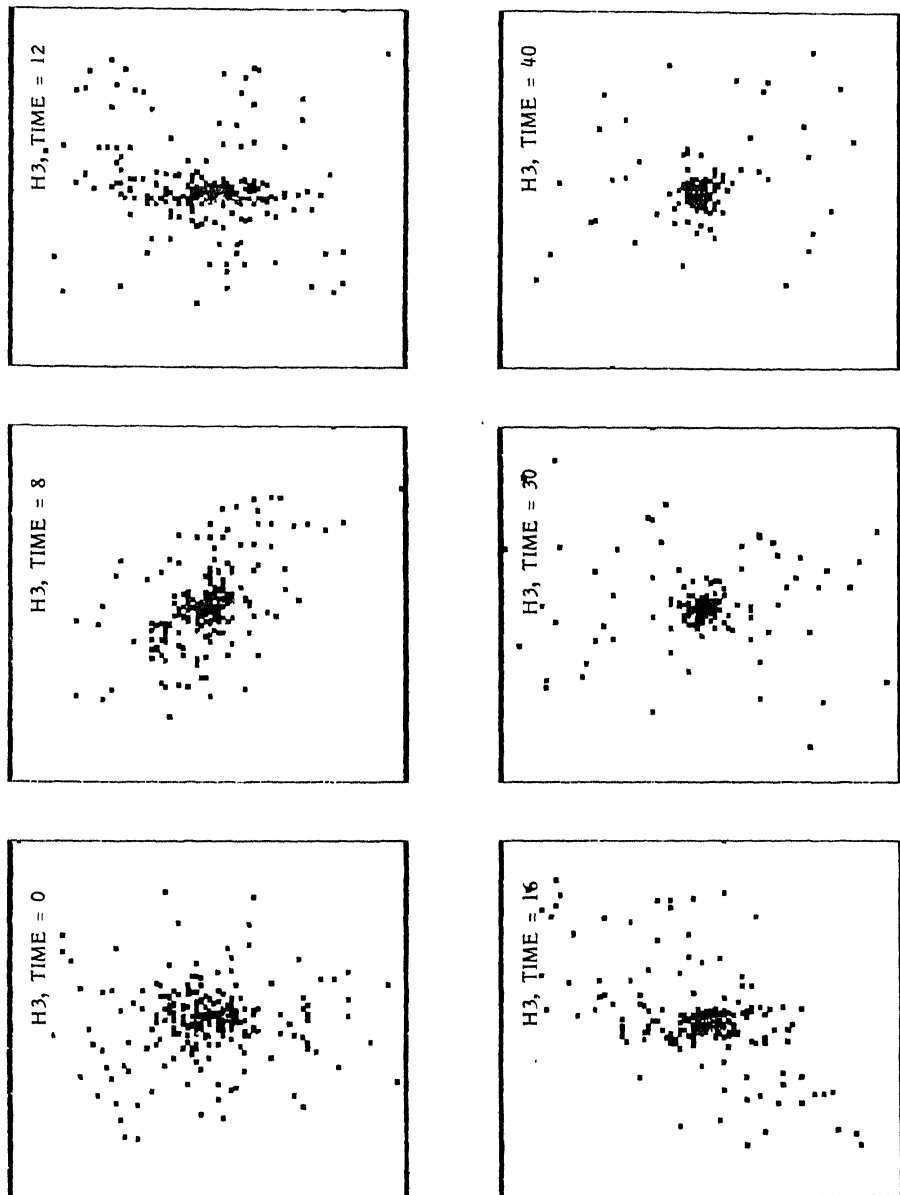
Figure 14. Same as figure 12, but for model H3. The rotation of the major axis can be seen at time = 8.
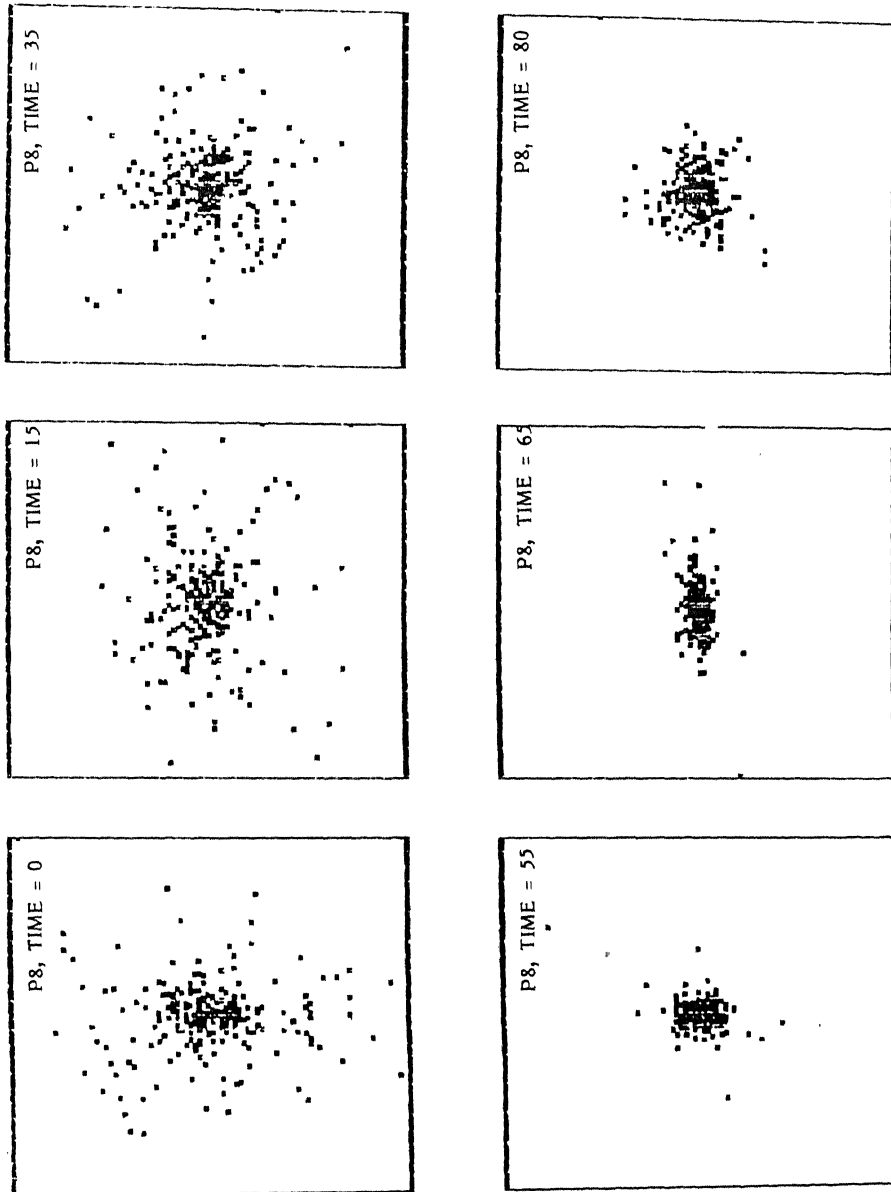
Figure 15. Same as figure 12, but for model H4.
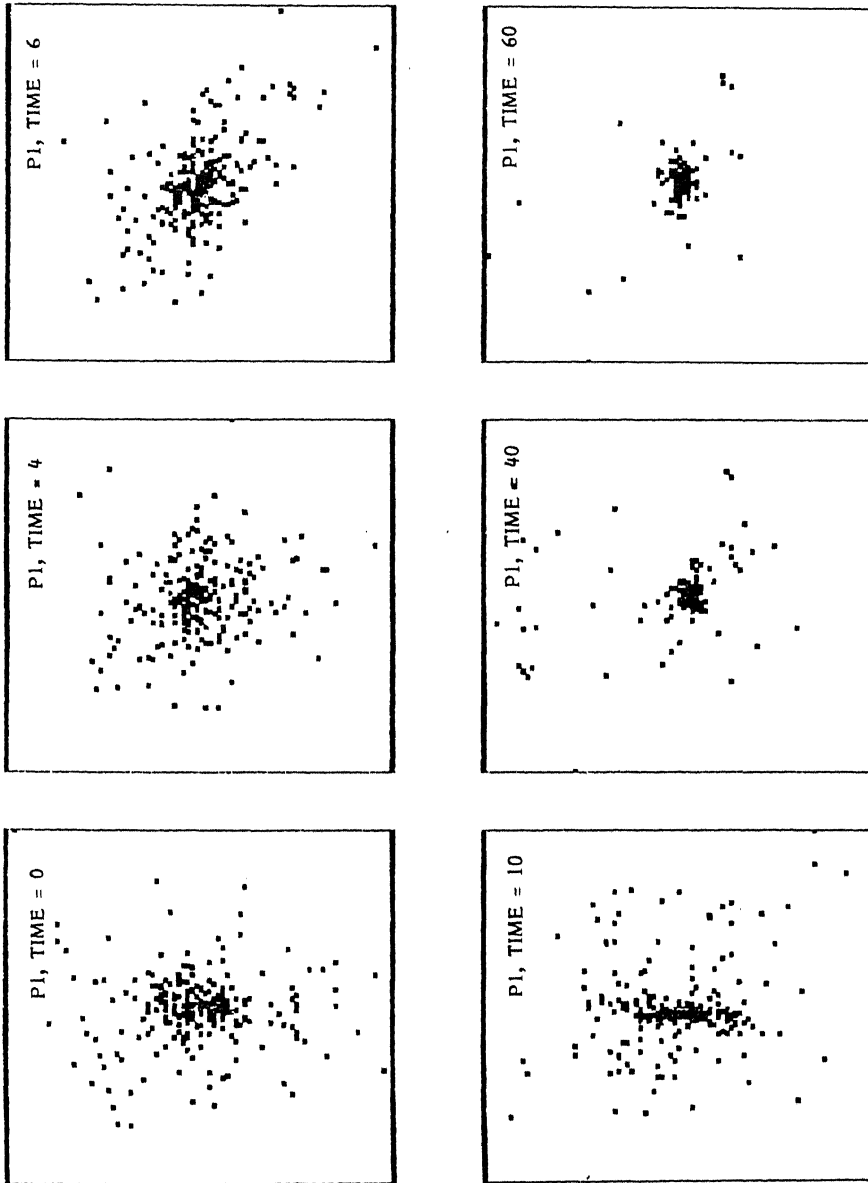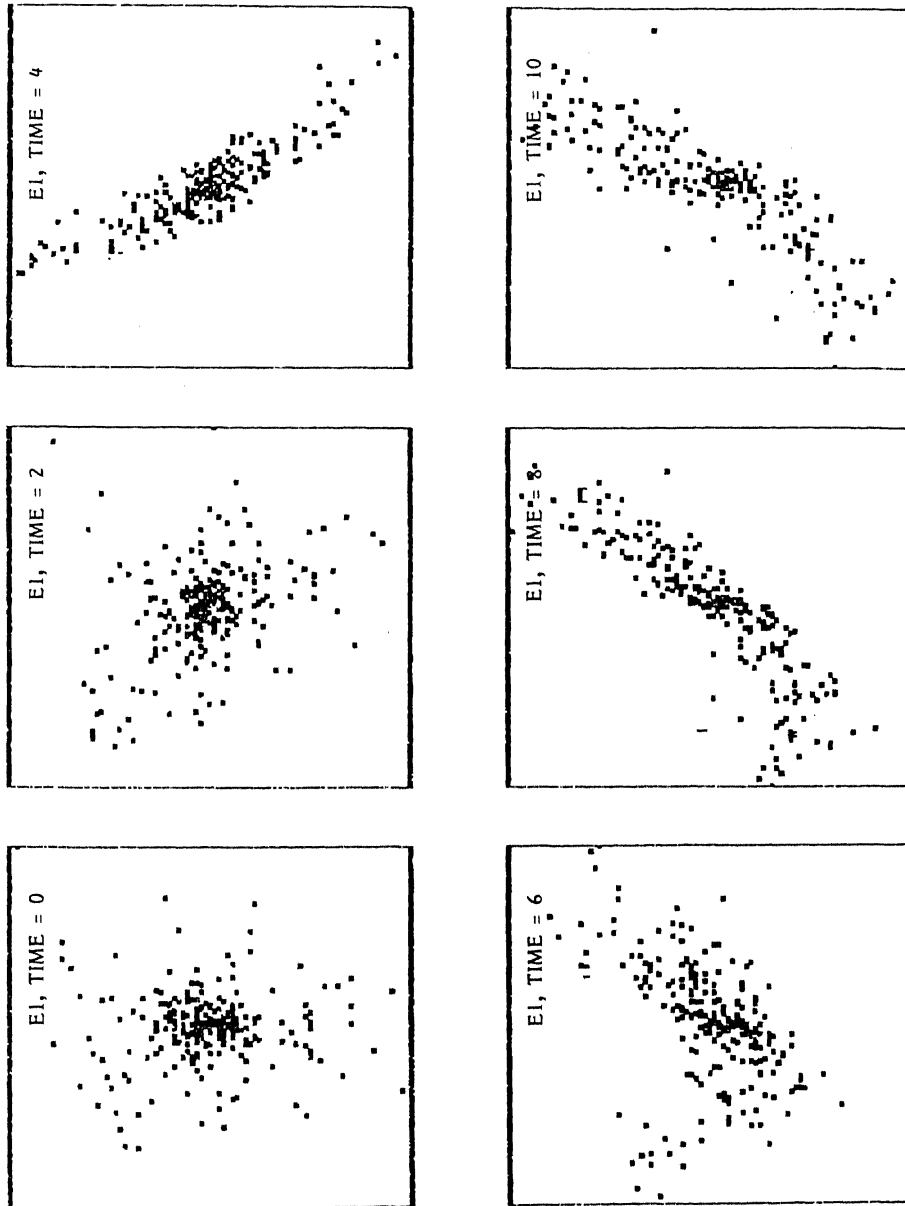
Figure 16. Same as figure 12, but for 'parabolic' model P1.

P2, TIME = 10

P2, TIME = 48

P2, TIME = 6

P2, TIME = 28

P2, TIME = 0

P2, TIME = 16
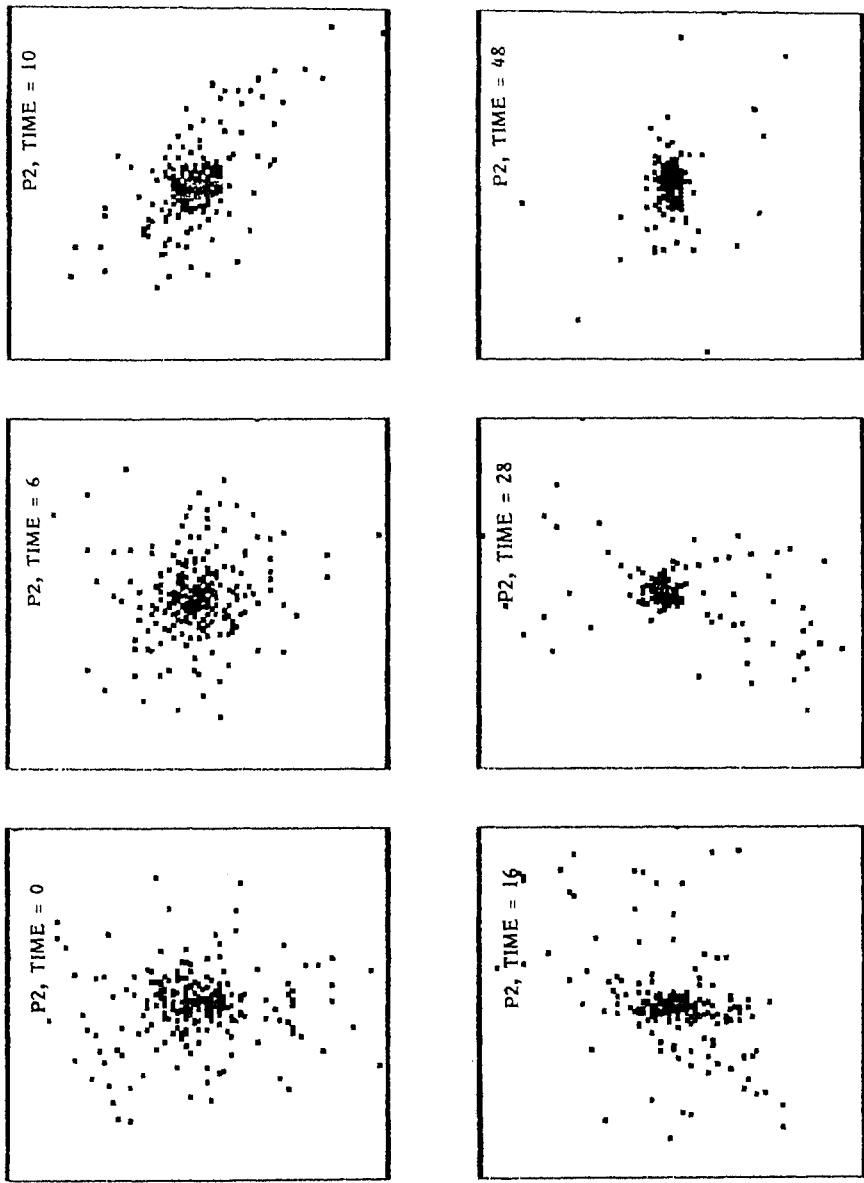
Figure 17. Same as figure 12, but for model P2.

65

P3, TIME = 0

P3, TIME = 6

P3, TIME = 8

P3, TIME = 22

P3, TIME = 36

P3, TIME = 66
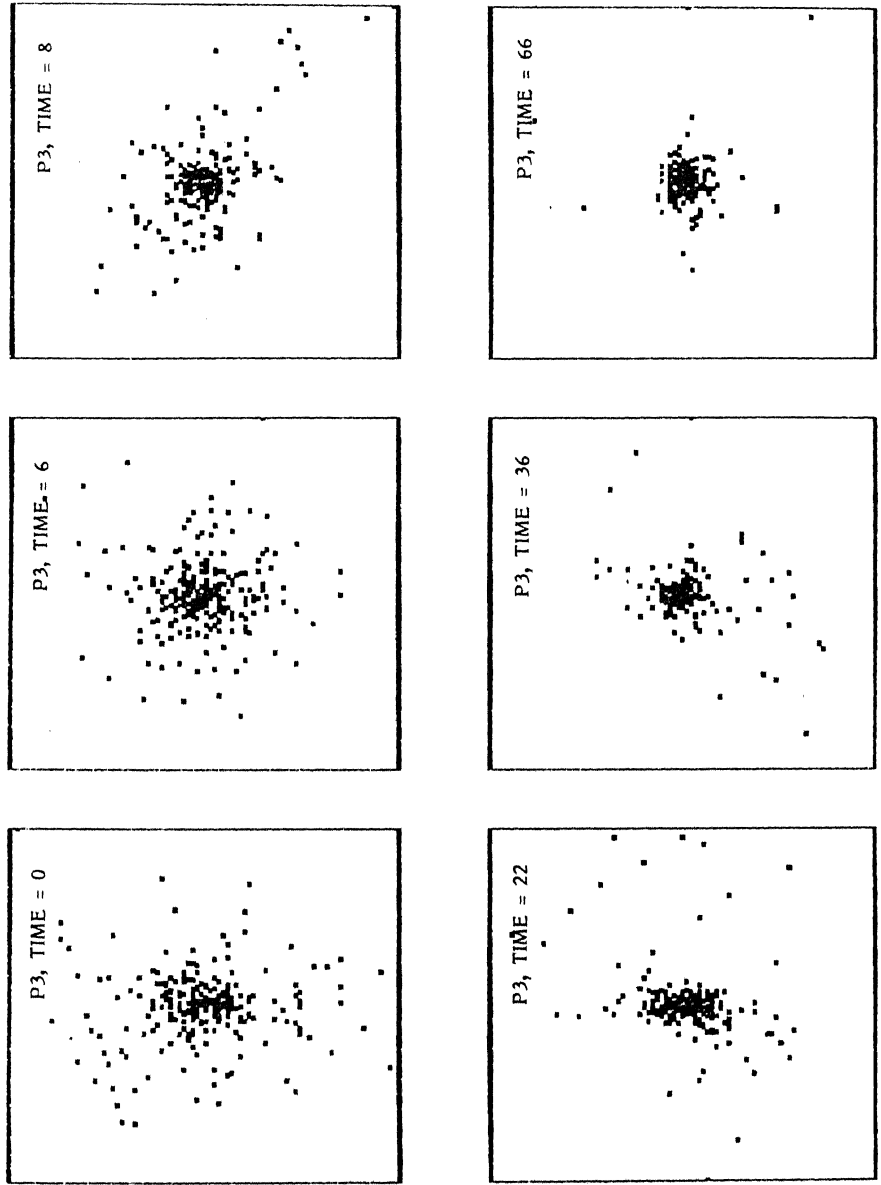
Figure 18. Same as figure 12, but for model P3.

P4, TIME = 18

P4, TIME = 10

P4, TIME = 0

P4, TIME = 66

P4, TIME = 36

P4, TIME = 30
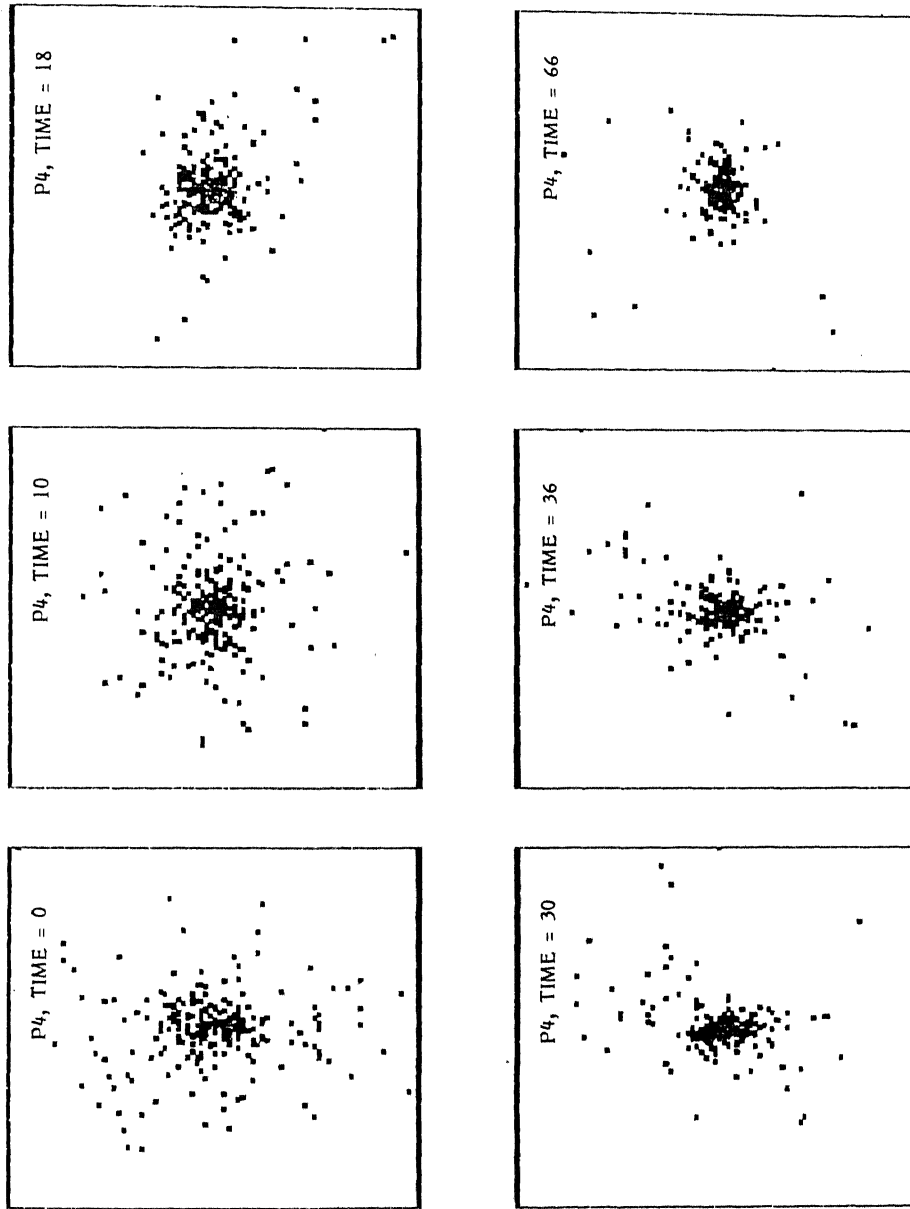
Figure 19. Same as figure 12, but for model P4.

67
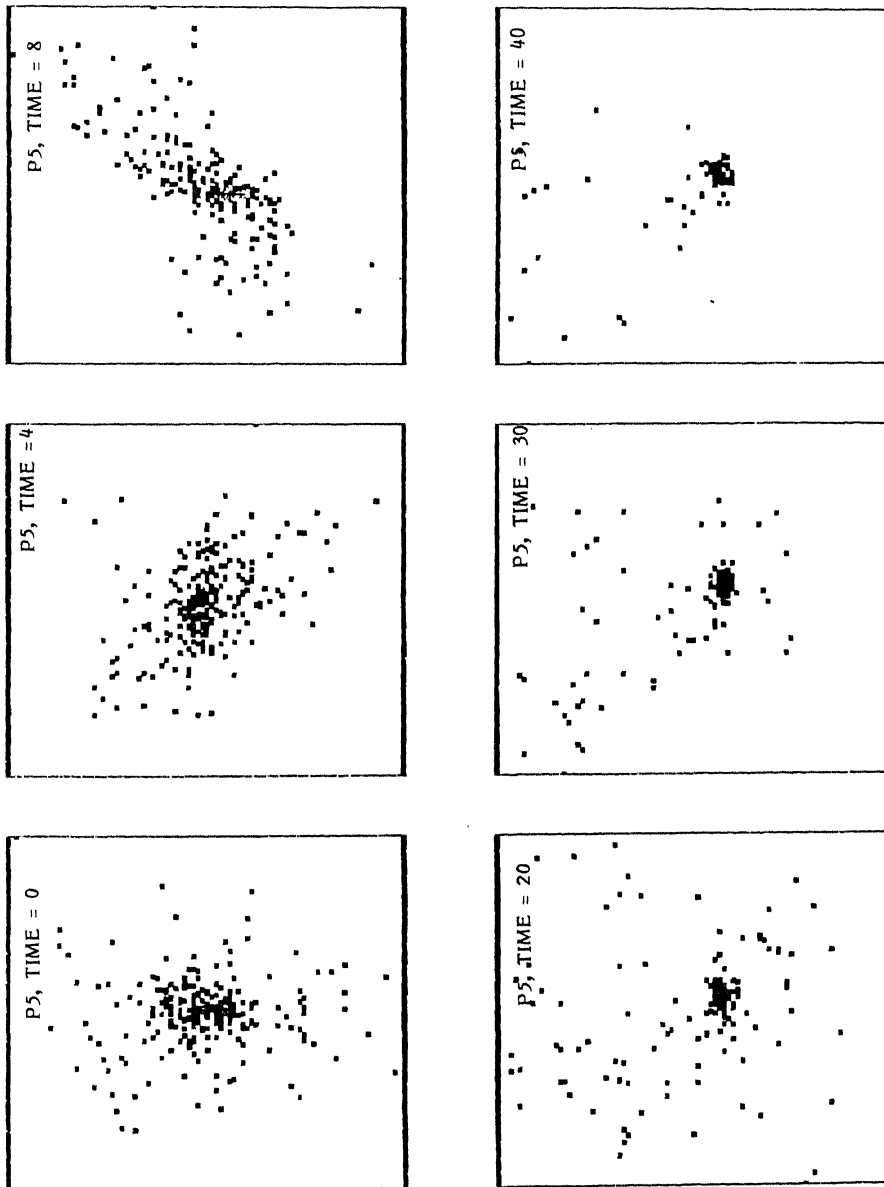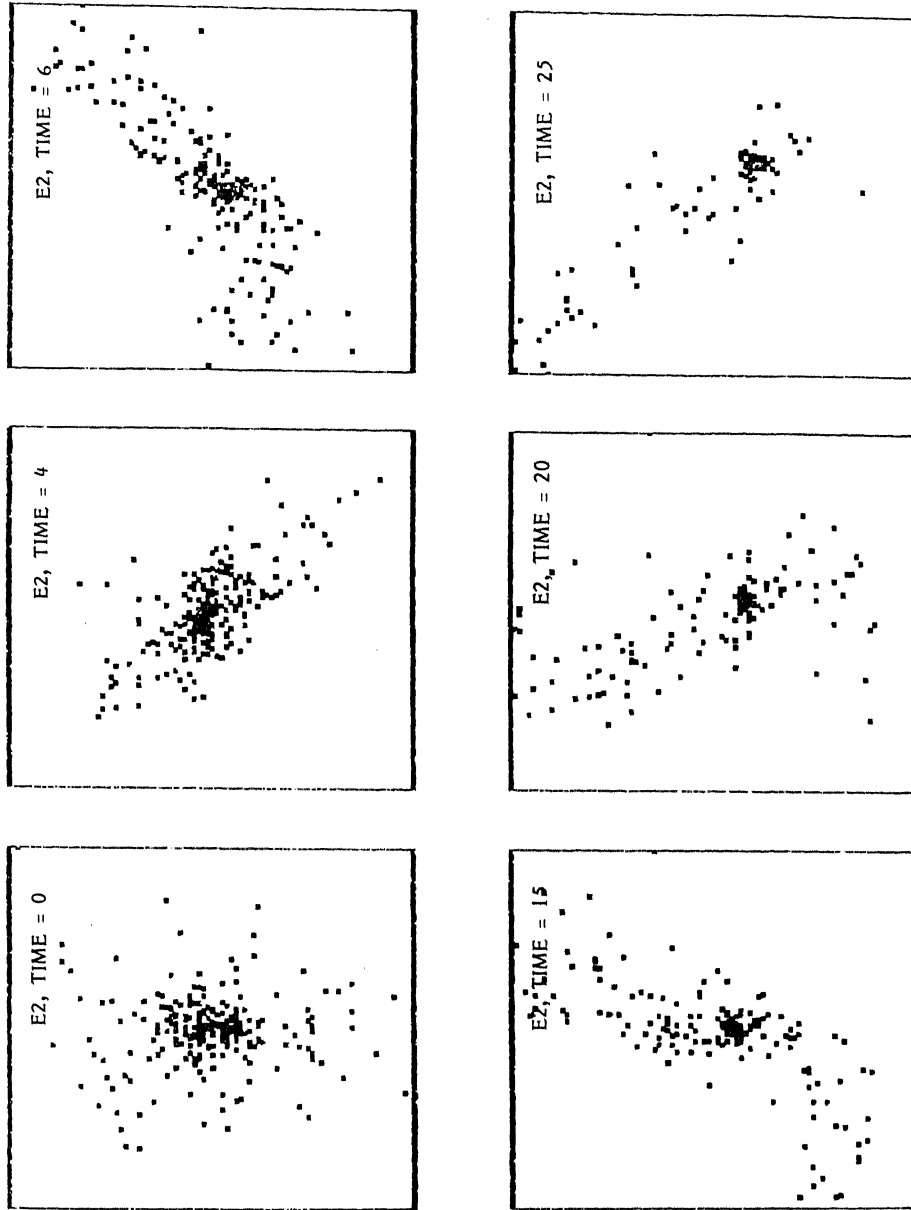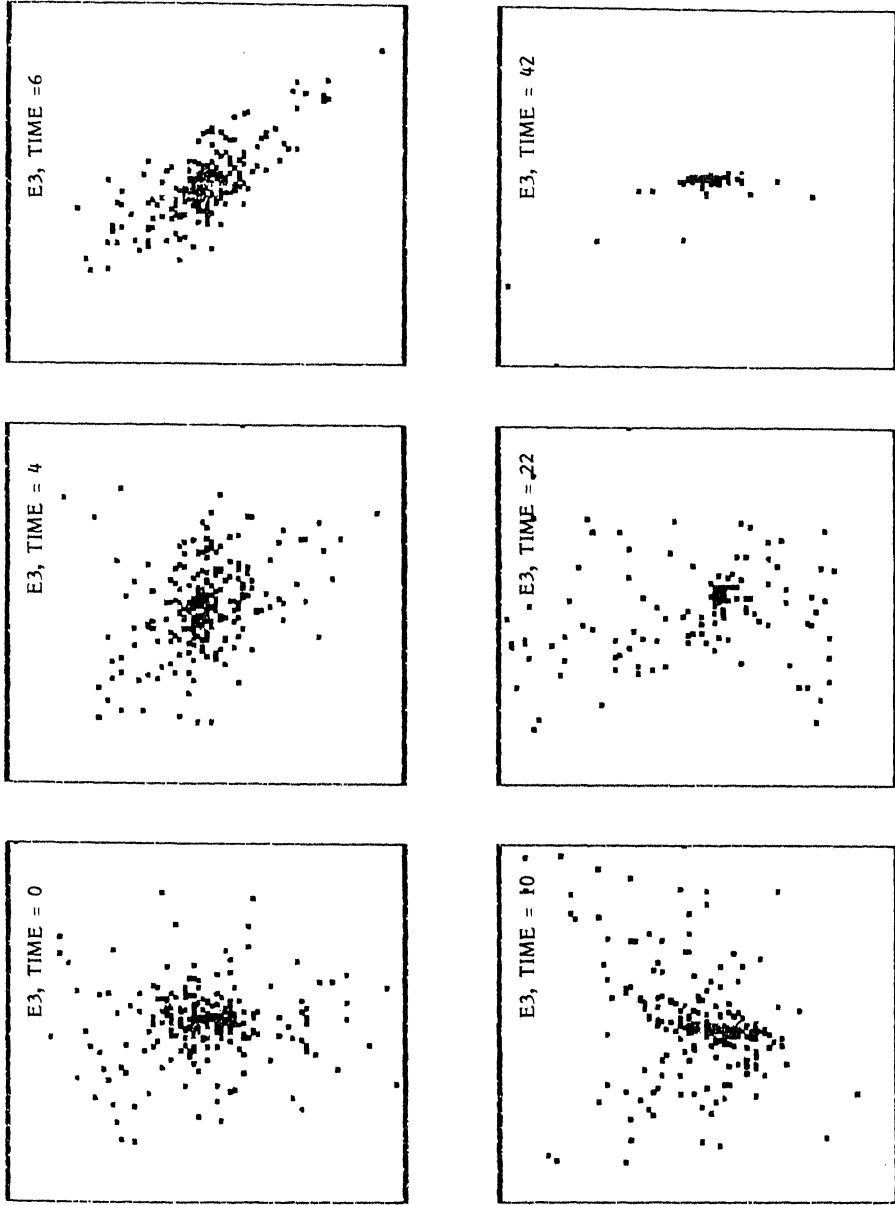
Figure 20. Same as figure 12, but for model P5. The rotation of the major axis can be seen at times 4 and 8.
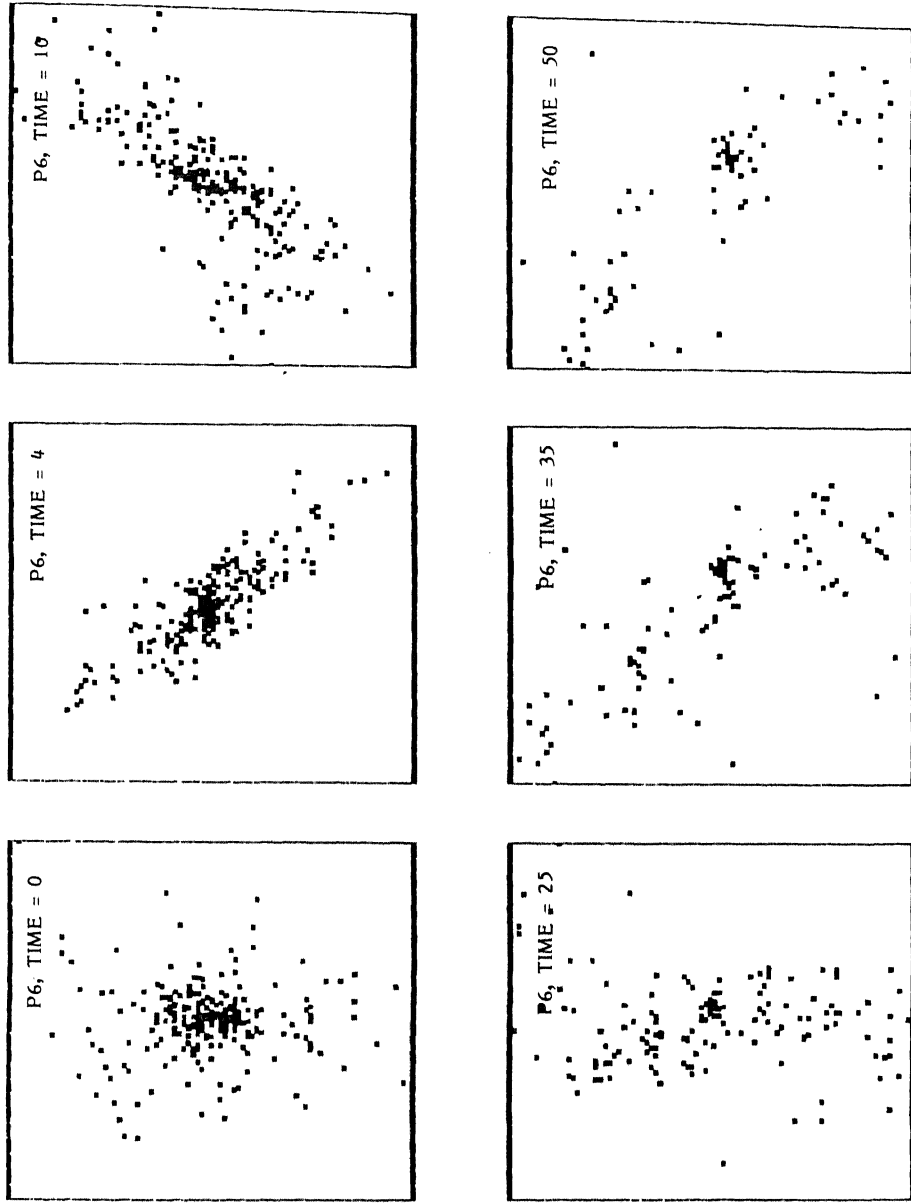
Figure 21. Same as figure 12, but for model P6. The rotation of the axis can be seen at times 4,10,25,35 and 50.

Figure 22. Same as figure 12, but for model P7.

P8, TIME = 35

P8, TIME = 80

P8, TIME = 15

P8, TIME = 65

P8, TIME = 0

P8, TIME = 55

Figure 23. Same as figure 12, but for model P8.

P10, TIME = 60

P10, TIME = 140

P10, TIME = 30

P10, TIME = 120

P10, TIME = 0

P10, TIME = 90
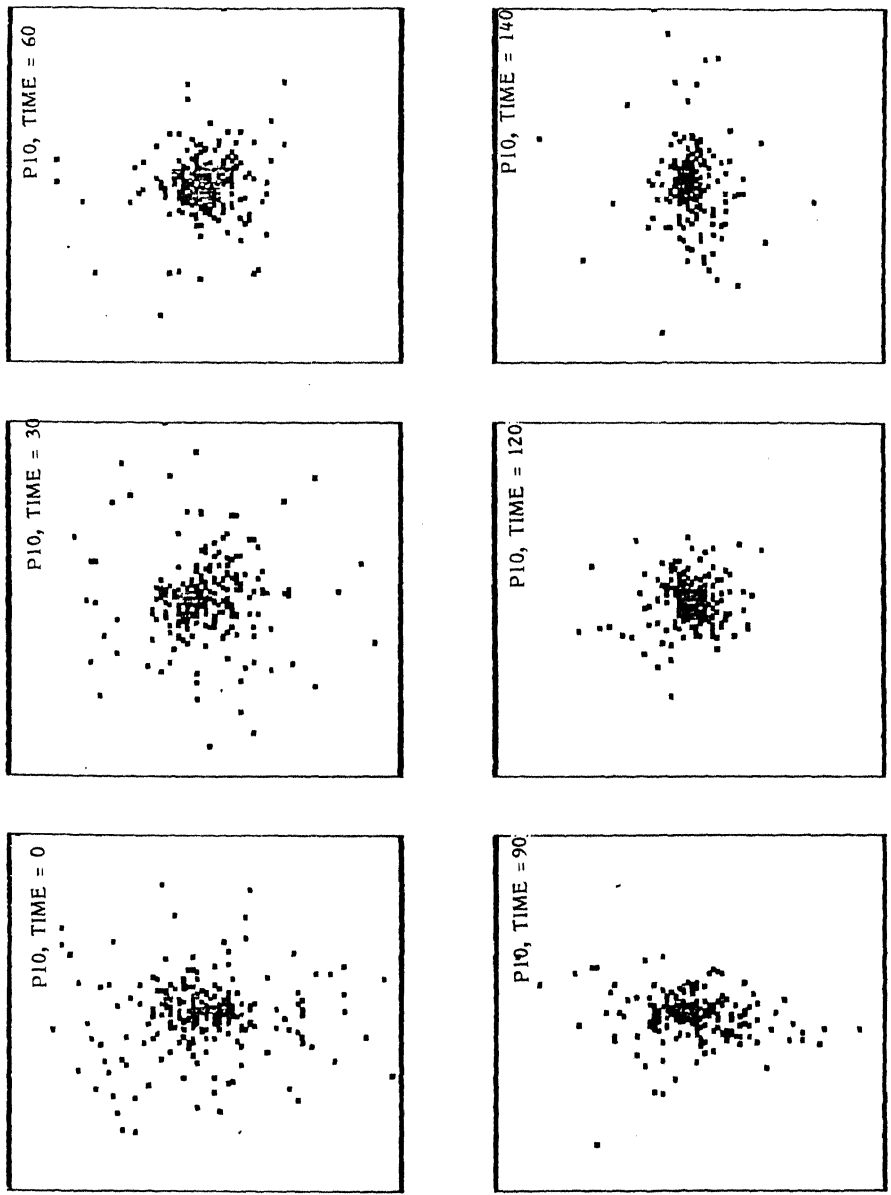
Figure 24. Same as figure 12, but for model P10.

72

Figure 25. Same as figure 12, but for 'elliptic' model E1. The rotation of the major axis can be seen at times 4, 6, 8, and 10.

Figure 26. Same as figure 12, but for model E2. The rotation
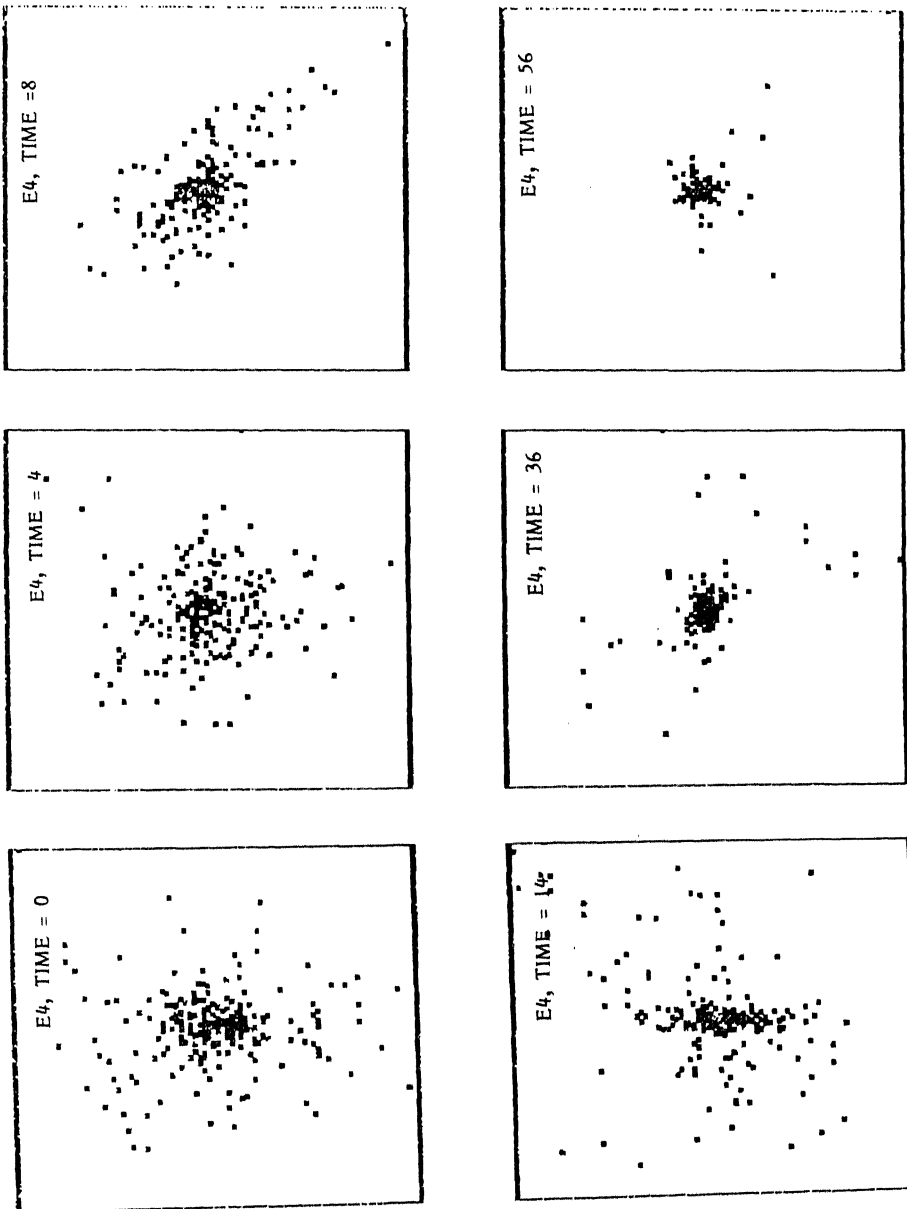of the major axis can be seen at times 4, 6, 15, 20, and 25.

74

E3, TIME =6

E3, TIME = 4

E3, TIME = 0

E3, TIME = 42

E3, TIME =22

E3, TIME = 40

Figure 27. Same as figure 12, but for model E3. The rotation of the major axis can be seen at times 4 and 6.

Figure 28. Same as figure 12, but for model E4. The rotation of the major axis can be seen at time 8.
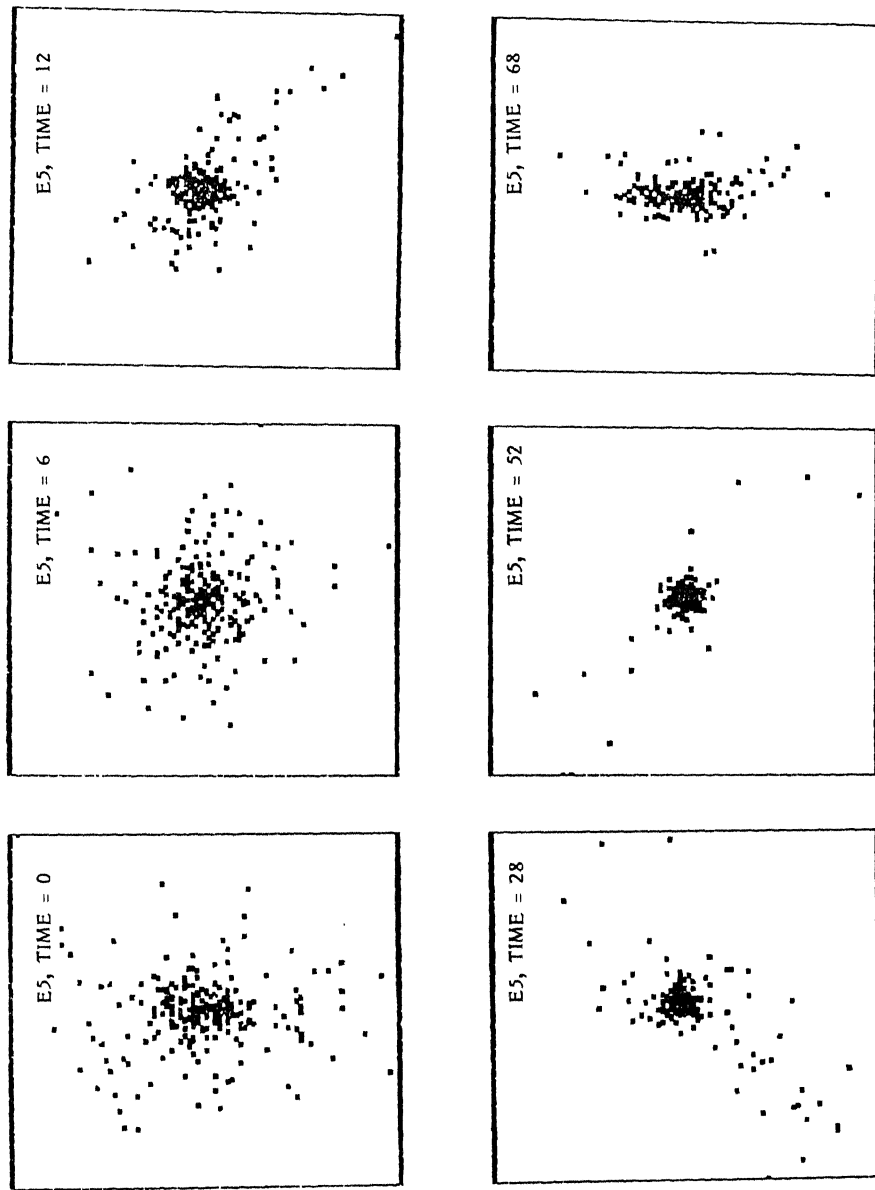
Figure 29. Same as figure 12, but for model E5. Note the formation of spiral structure at time 52.
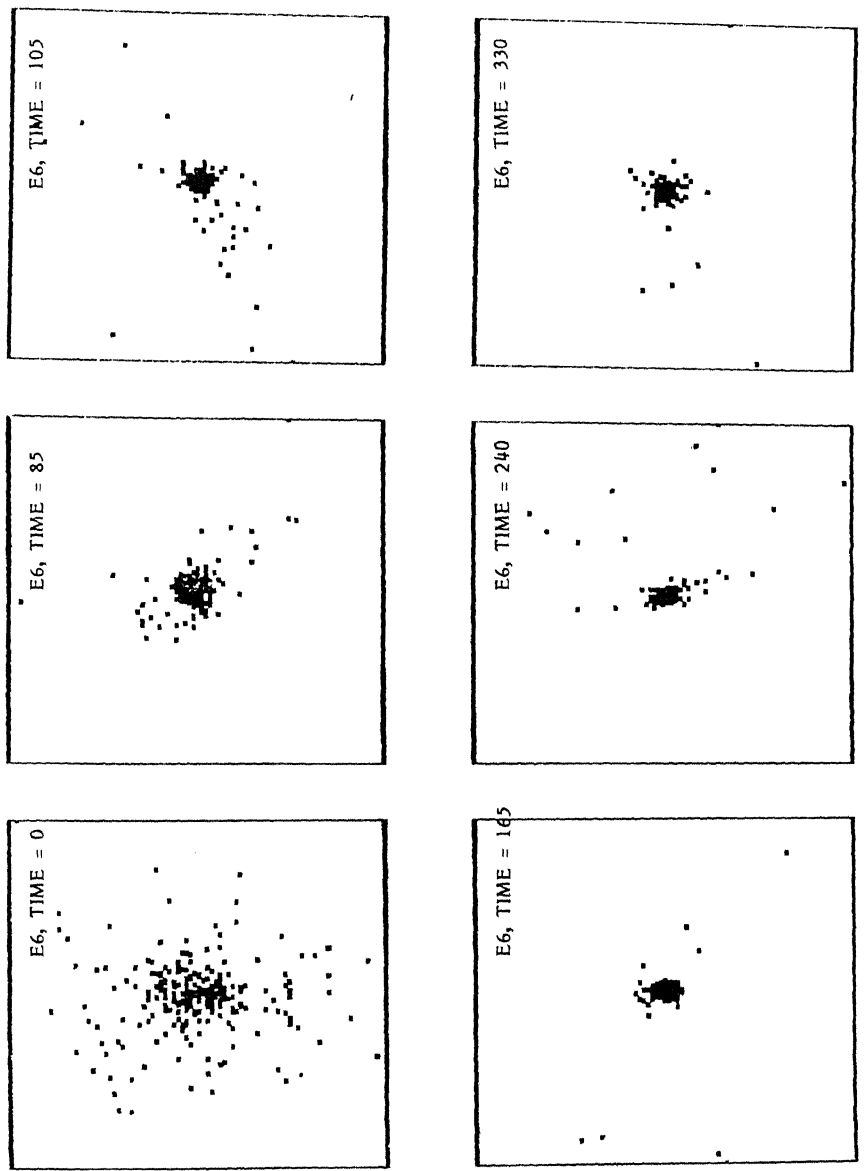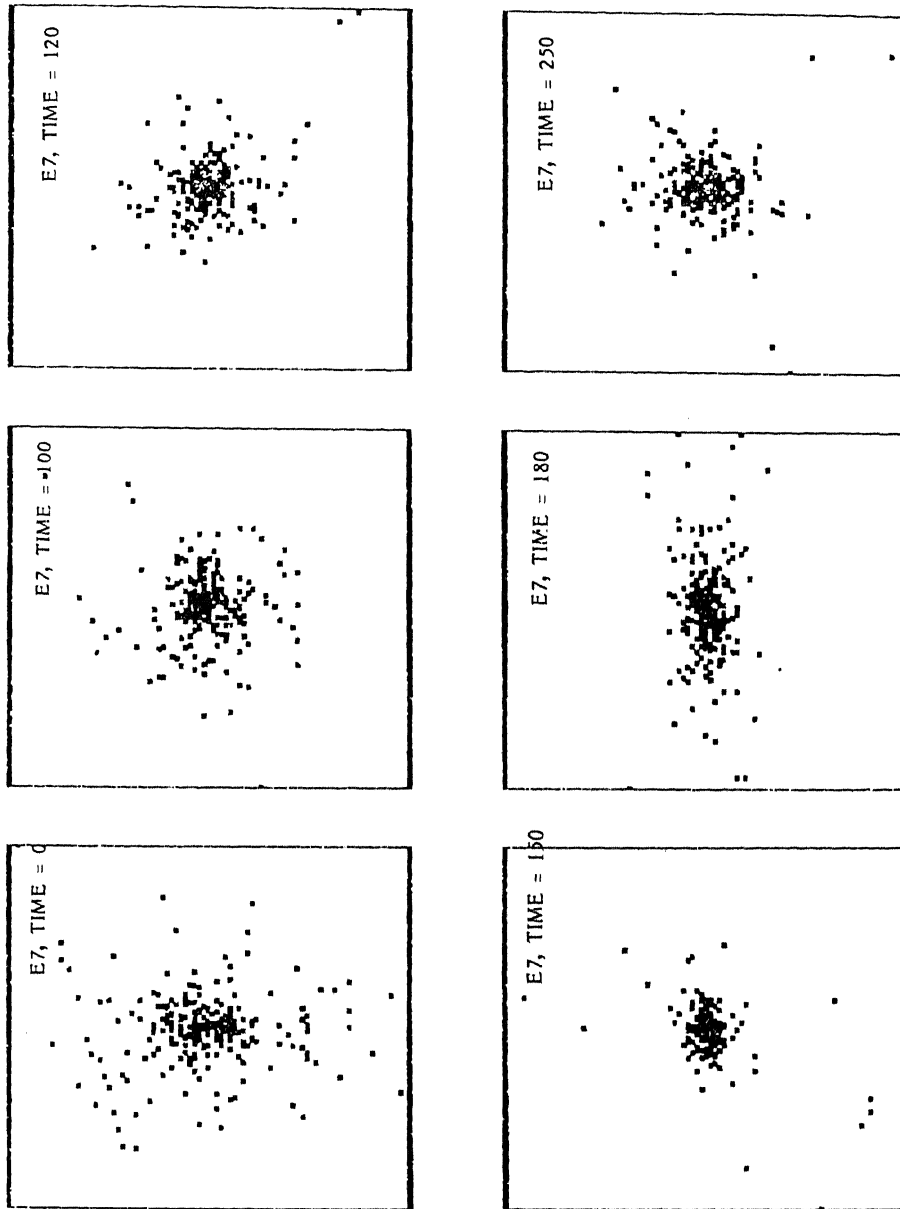
Figure 30. Same as figure 12, but for model E6.

E6, TIME = 105

E6, TIME = 85

E6, TIME = 0

E6, TIME = 330

E6, TIME = 240

E6, TIME = 165

E7, TIME = 120

E7, TIME = 250

E7, TIME = 100

E7, TIME = 180

E7, TIME = 0

E7, TIME = 150

Figure 31. Same as figure 12, but for model E7. Note the elongation in the orbital plane at time 180.
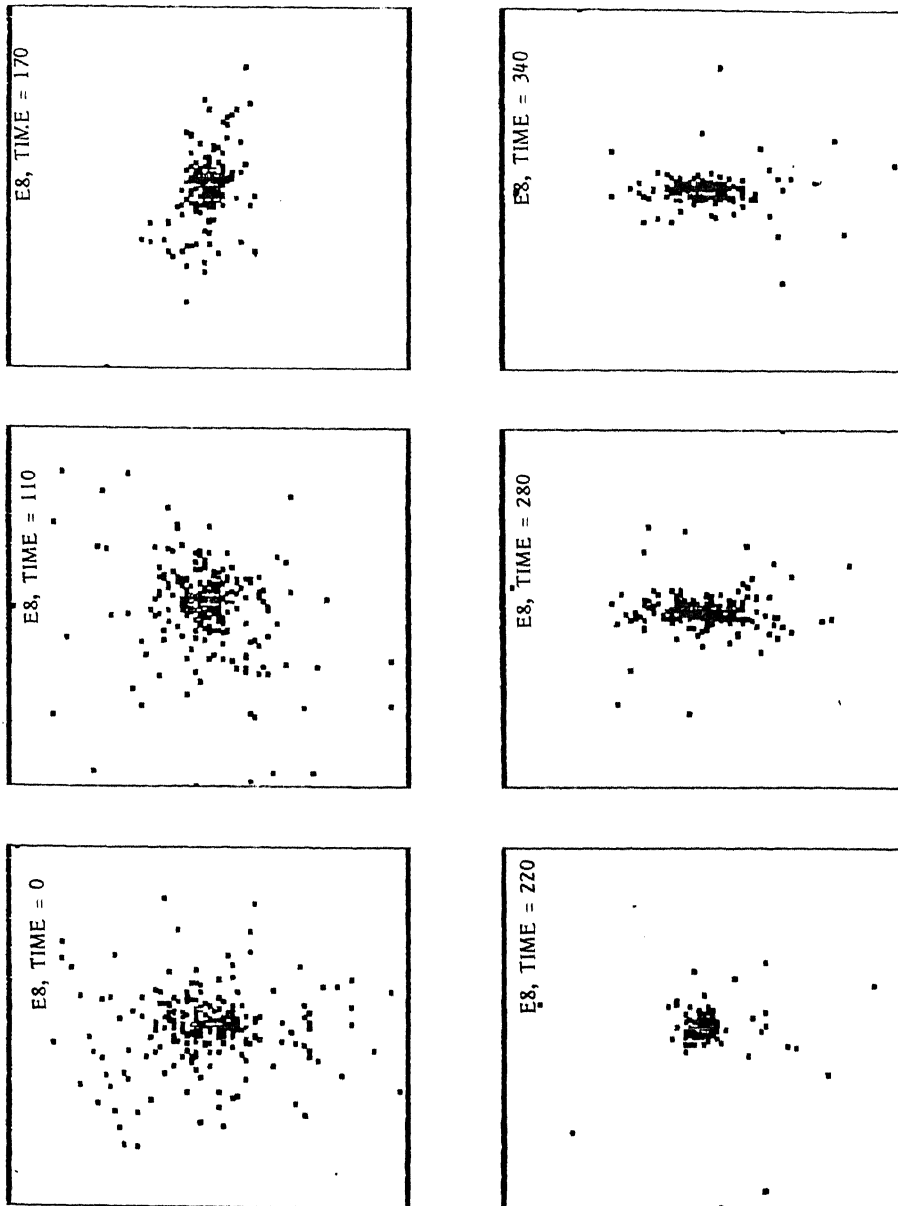
79

Figure 32. Same as figure 12, but for model E8. Note the elongation in the orbital plane at times 280 and 340.
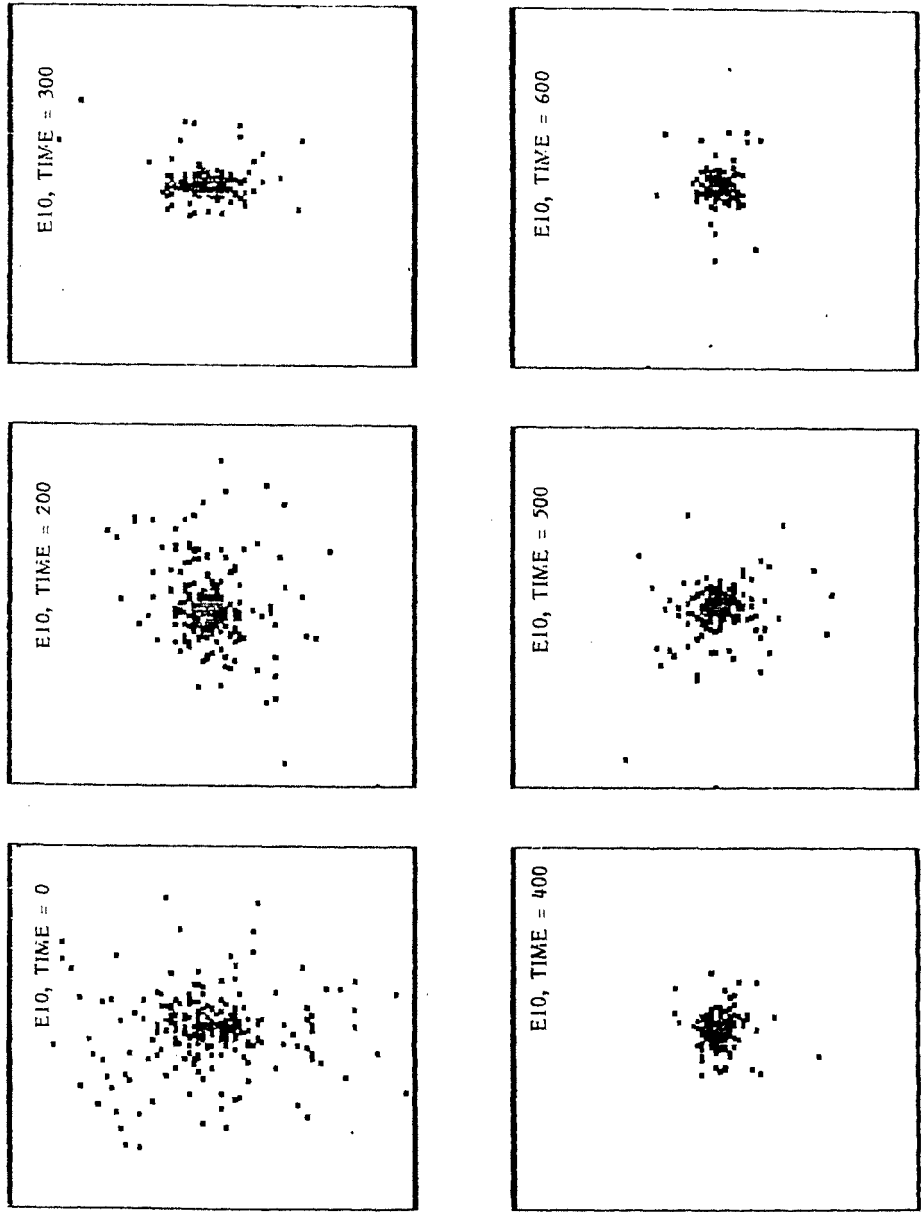
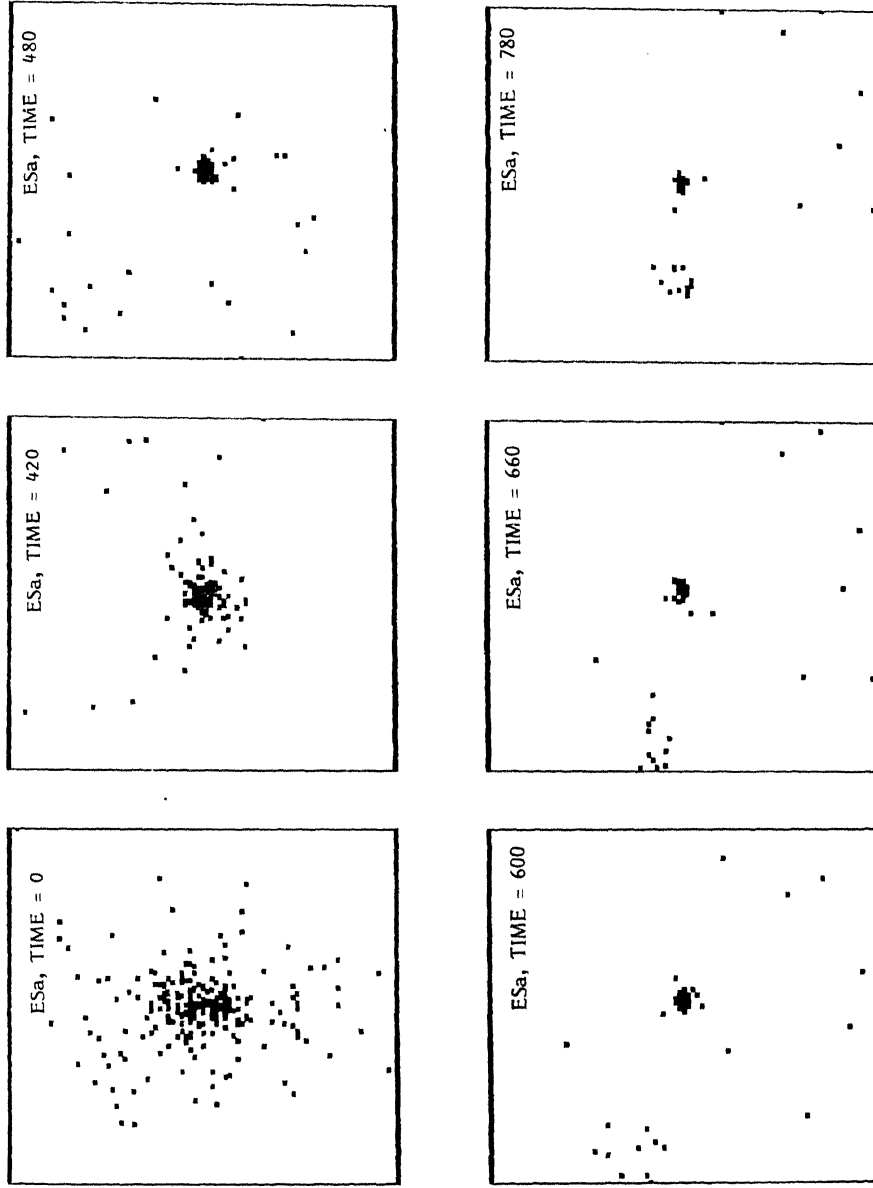Figure 33. Same as figure 12, but for model E10.

81

ESa, TIME = 480

ESa, TIME = 420

ESa, TIME = 0

ESa, TIME = 780

ESa, TIME = 660

ESa, TIME = 600

Figure 34. Same as figure 12, but for model ESa.

ESb, TIME = 1120

ESb, TIME = 1460

ESb, TIME = 1080

ESb, TIME = 1240

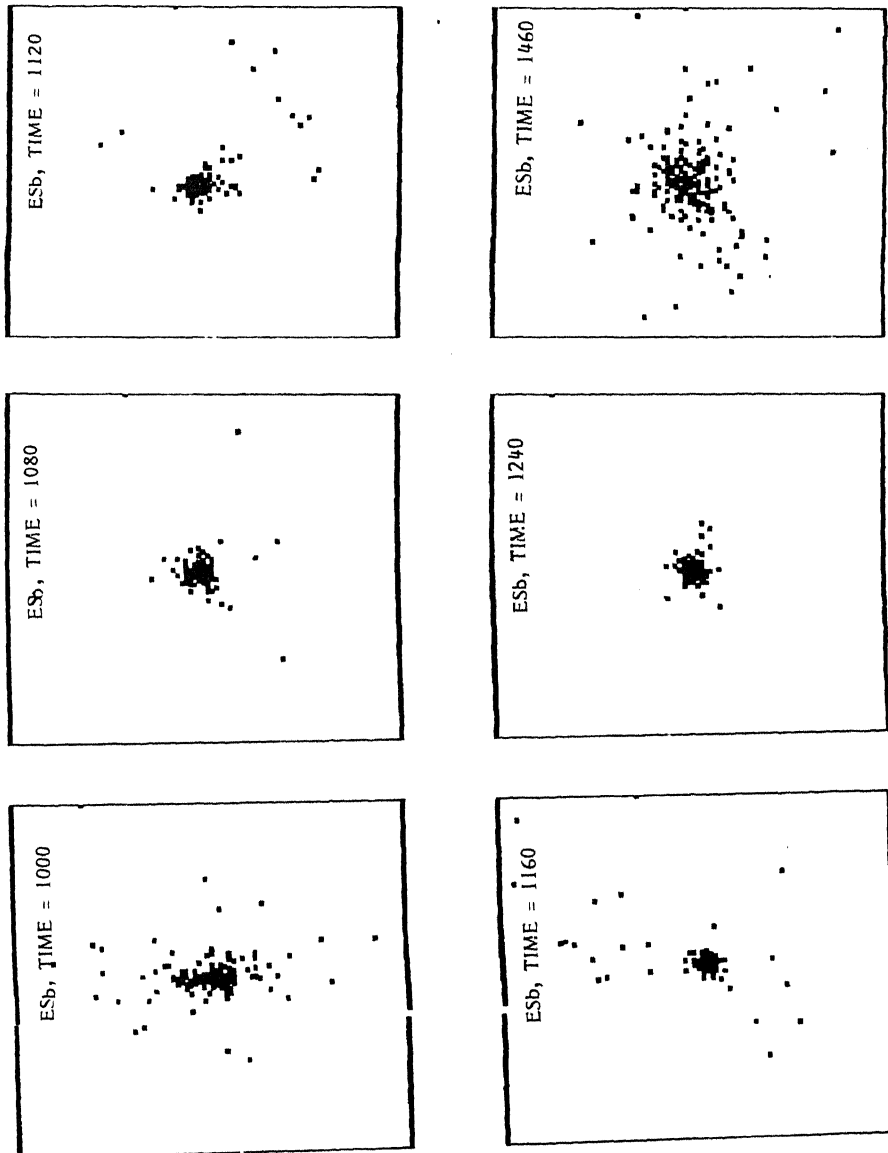ESb, TIME = 1000

ESb, TIME = 1160

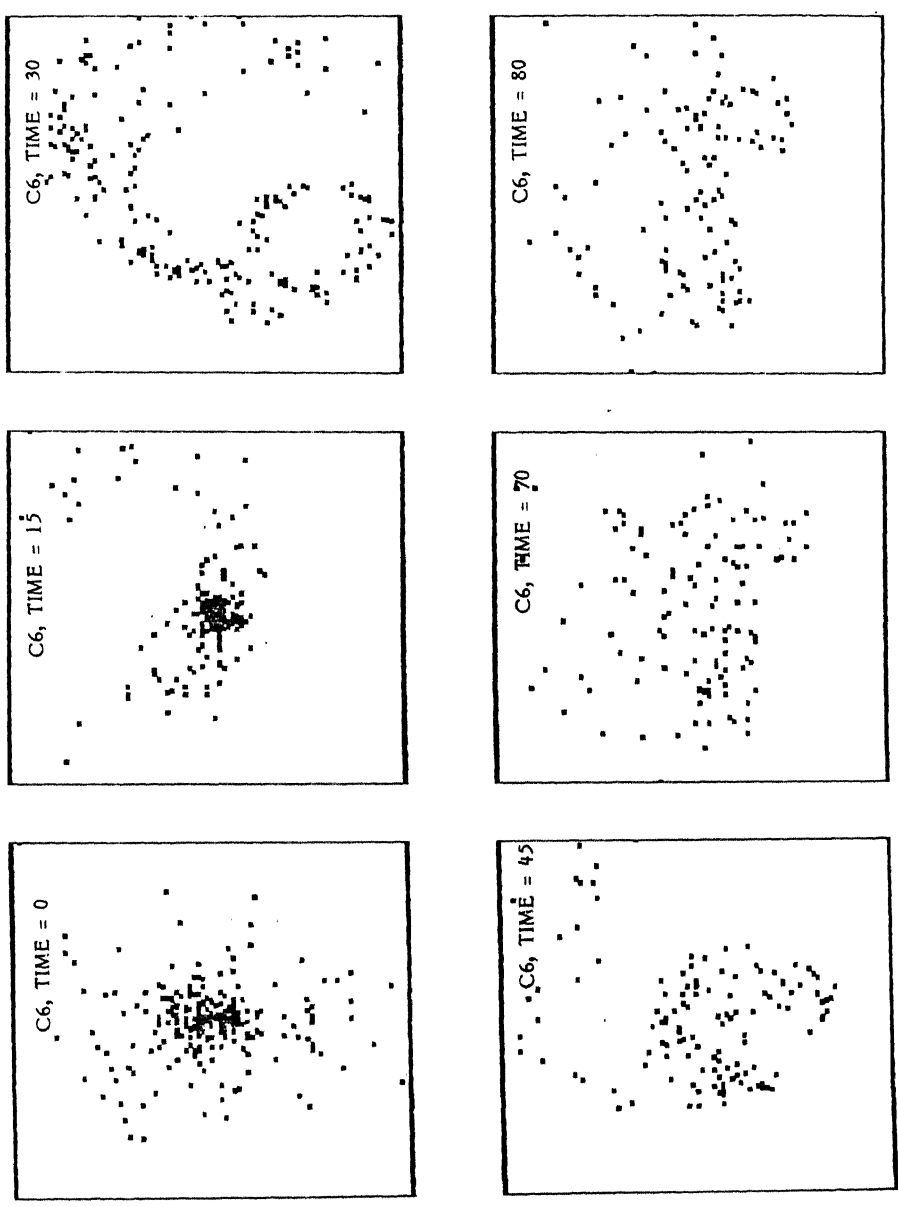Figure 35. Same as figure 12, but for model ESb.

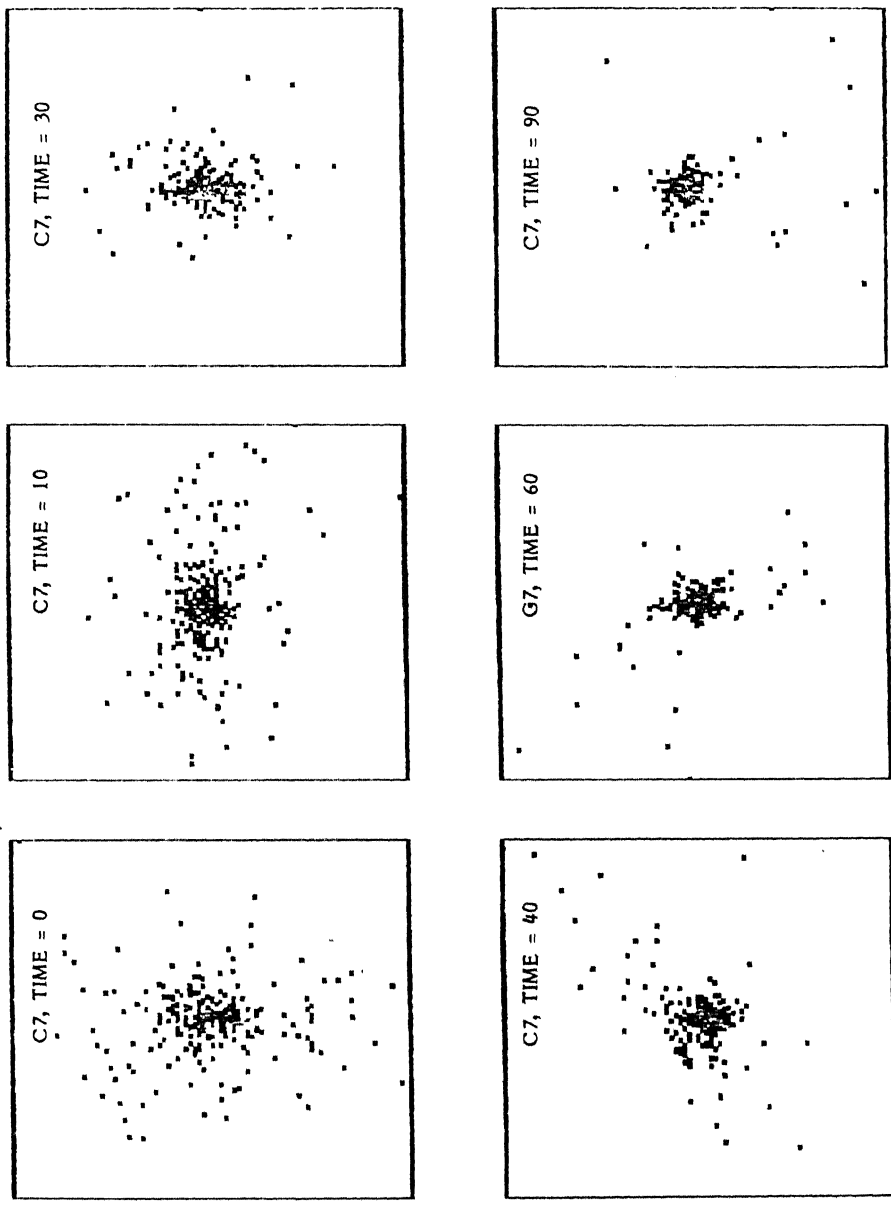Figure 36. Same as figure 12, but for 'circular' model C6.
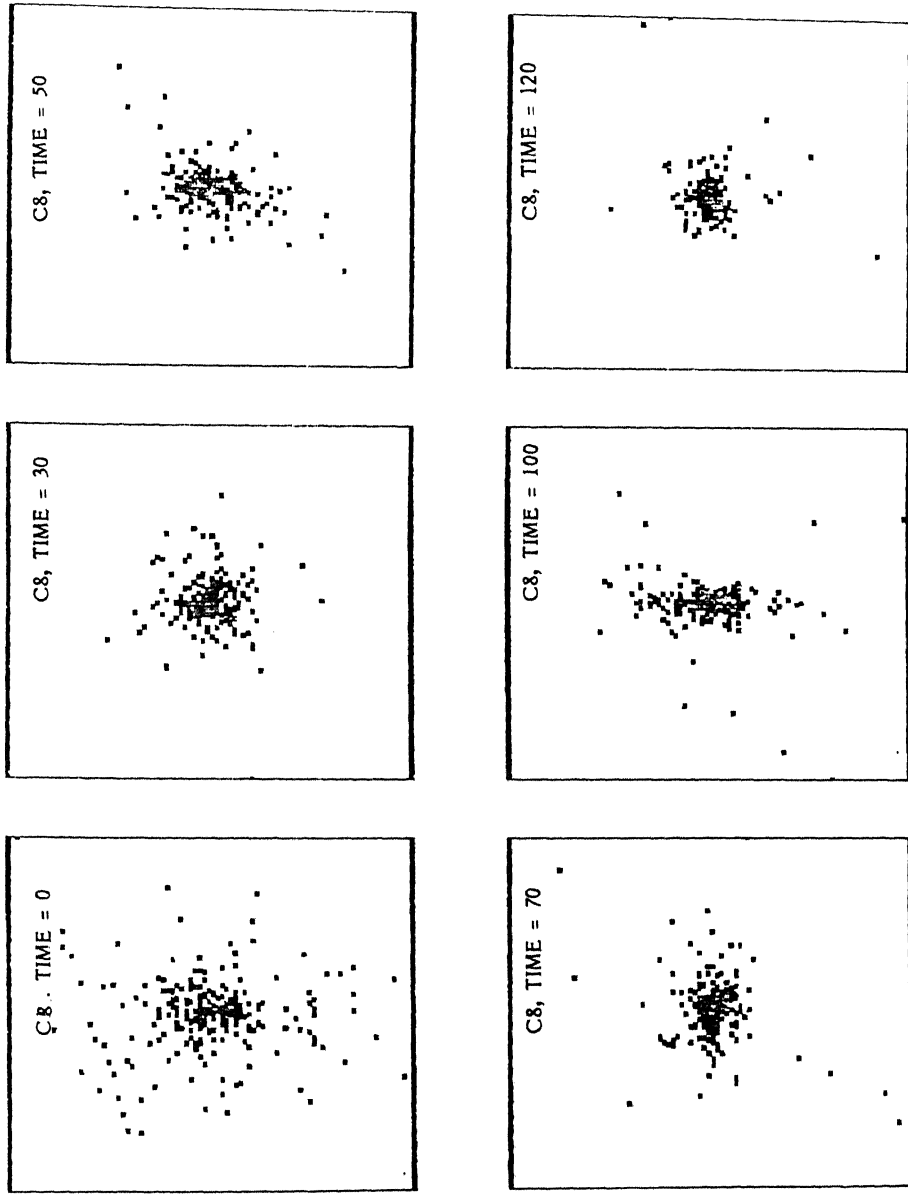
Figure 37. Same as figure 12, but for model C7.

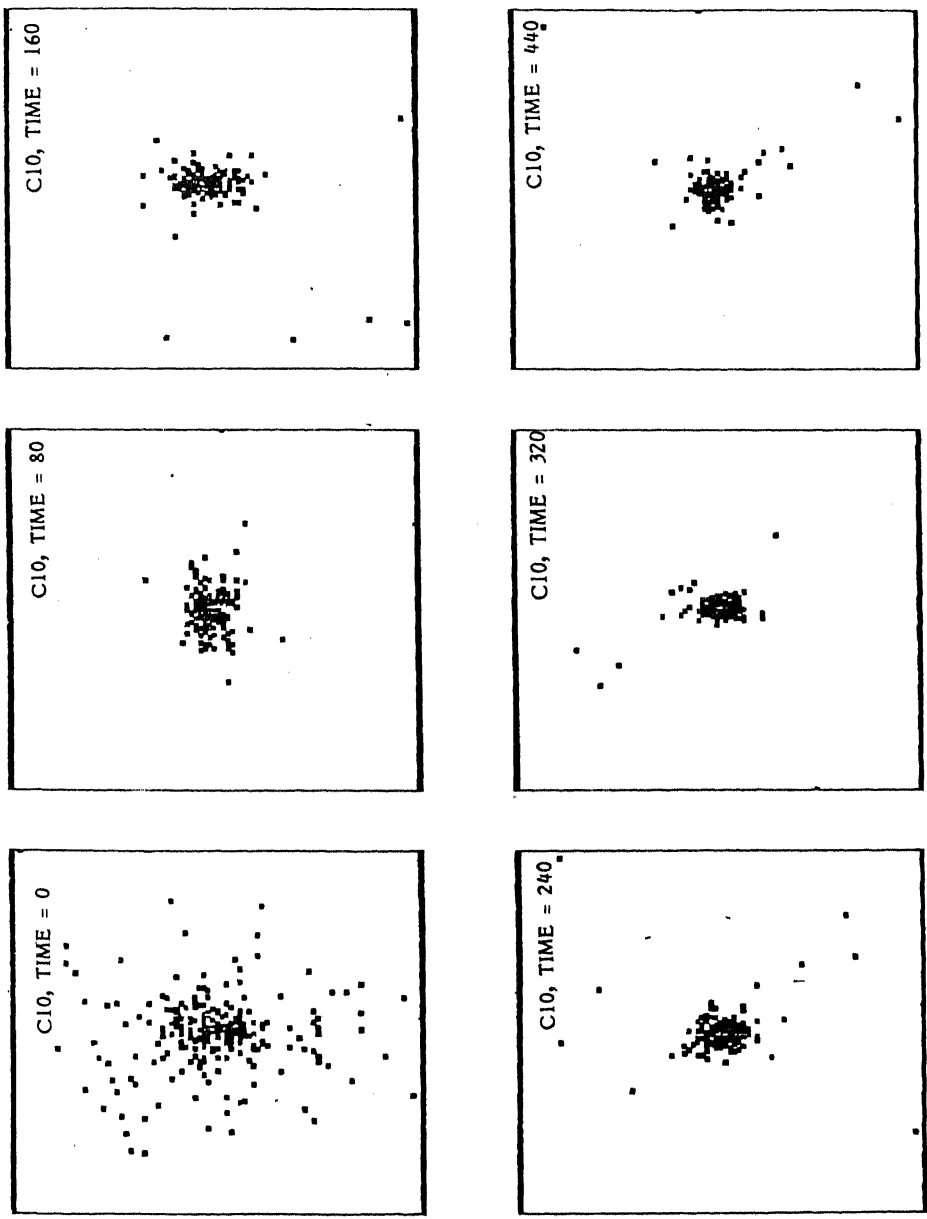Figure 38. Same as figure 12, but for model C8.

Figure 39. Same as figure 12, but for model C10.

87

17. Mass loss

For the purpose of computing the mass loss, the total energy U_1 of each particle is evaluated using equation (2) with respect to the CM of the test galaxy as defined above. Then particles with $U_1 > 0$ are identified as escapers and thus the fractional mass loss $\Delta M/M$ is obtained. Here $\Delta M = M - M_B$ where M_B is the mass of the final bound system. As expected there is a significant mass loss from the test galaxy especially in models having density ratio $\rho_h/\rho_R < 1$. The percentage of mass loss is almost 40 or more in models H1, P1-P3, E1-E4, and C6. In these models, the test galaxy is either completely or significantly disrupted.

Miller (1986) performed computations with 100352 particles in a galaxy orbiting within a cluster in a highly eccentric orbit and showed that disruption occurs when mass loss exceeds 30 - 40 %. He also obtained the strength of interaction in terms the ratio of the maximum tidal force F_T and the internal force F_I at median radius of the satellite. Miller's condition for a galaxy not to be disrupted is $F_T/F_I < 1/4$. The ratio F_I/F_T is nearly equivalent to the density ratio ρ_h/ρ_R. It can be seen that disruption occurs when $\rho_h/\rho_R < 4$ which is in conformity with Miller's result.

Figures 40 - 47 show the fractional mass loss as a function of time for all models. The mass loss reaches a

88
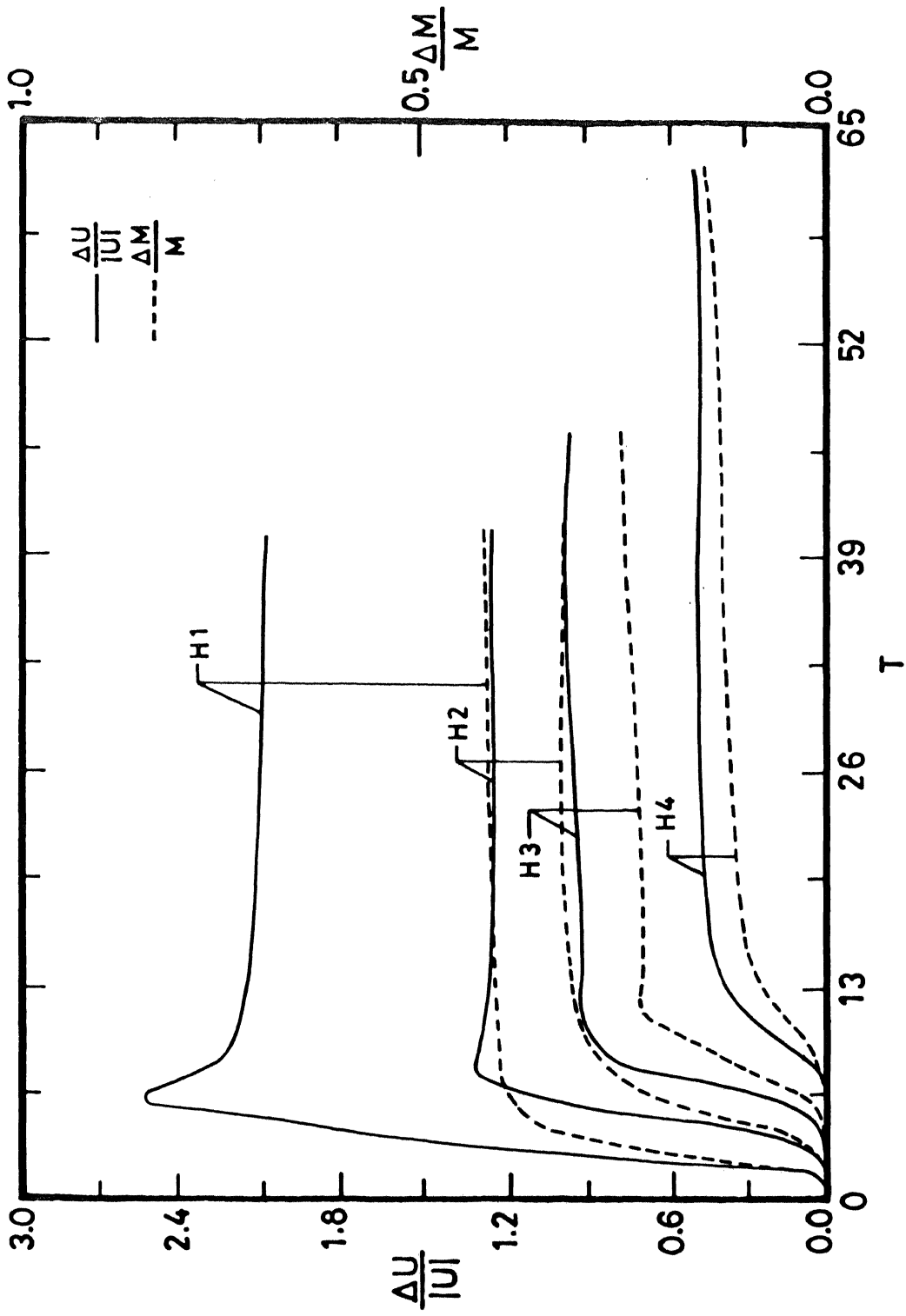
Figure 40. Fractional change in the energy and mass loss as a function of time for H models.
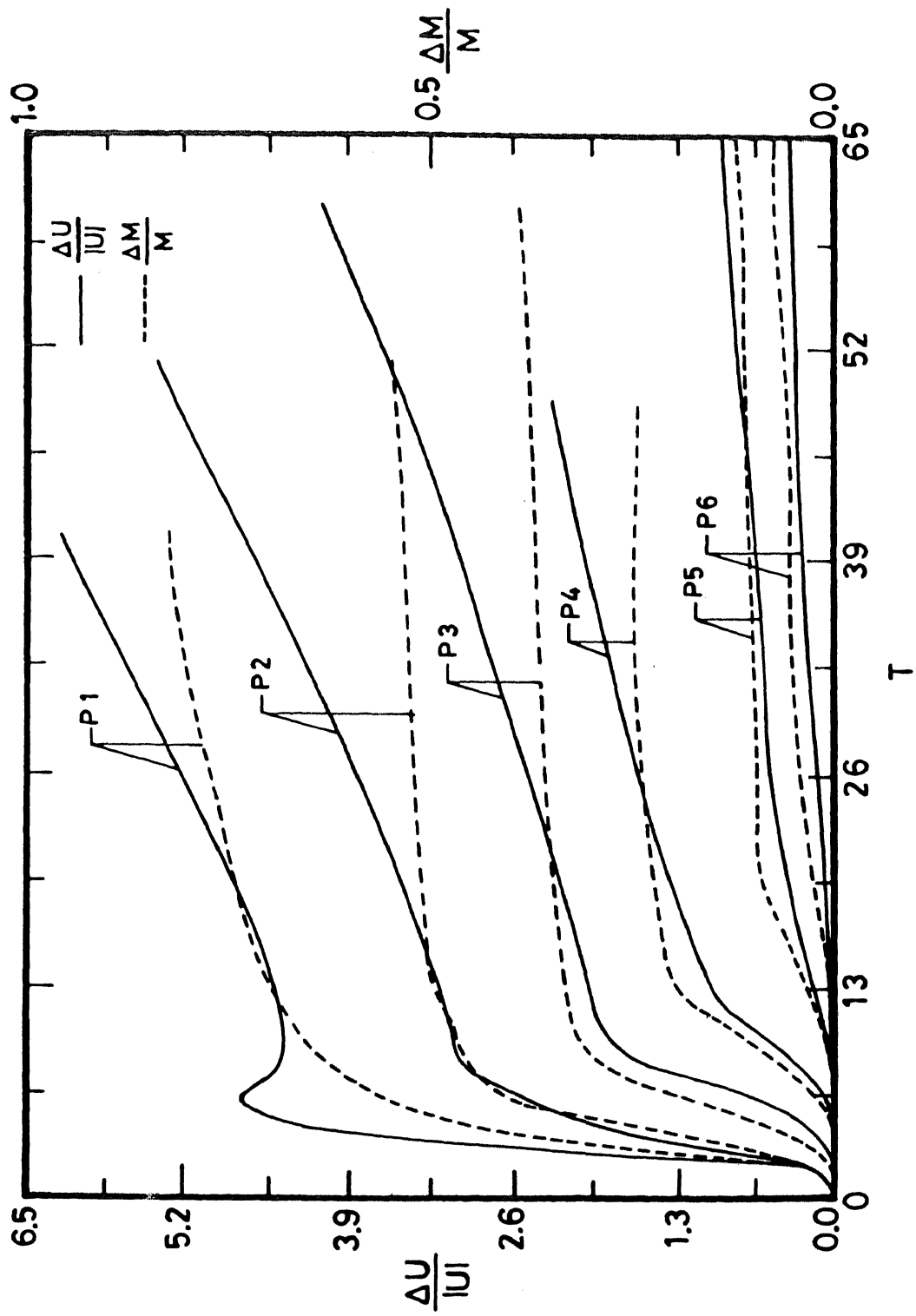
Figure 41. Same as figure 40, but for models P1 - P6.
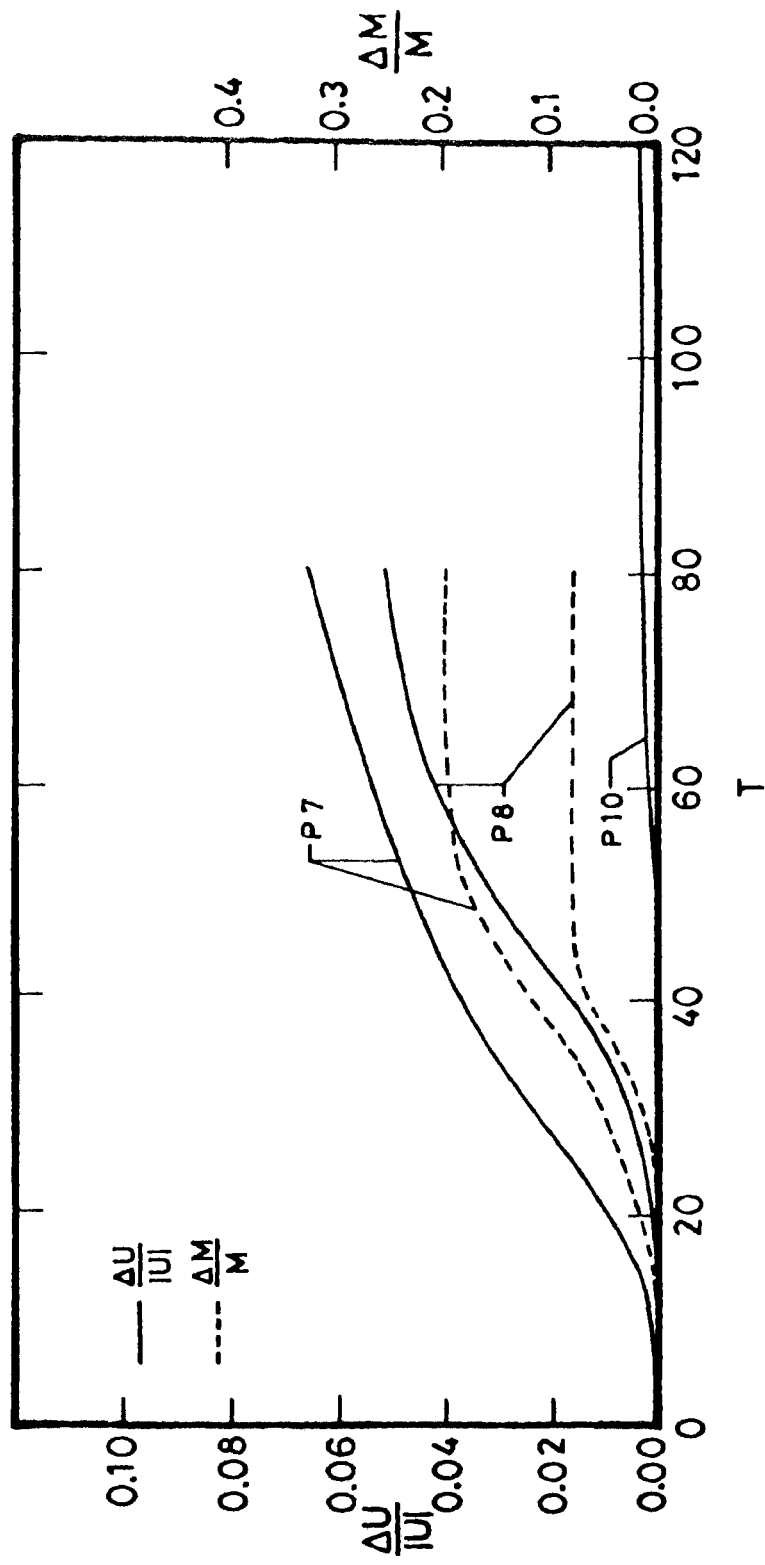
Figure 42. Same as figure 40, but for models P7 - P10.
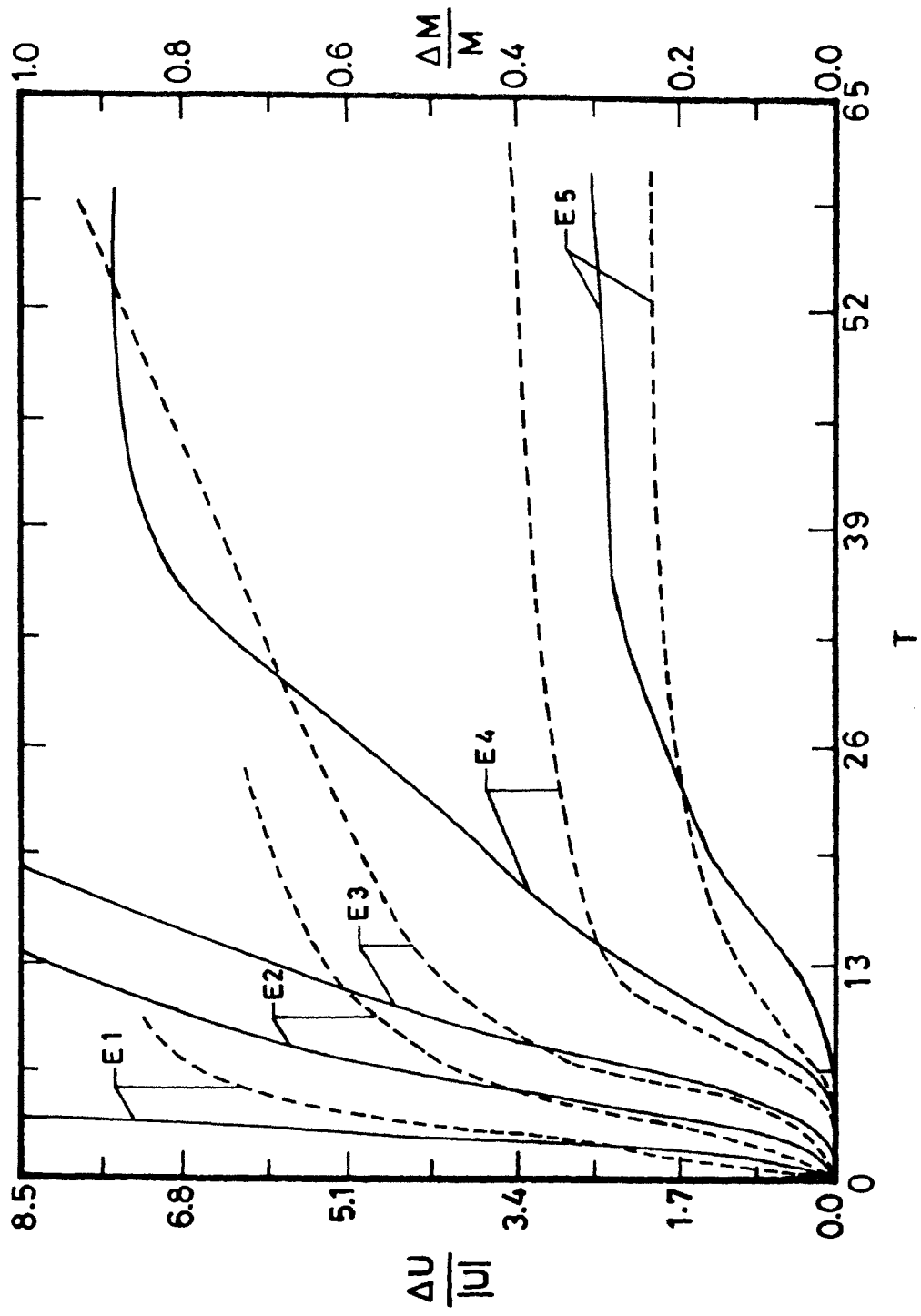
Figure 43. Same as figure 40, but for models E1 – E5.
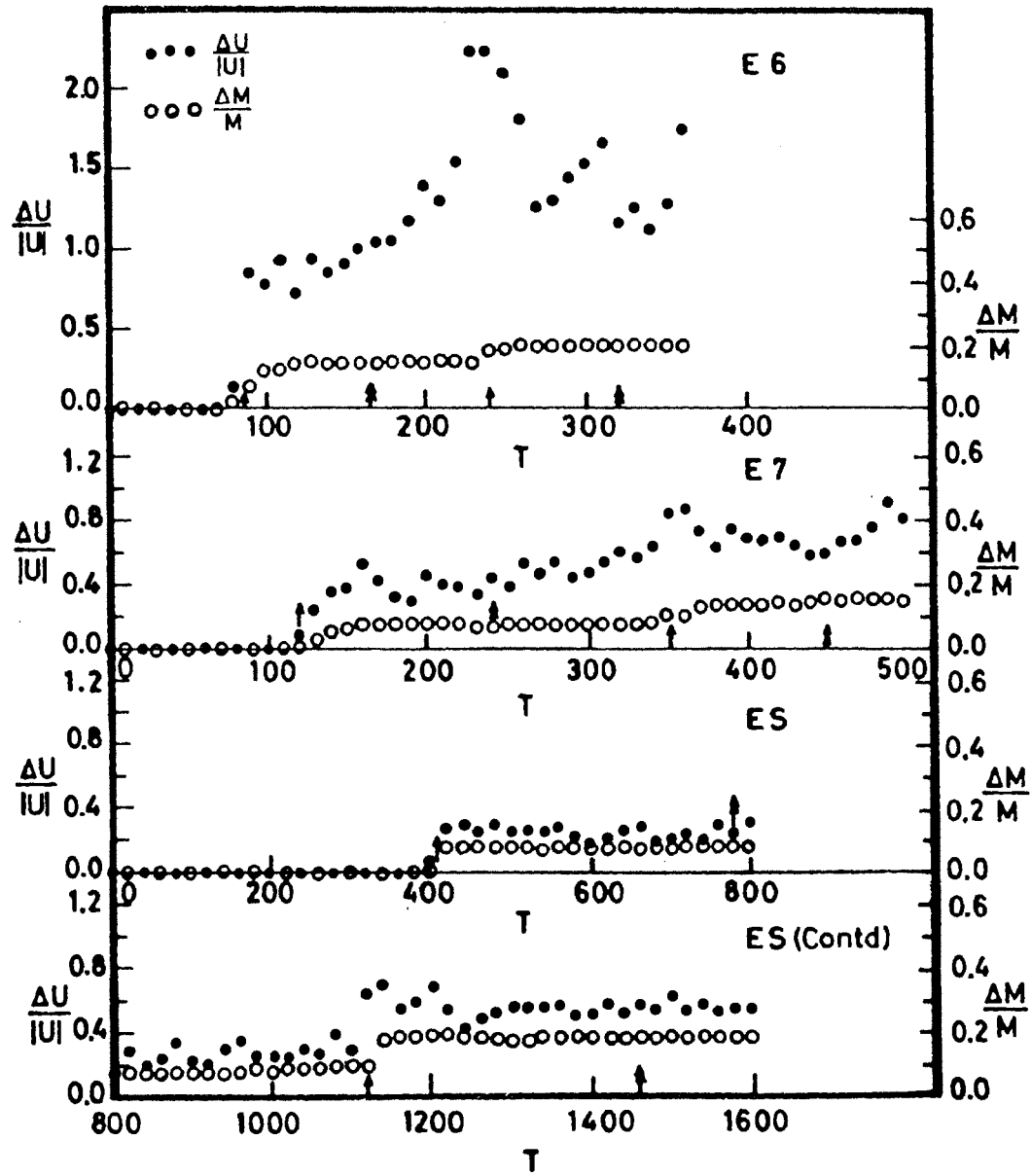
Figure 44. Same as figure 40, but for model E6, E7, and ES. Symbols ↑ and ⬆ respectively indicate times of minimum and maximum separation.
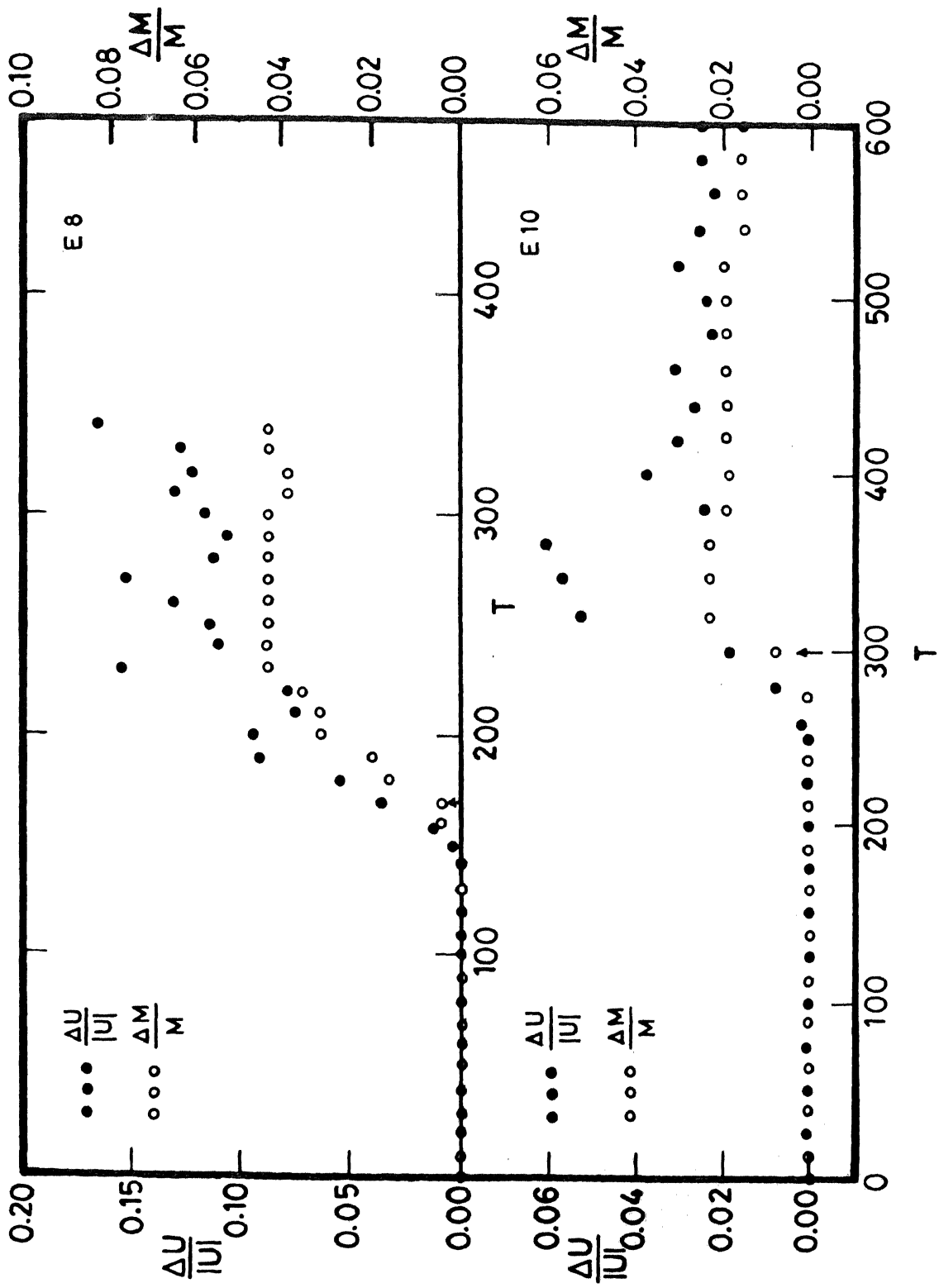
Figure 45. Same as figure 40, but for models E8 and E10.

94
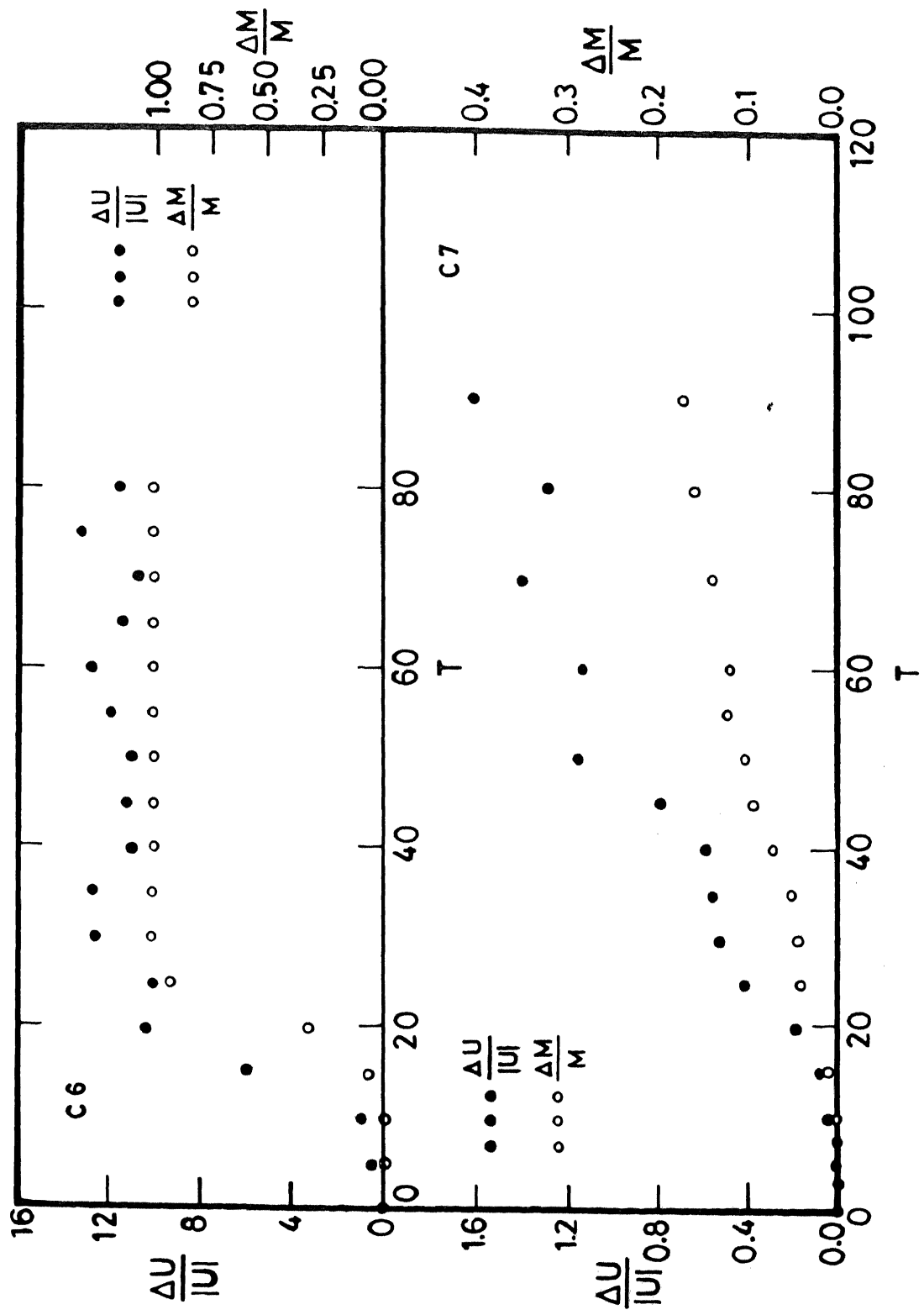
Figure 46 Same as figure 40, but for models C6 and C7.
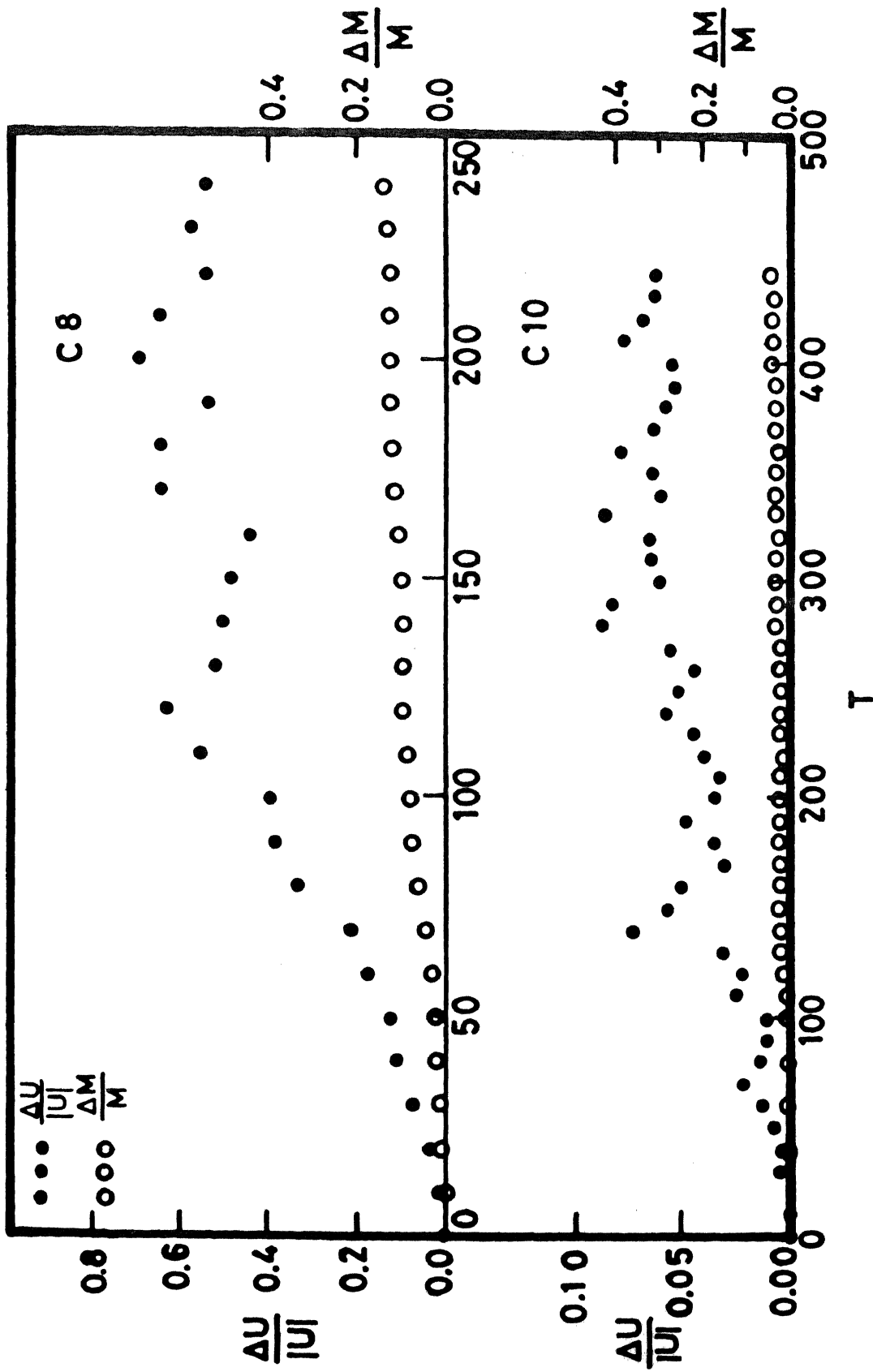
Figure 47. Same as figure 40, but for models C8 and C10.

maximum during the first contact and remains almost constant during subsequent encounter. The values of $\Delta M/M$ at the end of our simulations are given in table 4. In H and P models, the escaping particles show a preferential direction which is same as the direction of motion of the perturber and some of them are captured by the perturber. In bound orbit encounters, particles escape in various directions.

18. Energy transfer

The total kinetic and potential energy of the system are respectively given by

$$T = \sum_{i=1}^{N} (1/2) \, m_i v_i^2 \quad , \tag{3}$$

$$W = (1/2) \sum_{i=1}^{N} W_i \quad , \tag{4}$$

where

$$W_i = -G \, m_i \sum_{j=1}^{N} \frac{m_j}{(r_{ij}^2 + \varepsilon^2)^{1/2}} \quad , \tag{5}$$

and various symbols have their usual meaning. The total internal energy U_f after the encounter is given by

$$U_f = T + W \, . \tag{6}$$

The fractional change in the energy is denoted by $\Delta U/|U|$ where

$\Delta U = U_f - U$ and U is the unperturbed initial energy of the system. Ideally one should use energy per unit mass of the test galaxy. But since we are dealing with ratios, the quantity we use is the total energy. One can easily obtain energy per unit mass by dividing the above quantities by $\frac{1}{2}< v^2 >$ where $< v^2 >$ is the mean square speed at median radius of the test galaxy.

The fractional change in the total internal energy $\Delta U/|U|$ is a good measure of the tidal damage done to the test galaxy. The damage is considered negligible if $\Delta U/|U|$ is small and significant if it is nearly unity. If it is much greater than unity, severe disruption of the test galaxy is expected.

The values of $\Delta U/|U|$ obtained from the simulations after the encounter are given in table 4. Figures 40 - 47 show the variation of $\Delta U/|U|$ as a function of time for all models. We first consider the behaviour of energy transfer in unbound orbit models. It can be seen that most of the change in the energy occurs after the perturber has passed the perigalactic point. In H and P models the energy transferred during second half is almost twice the energy transferred during first half. Thus the energy transfer is asymmetric with respect to the perigalactic point. As the density ratio increases, the fractional change in the energy decreases. Disruption occurs when $\Delta U/|U| > 2$ which approximately corresponds to a mass loss of 30 - 40 % . In disruptive cases the energy of the satellite continues to increase whereas in non-disruptive cases it remains nearly constant after attaining a maximum. In these

models the variation of $\Delta U/|U|$ with time is smooth. This is because the perturber is always on one side of the satellite so that the direction of the tidal acceleration does not change significantly. The tidal effects become negligible after the perturber recedes from the test galaxy without causing much disruption.

In bound orbit encounters computations have been performed for half orbital period in models E1 - E5. Models E8, E10, C6, and C7 were followed for one orbital period. The response of the test galaxy for two orbital periods was determined in models E6, E7, ES, C8, and C10. The results are designated by the letters 'a' and 'b' where 'a' refers to first orbit and 'b' to the second. It is interesting to note that $\Delta U/|U|$ shows irregular variation with time in models E6, E7, E8, E10, ES, C6, C7, C8, and C10. This is due to the fact that in these models the perturber is moving in a closed orbit as a result of which the direction of the tidal acceleration gets partially reversed. $\Delta U/|U|$ slowly builds up during first close contact and afterwards shows irregular variation. It can also be noted that the value of $\Delta U/|U|$ and $\Delta M/M$ during second close contact are higher than the corresponding values during first close contact.Energy change in a single collision only affects stars in the outer parts rather weakly but repeated collisions may have significant effects at considerably smaller radii.

19. Angular momentum transfer

Considerable amount of orbital angular momentum is imparted to the test galaxy especially in the case of bound orbit encounters. Most of the angular momentum transfer occurs when the components are at minimum separation. A large fraction of the angular momentum transferred is carried away by the escaping particles and consequently the remaining bound system acquires very little spin. The magnitude of orbital and total internal angular momentum J_{orb} and J_{T} are given by

$$J_{orb} = \frac{M\,M_1}{M + M_1}\, p\, V_p \quad , \tag{7}$$

$$J_{T} = \sum_{i=1}^{N} m_i\, \mathbf{r}_i \times \mathbf{v}_i \quad . \tag{8}$$

The variation of J_{T}/J_{orb} with time is shown in figures 48-55. As in the case of energy transfer, the angular momentum transfer also shows irregular variation with time in bound orbit encounters and smooth variation in unbound orbit cases. The values of J_{T}/J_{orb} and J_{B}/J_{orb} are given in table 4. It can be seen that the amount of angular momentum transfer decreases as the eccentricity of the relative orbit increases.

20. Particle orbits

An idea of the type of particle orbits may be

100
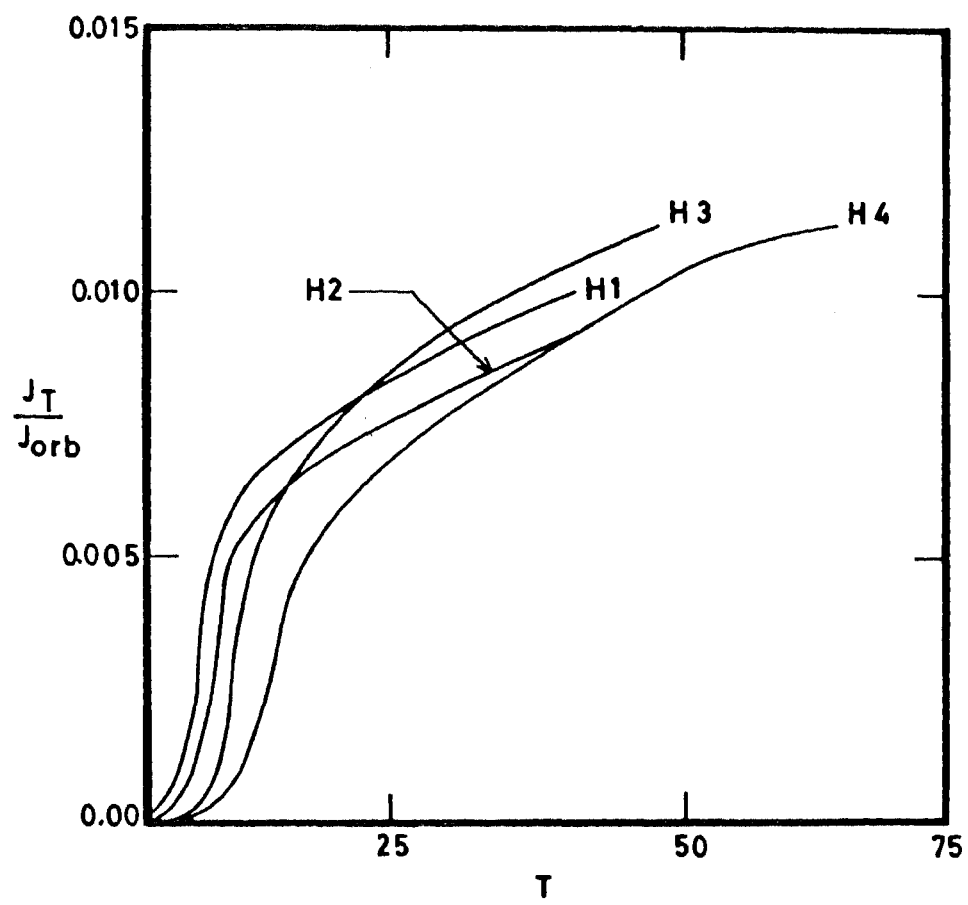
Figure 48. Angular momentum variation for the total system as a function of time for H models. J_T is the total internal angular momentum and J_{orb} is the initial orbital angular momentum of the pair.
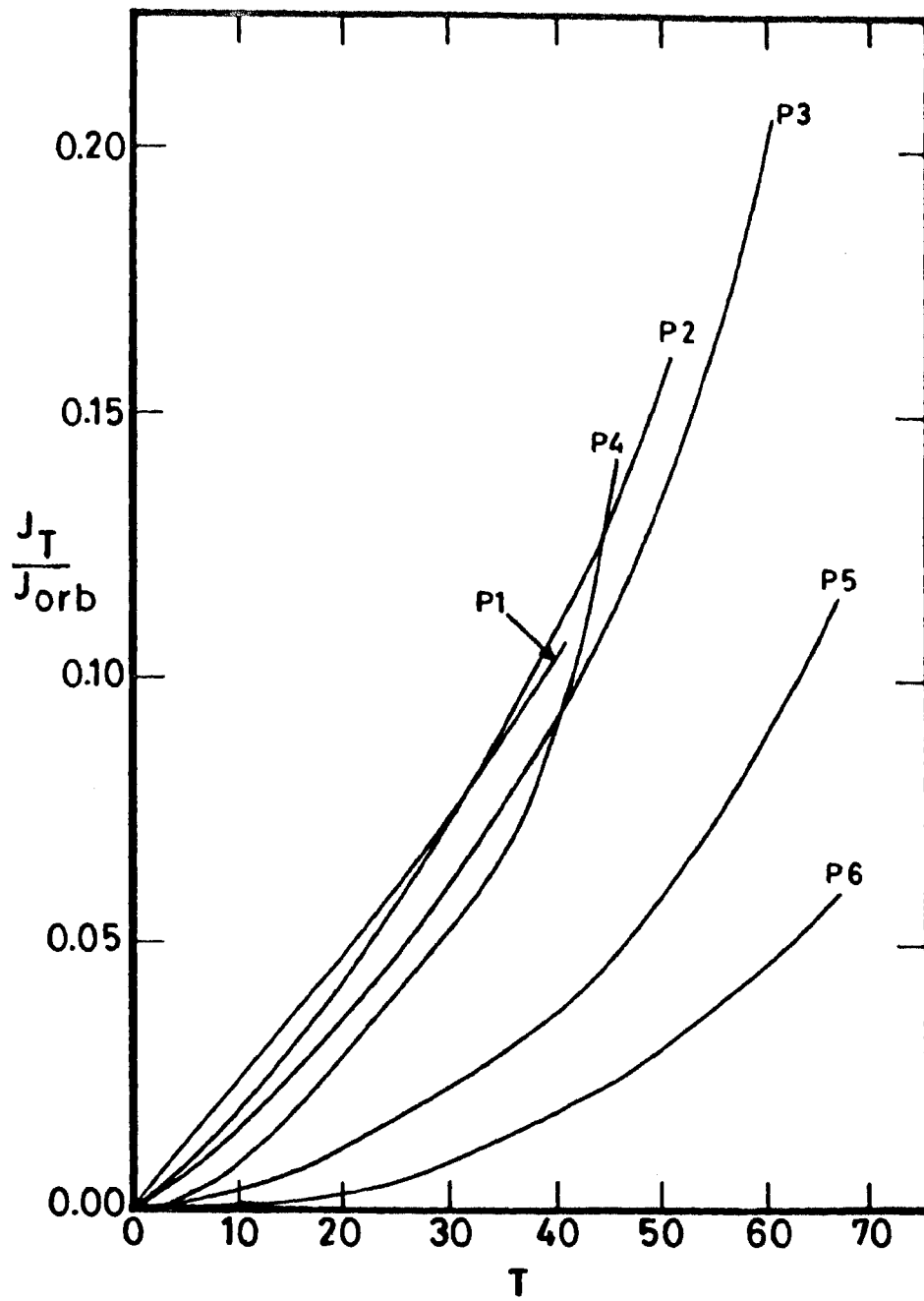
Figure 49. Same as figure 48, but for models P1 - P6.
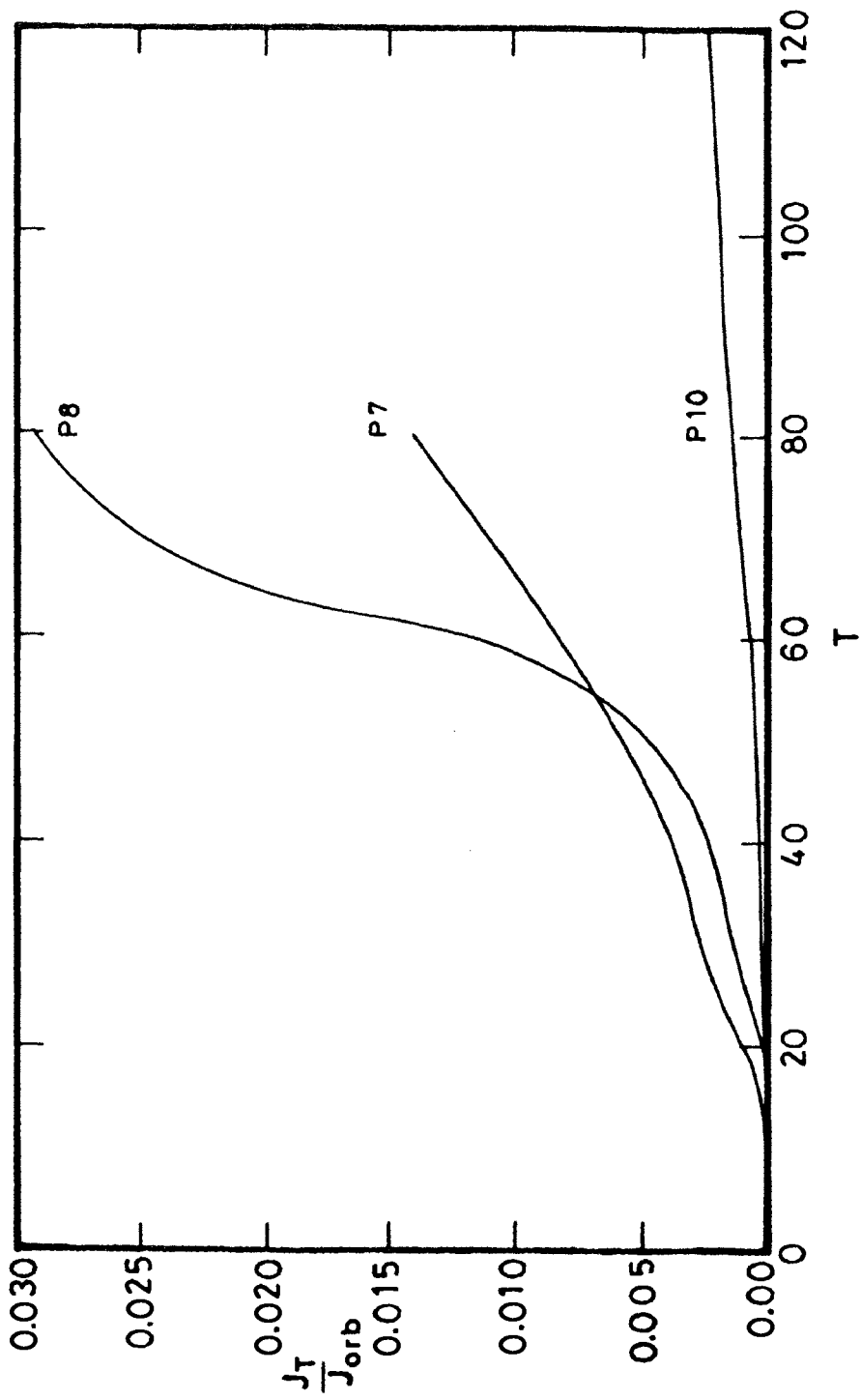
Figure 50. Same as figure 48, but for models P7, P8, and P10.
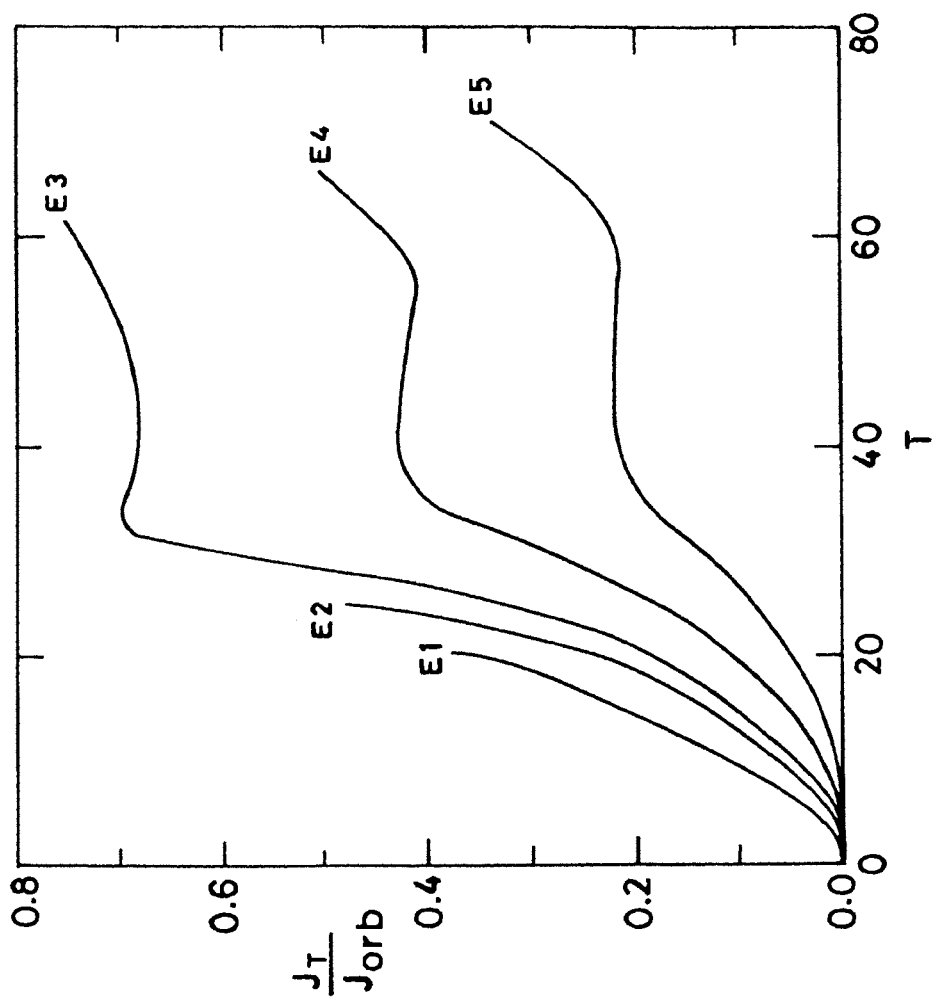
Figure 51. Same as figure 48, but for models E1 - E5.
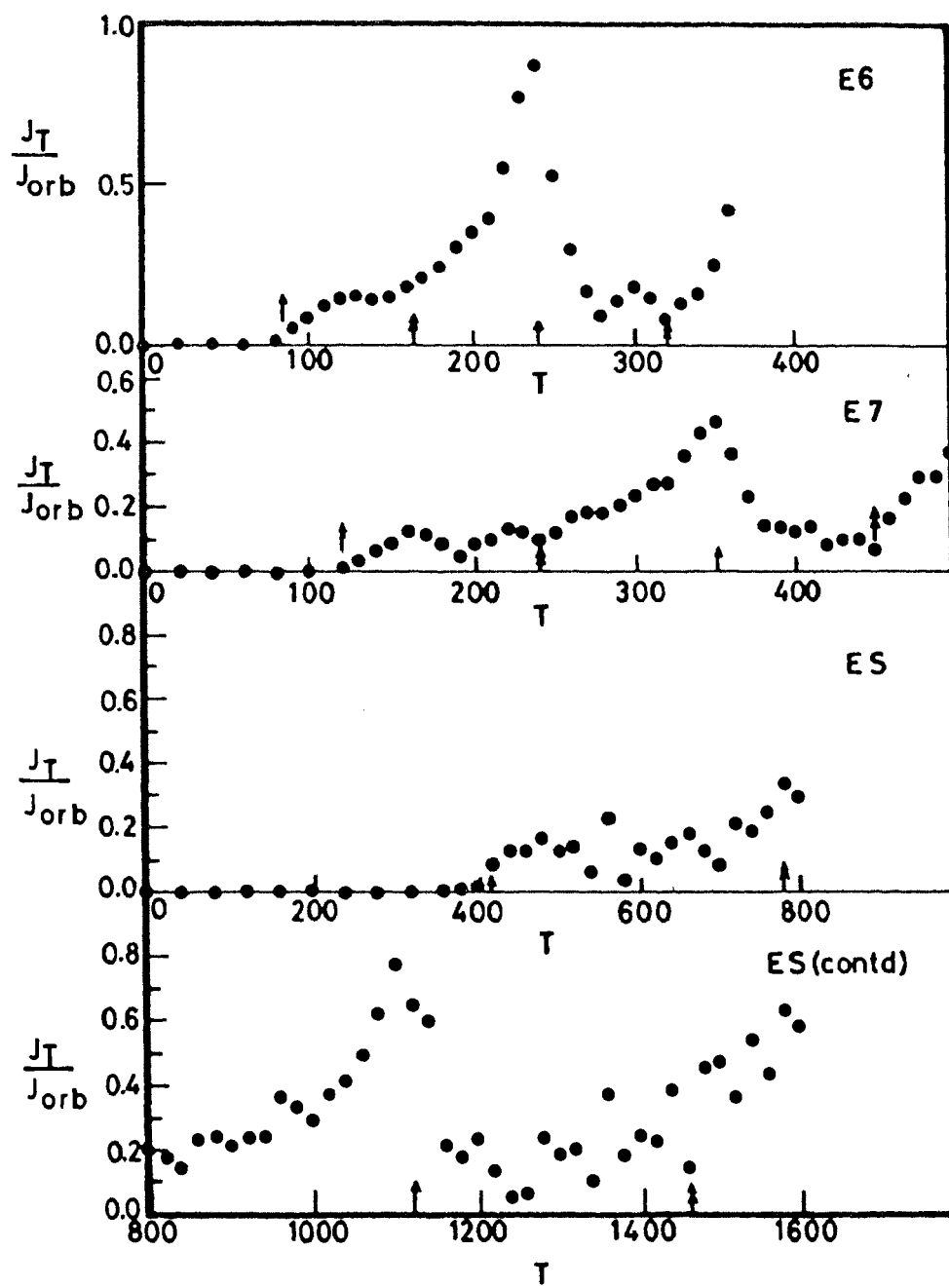
Figure 52. Same as figure 48, but for models E6, E7, and ES.
Symbols ↑ and ⤊ respectively indicate the times of minimum
and maximum separation.
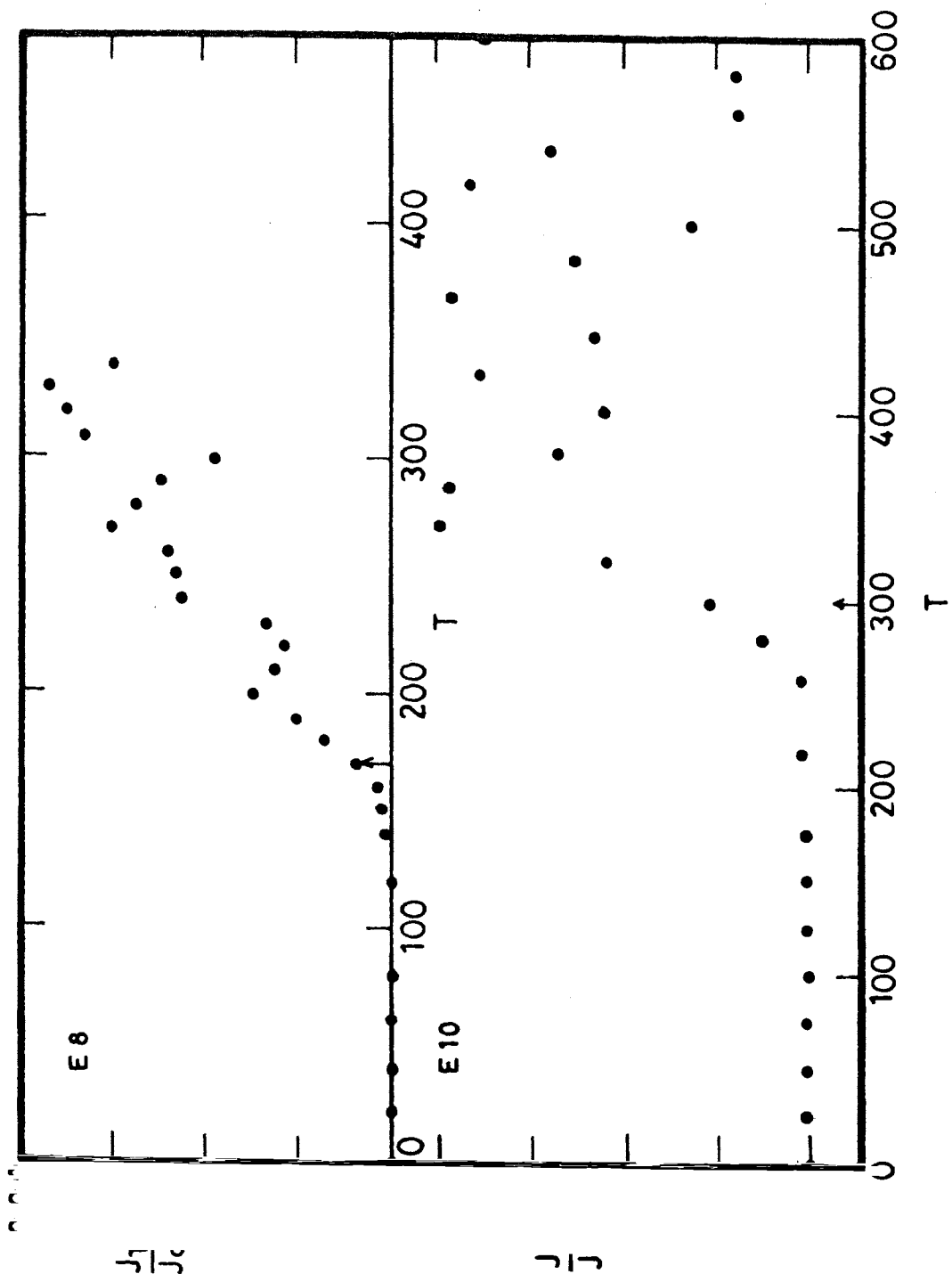
Figure 53. Same as figure 48, but for models E8 and E10.
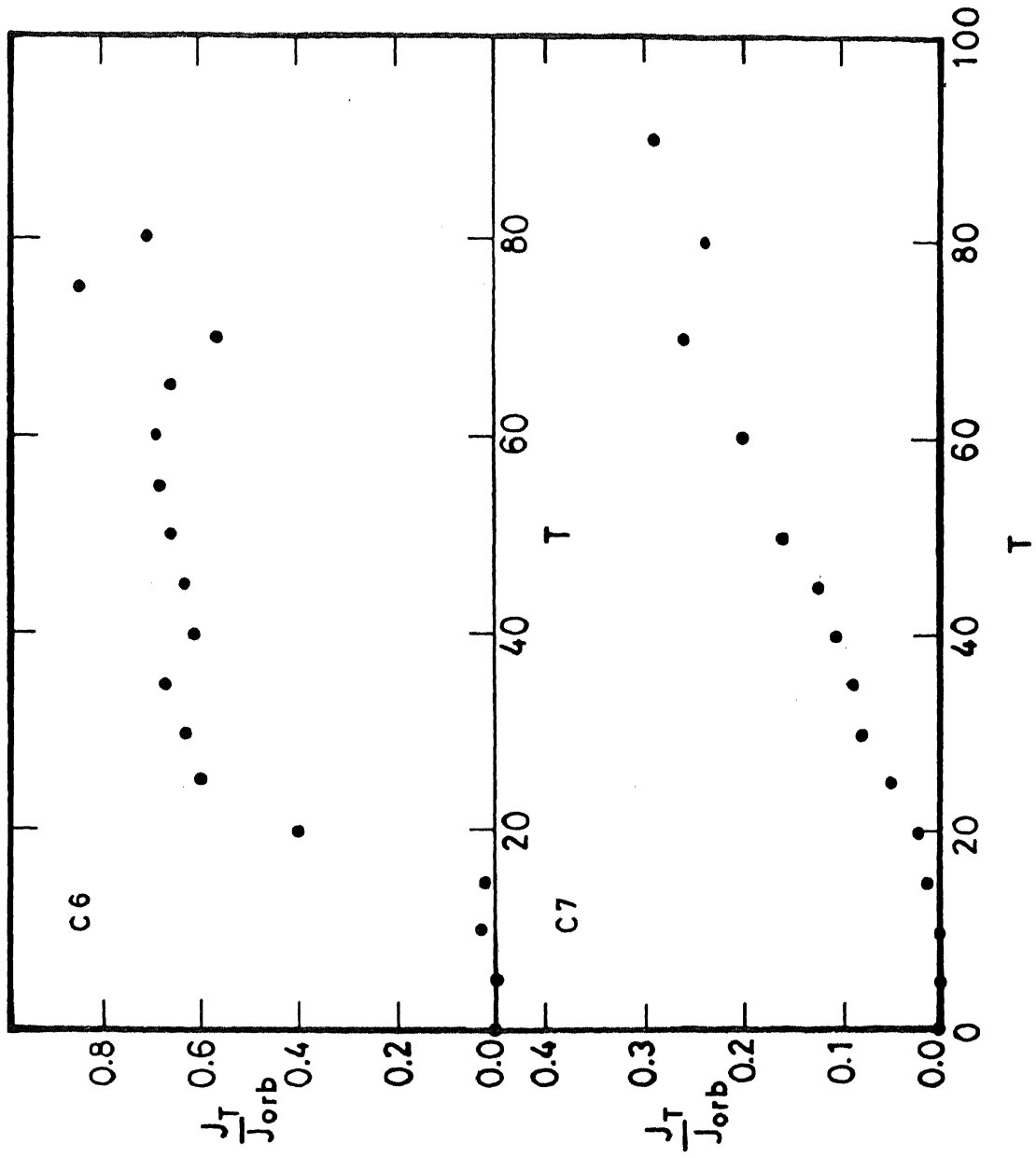
Figure 54. Same as figure 48, but for models C6 and C7.
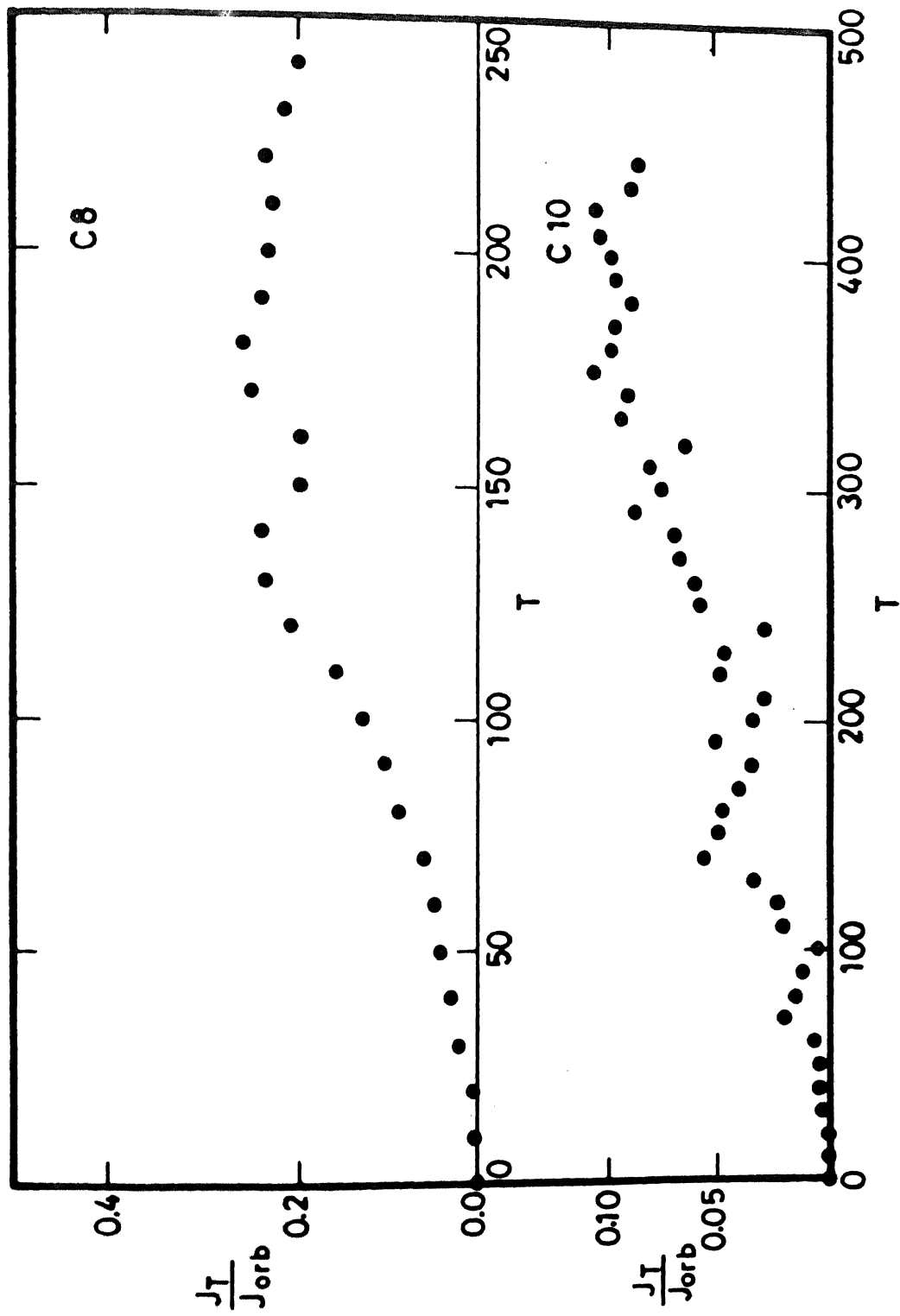
Figure 55. Same as figure 48, but for models C8 and C10.

obtained from the ratio v_{rrms}/v_{trms} where v_{rrms} and v_{trms} are respectively the root mean square radial and tangential velocities of the particles. These values are given in table 5. This table shows that the increase in root mean square radial velocity is larger than the corresponding increase in tangential velocity for the total system. Particles initially in circular orbits move in radial orbits after the encounter especially in models H and P. Consequently the test galaxy becomes elongated in the plane of the orbit. The elongation is less in bound orbit models. The increase in v_{rrms} and v_{trms} is mainly, therefore, due to the escaping particles. For the bound system, this ratio nearly coincides with that of the initial system.

The values of velocity dispersion σ of the remnant bound system are given in table 5. We note that in models where disruptive effects are significant the value of σ is smaller than that of the initial system. In other models σ remains almost constant to within 10 %.

21. Shape of the system after the encounter

To determine the shape of the system, we have computed the average expansion in the X, Y, and Z directions of the test galaxy after the encounter. To obtain the average expansion in the three directions we use the following formulae:

Table 5. Values of v_{rrms}/v_{trms} and velocity dispersion σ

	v_{rrms}/v_{trms}		σ
MODEL	TOTAL	BOUND	(BOUND)
INITIAL	0.75	0.75	1.45
H1	2.76	0.68	1.06
H2	1.79	0.65	1.27
H3	1.61	0.74	1.20
H4	1.13	0.63	1.28
P1	2.32	0.75	0.74
P2	2.16	0.62	0.96
P3	1.76	0.76	1.13
P4	1.22	0.68	1.30
P5	0.97	0.71	1.23
P6	0.94	0.79	1.26
P7	0.74	0.69	1.36
P8	0.67	0.79	1.30
P10	0.70	0.70	1.45
E4	0.86	0.74	1.11
E5	0.74	0.74	1.27
E6a	0.79	0.73	1.44
E6b	0.94	0.66	1.28
E7a	0.89	0.71	1.27
E7b	0.87	0.66	1.25
E8	0.75	0.68	1.35
E10	0.68	0.71	1.35
ESa	0.75	0.66	1.38
ESb	0.99	0.71	1.22
C7	0.60	0.73	1.26
C8a	0.59	0.65	1.38
C8b	0.72	0.75	1.34
C10a	0.66	0.67	1.45
C10b	0.65	0.71	1.37

$$E_x = \left[\frac{\sum x_i^2}{N} \right]^{1/2} \quad , \tag{9}$$

$$E_y = \left[\frac{\sum y_i^2}{N} \right]^{1/2} \quad , \tag{10}$$

$$E_z = \left[\frac{\sum z_i^2}{N} \right]^{1/2} \quad . \tag{11}$$

We have also computed the flattening f and spin parameter Λ for the bound part:

$$f = 1 - 2 \frac{I_{33}}{I_{11} + I_{22}} \quad , \tag{12}$$

$$\Lambda = J |U|^{1/2} M^{5/2} \quad , \tag{13}$$

where I_{11} , I_{22} , I_{33} are the components of the moments of inertia in the three directions; J is the internal angular momentum; U is the total energy and M is the mass of the bound part. As the encounter proceeds, the X-axis which is directed toward the closest approach point increases till the perturber reaches this point. The Y-axis remains almost constant during this period but starts expanding afterwards. We observe a shortening of Z-axis till the perturber reaches the pericentric point and a small expansion afterwards. The flattening is also maximum during the closest approach. The system generally expands in all directions during the later

111

stages of the encounter, the elongation in the Y direction being the maximum. The final values of the expansion, flattening, and spin parameters are given in table 6. This table clearly shows that the radial expansion is anisotropic.

The line of elongation is seen to rotate about the Z-axis. It is evident from models E6, E7, ES, C8, and C10 that repeated collisions make the test galaxy more and more elongated in the orbital plane. The final bound system has the characteristics of a triaxial galaxy close to an oblate system, i. e., $E_x \approx E_y > E_z$.

22. Mass and density distribution

The change in the radial structure of the test galaxy due to an encounter can be tabulated in a dimensionless way by computing the radius containing 10, 20, 30,........,100 % of the mass. This was done for the bound system where the test galaxy does not show significant tidal disruption. The results of the computations are presented in table 7 for several models. The last row in this table gives the half mass radius R_h of the respective systems. The data given in table 7 are normalized with respect to the half-mass radius of the corresponding system. Comparing radii containing 50 % of the mass for various models with the initial one, we find that the inner region containing 50 % of the mass remains intact. Similarly radii containing 90 % of the mass generally shows expansion. There is significant expansion in the region

Table 6. Expansion, flattening and spin parameters

MODEL	TOTAL			BOUND				
	E_x	E_y	E_z	E_x	E_y	E_z	f	Λ
Initial	5.98	6.22	6.50	5.98	6.22	6.50	–	–
H2	61.07	88.27	38.86	13.54	18.12	12.16	0.42	0.05
H3	56.49	91.37	38.86	12.00	15.84	14.84	0.12	0.02
H4	44.78	87.27	29.82	11.68	12.64	11.84	0.05	0.04
P4	53.60	137.91	23.41	11.41	9.67	8.62	0.34	0.04
P5	50.03	112.43	17.22	11.00	12.13	9.79	0.29	0.03
P6	24.69	65.74	11.77	8.16	13.59	9.43	0.29	0.04
P7	9.87	29.74	7.90	5.96	7.83	7.14	0.05	0.01
P8	9.28	24.69	7.25	7.02	8.17	7.17	0.11	0.02
P10	6.62	8.62	7.11	6.62	8.62	7.11	0.15	0.01
E5	96.86	127.65	16.73	6.02	4.96	5.15	0.13	0.03
E6a	78.69	115.04	15.35	7.88	5.87	5.78	0.31	0.02
E6b	230.47	280.83	40.71	7.83	7.94	5.88	0.45	0.03
E7a	73.99	104.37	17.09	7.26	6.74	5.95	0.28	0.02
E7b	230.47	275.51	40.66	5.56	6.42	6.30	0.10	0.01
E8	64.61	90.10	17.38	14.57	8.52	6.49	0.70	0.03
E10	44.03	33.54	9.47	17.39	33.59	9.46	0.88	0.02
ESa	171.86	186.72	36.99	14.96	13.63	8.53	0.65	0.05
ESb	604.22	612.33	112.86	20.18	15.73	9.82	0.71	0.03
C7	50.84	52.49	29.55	5.15	6.04	4.77	0.28	0.02
C8a	28.17	43.37	9.26	6.03	6.10	4.79	0.33	0.03
C8b	68.87	100.45	17.35	6.29	8.45	5.05	0.52	0.04
C10a	13.11	15.12	7.46	7.04	9.76	6.94	0.34	0.02
C10b	29.76	32.83	10.31	23.87	17.18	8.96	0.81	0.03

Table 7. Radial structure of the remnant bound system

% of mass	Init-ial	H2	H3	H4	P5	P6	P7	P8	P10
10	0.32	0.32	0.29	0.29	0.26	0.27	0.28	0.26	0.28
20	0.48	0.44	0.45	0.43	0.38	0.41	0.43	0.42	0.46
30	0.71	0.58	0.66	0.60	0.62	0.55	0.60	0.58	0.60
40	0.84	0.76	0.84	0.78	0.83	0.81	0.77	0.80	0.79
50	1.00	1.00	1.00	1.00	1.00	1.00	1.00	1.00	1.00
60	1.26	1.22	1.44	1.25	1.77	1.19	1.22	1.18	1.28
70	1.62	1.81	2.01	1.57	1.57	1.39	1.60	1.44	1.76
80	2.12	2.57	3.11	2.12	1.94	1.90	1.99	1.89	2.24
90	2.84	8.71	7.58	3.22	3.11	2.82	2.89	2.45	2.85
100	5.59	13.37	15.75	20.97	15.32	13.18	7.58	10.67	10.71
R_h	6.55	6.24	5.83	6.51	6.97	7.26	6.88	7.44	6.42

TABLE 7 (Continued)

% of mass	E6a	E6b	E7a	E7b	ESa	ESb	E8	E10
10	0.28	0.34	0.39	0.41	0.36	0.35	0.36	0.30
20	0.49	0.49	0.51	0.53	0.52	0.51	0.48	0.38
30	0.64	0.61	0.65	0.68	0.65	0.62	0.64	0.52
40	0.84	0.81	0.85	0.86	0.80	0.80	0.78	0.70
50	1.00	1.00	1.00	1.00	1.00	1.00	1.00	1.00
60	1.16	1.26	1.15	1.21	1.32	1.22	1.28	1.22
70	1.48	1.47	1.37	1.44	2.03	1.47	1.61	1.64
80	1.91	1.98	1.73	1.96	2.74	2.06	2.04	2.11
90	2.55	2.80	2.52	3.05	4.23	3.74	3.31	3.06
100	12.59	16.88	7.42	8.72	32.11	46.03	23.66	74.32
R_h	5.91	5.50	6.66	5.47	5.36	5.34	6.06	7.01

TABLE 7 (Continued)

% of Mass	C7	C8a	C8b	C10a	C10b
10	0.24	0.24	0.30	0.30	0.37
20	0.45	0.41	0.47	0.46	0.48
30	0.60	0.56	0.61	0.67	0.63
40	0.76	0.77	0.79	0.79	0.79
50	1.00	1.00	1.00	1.00	1.00
60	1.18	1.14	1.33	1.30	1.28
70	1.40	1.42	1.70	1.60	1.58
80	1.70	1.88	2.10	2.10	1.97
90	2.38	2.55	2.67	2.71	2.60
100	6.74	6.27	10.54	13.18	69.08
R_h	6.21	6.63	5.77	6.49	6.28

containing 90 - 100 % of the mass. In all simulations carried out, the remnant profile has been found to have very extensive outer envelopes compared to the profiles of the galaxy from which it formed. Observations indicate that mild encounters produce a distension in the victim's envelope. This was interpreted as due to reversible tidal stretching and substantial tidal heating (Kormandy, 1977). A similar effect can be observed in our models.

The data in table 7 can be graphically represented by plotting the radii containing various percentages of mass. Figures 56 - 59 show the mass profiles of the bound system after the encounter. The mass profiles containing 50 % of the mass generally follows the law $M(r) \propto r$. The deviations from this law occurs beyond $R = R_h$. We note that in hyperbolic encounters where $p > 5 R_h$, the expansion of the region containing 50 % of the mass is negligible (cf. Dekel et al., 1980). It can be seen from table 7 that except in models C8 and C10, the half-mass radius of the final bound system does not increase significantly. It thus appears that no collision signature is to be expected at least in the inner regions of the density profiles.

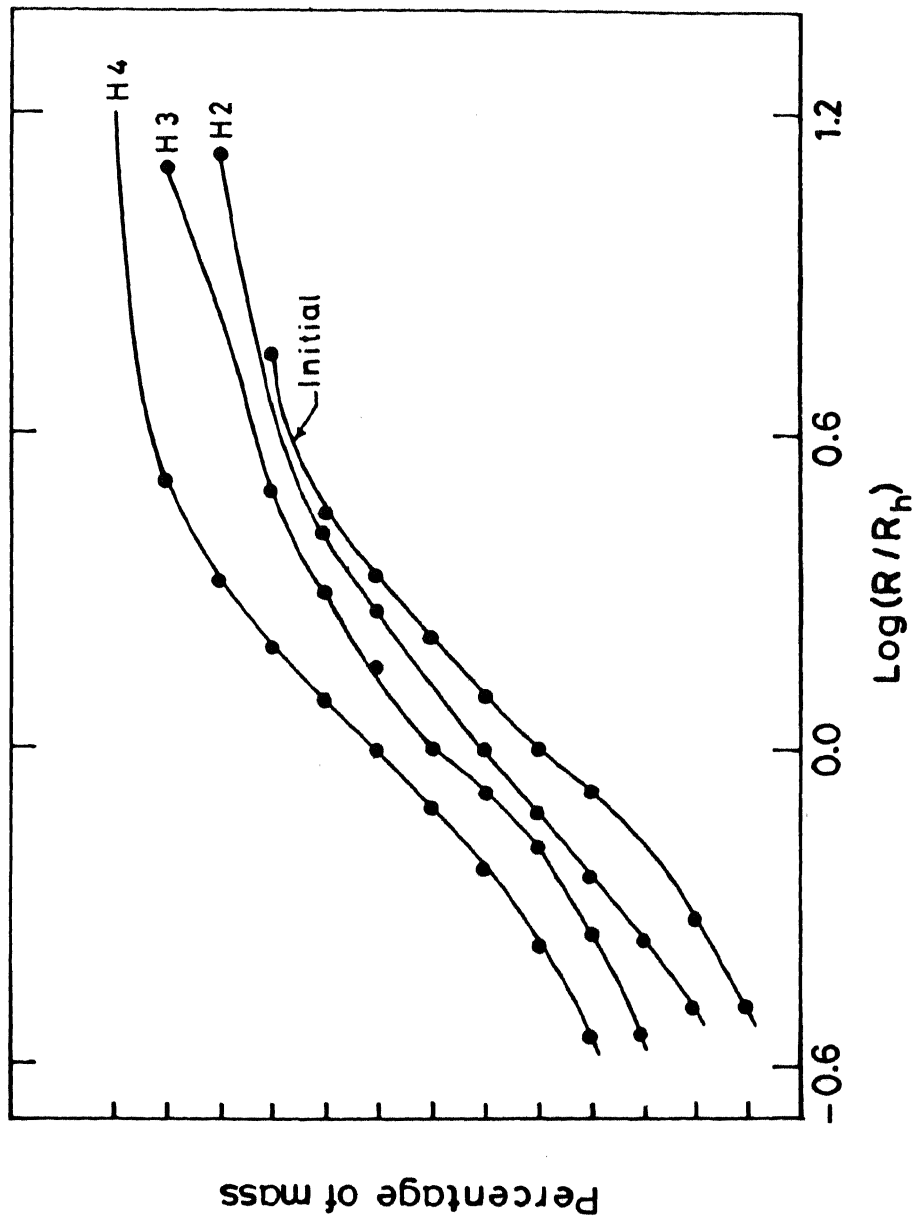Figure 56. Radial distribution of the remnant bound mass for models H2, H3, and H4. The marks on the ordinate represent steps of 10 % mass. Successive graphs from bottom to top are vertically displaced by 10 % mass.
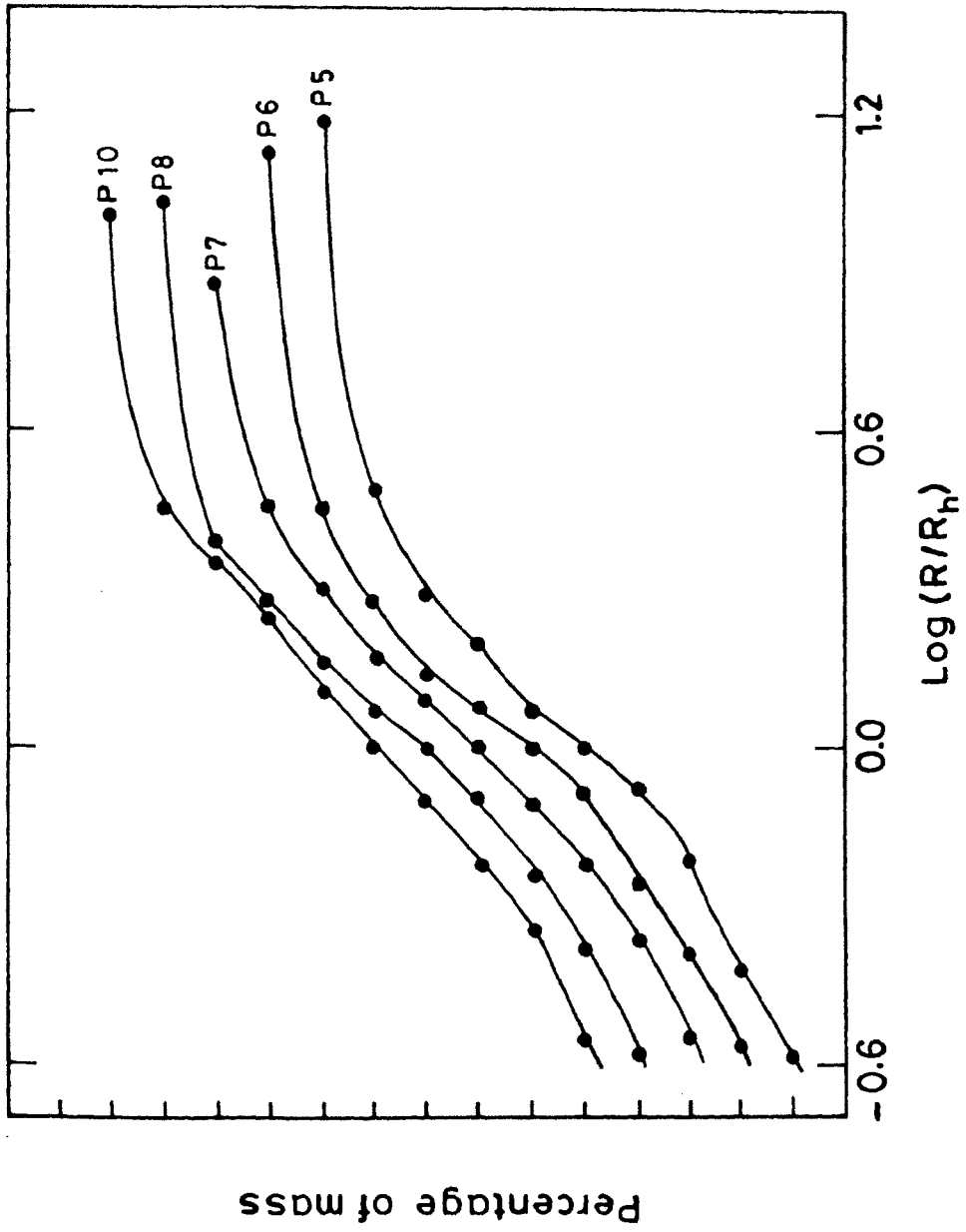
117

Figure 57. Same as figure 56, but for models P5, P6, P7, P8, and P10.
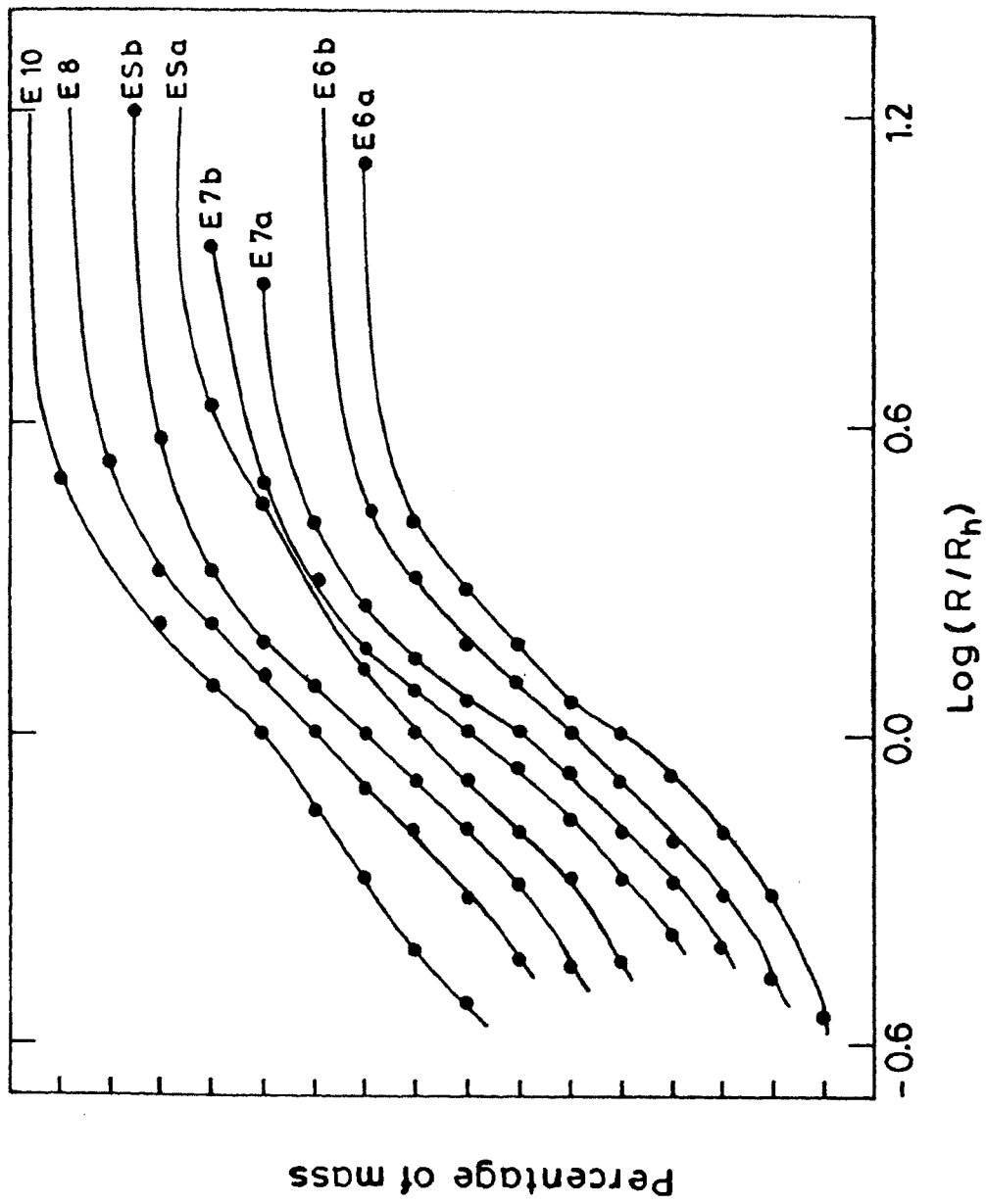
Figure 58. Same as figure 56, but for models E6, E7, Es, E8, and E10.
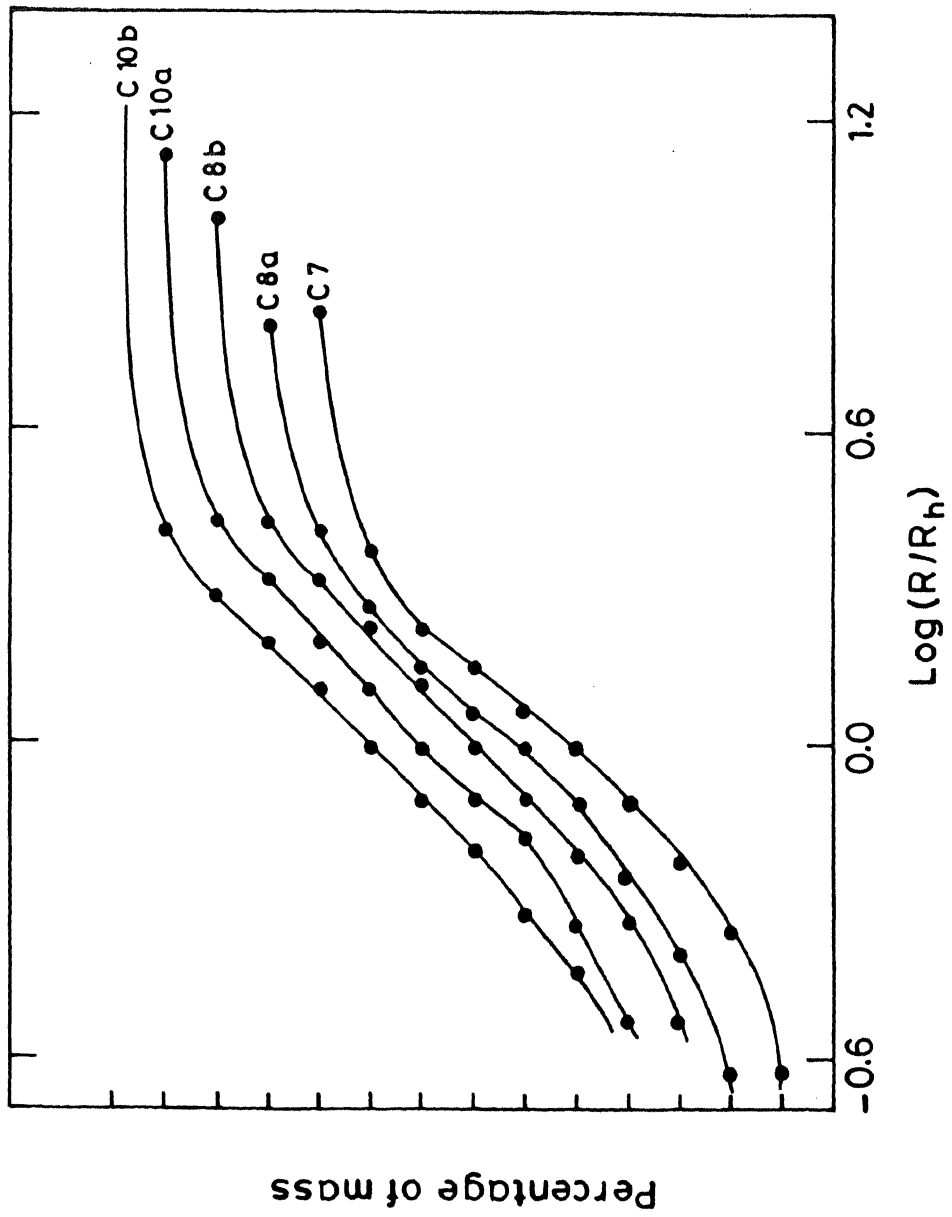
Figure 59. Same as figure 56, but for models C7, C8, and C10.

120

CHAPTER FIVE

DISCUSSION OF THE RESULTS

23. Comparison of energy change with predictions of analytic formulae

During the course of an encounter, a part of the orbital energy is transferred to the total internal energy of the test galaxy. Individual stars in the test galaxy gain energy and consequently start moving in elongated orbits. This causes an overall expansion of the system. Those particles which acquire velocity greater than escape velocity will leave the system. The increase in the energy of the system can fairly well be estimated by using the impulse approximation (IA). This has been shown to be a good approximation by several investigators over a wide range of collision parameters in spite of its simplifying assumptions.

To obtain the fractional change in the internal energy of the test galaxy due to the passage of a perturber moving in a relative orbit of eccentricity e within the framework of IA, we use the following formulae (Alladin & Narasimhan, 1982; Narasimhan & Alladin, 1983). These will be denoted by the subscript AN.

$$\left[\frac{\Delta U}{|U|}\right]_{AN} = \frac{2\,\Pi^2}{(1+e)^2}\,\frac{G^2\,M_1^2}{p^4\,V_p^2}\left(\frac{R_{rms}}{V_{rms}}\right)^2 \quad , \qquad e \leq 1 \quad , \qquad (1)$$

$$\left[\frac{\Delta U}{|U|}\right]_{AN} = (1+e)\,<e_1^2>\,\frac{G^2\,M_1^2}{p^4\,V_p^2}\left(\frac{R_{rms}}{V_{rms}}\right)^2 \quad , \qquad e > 1 \quad , \quad (2)$$

where $<e_1^2>$ is a complicated function of e given by

$$<e_1^2> = (e_1^2 + e_2^2 + e_3^2) / 3 \qquad , \qquad\qquad (3)$$

$$e_1 = \frac{1}{(e+1)^2}\left[\frac{1}{(e+1)}\cos^{-1}(-e^{-1}) + \frac{2e^2-1}{e^2}\sqrt{\frac{e-1}{e+1}}\right] ,$$

$$e_y = \frac{1}{(e+1)^2}\left[\frac{1}{(e+1)}\cos^{-1}(-e^{-1}) + \frac{1}{e^2}\sqrt{\frac{e-1}{e+1}}\right], (4)$$

$$e_z = \frac{-1}{(e+1)^2}\left[\frac{1}{(e+1)}\cos^{-1}(-e^{-1}) + \sqrt{\frac{e-1}{e+1}}\right] .$$

Here ΔU is the increase in the internal energy; U the unperturbed initial energy; M_1 the mass of the perturber; p the distance of closest approach; and V_p the velocity at closest approach. R_{rms} and V_{rms} are respectively the root mean square radius and velocity of the particles in the test galaxy. If $\Delta U/|U|$ < 1, the collision results in negligible disruption whereas for $\Delta U/|U|$ >> 1 we could expect significant disruption of the test galaxy. It should however be noted that $\Delta U/|U|$ ≈ 1 does not necessarily imply disruption: a significant portion of its mass may still remain bound to the

122

system. The ratio $\Delta U / |U|$ thus gives an order of magnitude estimate of the tidal effects.

For fast encounters, we can derive a similar expression from Spitzer's (1958) theory. This is denoted by the subscript Sp.

$$\left[\frac{\Delta U}{|U|} \right]_{Sp} = \frac{8}{3} \frac{G^2 M_1^2}{p^4 v_p^2} \left(\frac{R_{rms}}{V_{rms}} \right)^2 \quad . \tag{5}$$

$\Delta U / |U|$ obtained from the present work, $(\Delta U / |U|)_{AN}$ and $(\Delta U / |U|)_{Sp}$ for various models are presented in table 8. It can be seen from this table that the agreement of these values is remarkably good in the case of H models as noted by earlier investigators. The validity of the formulae become less accurate as we decrease the eccentricity of the relative orbit.

Figure 60 shows the variation of $\log(\Delta U / |U|)$ with $\log(\rho_h / \rho_R)$. The dotted lines show the curves for IA values obtained using equations (1) and (2). It can be seen from table 8 and figure 60 that the IA estimates agree within a factor of two with numerical results in the range $0.1 < \Delta U / |U| < 2$. The IA underestimates the tidal effects when $\Delta U / |U| > 2$ and overestimates them when $\Delta U / |U| < 0.1$. This is due to the fact that for $\Delta U / |U| > 2$, there is much loosening of the test galaxy which enhances the tidal effects whereas for $\Delta U / |U| < 0.1$, the motion of the stars reduces the tidal effects and these factors are not taken into account in the derivation of the IA formulae. In the range of validity of the formulae,

Table 8. Values of $\Delta U / |U|$

| MODEL	$\Delta U / |U|$	$(\Delta U / |U|)_{AN}$	$(\Delta U / |U|)_{Sp}$
H1	2.080	3.334	2.631
H2	1.260	1.666	1.315
H3	0.986	0.934	0.738
H4	0.514	0.466	0.368
P1	6.203	7.304	3.947
P2	5.357	3.649	1.972
P3	4.100	2.048	1.107
P4	2.297	1.021	0.552
P5	0.970	0.507	0.274
P6	0.449	0.251	0.136
P7	0.066	0.122	0.066
P8	0.051	0.059	0.032
P10	0.003	0.012	0.006
E1	14.095	17.313	5.263
E2	13.222	8.650	2.629
E3	10.236	4.854	1.475
E4	8.711	2.420	0.736
E5	3.774	1.202	0.356
E6a	1.035	0.595	0.181
E7a	0.396	0.290	0.088
E8	0.167	0.139	0.042
E10	0.026	0.028	0.008
C6	11.470	2.008	0.271
C7	1.610	0.978	0.132
C8a	0.553	0.467	0.063
C10a	0.032	0.093	0.013
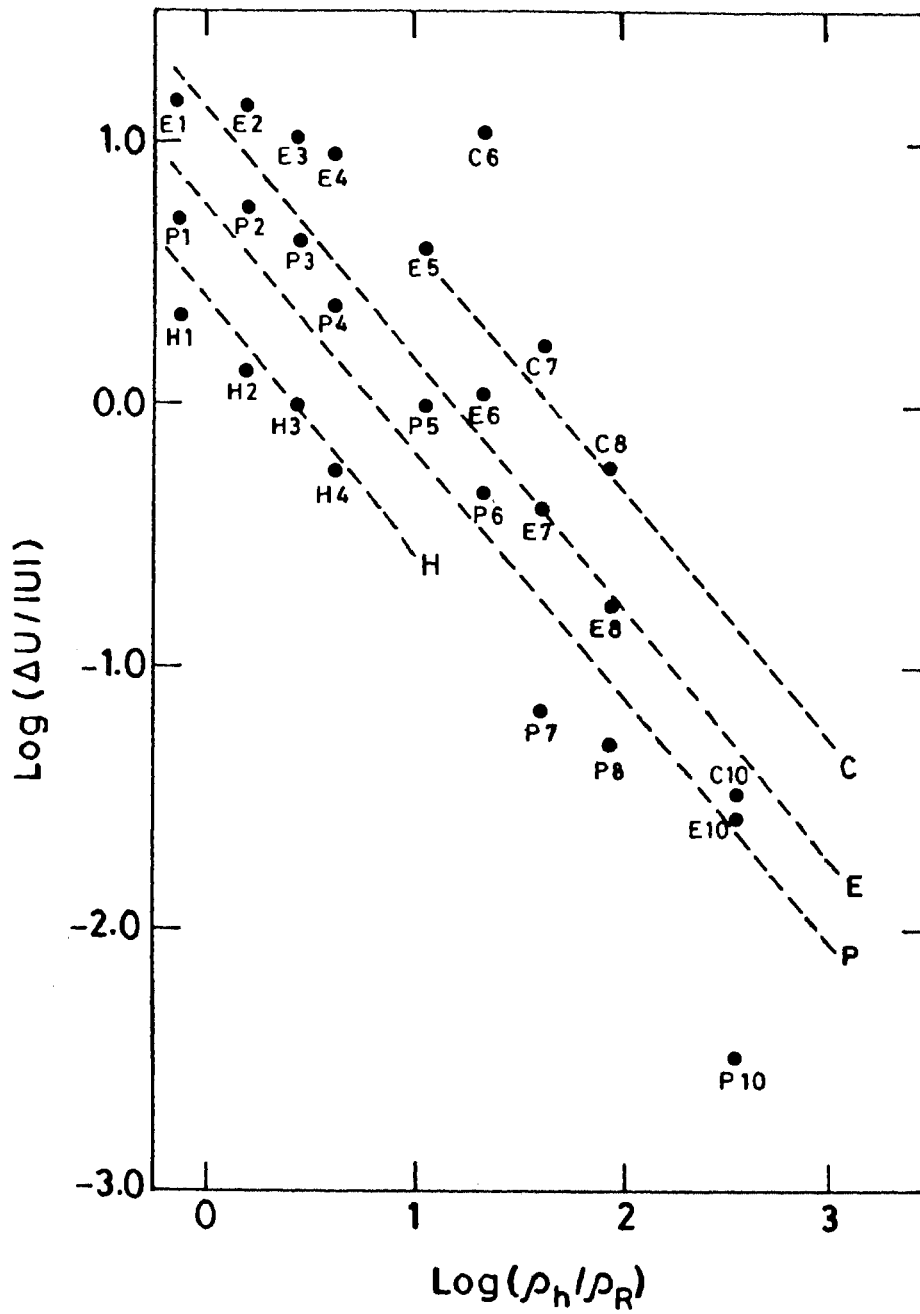
Figure 60. Variation of $\log(\Delta U/|U|)$ with $\log(\rho_h/\rho_R)$ for all models. The dotted lines show the results obtained from impulsive approximation calculation.

these opposite effects nearly balance each other. Disruption is observed when $\Delta U/|U| > 2$ and in this case nearly 40 % of the mass is stripped off from the test galaxy. Spitzer's formulae is valid in the case of H models only.

24. Dependence of $\Delta U/|U|$ on eccentricity and density ratio

Table 9 shows the values of $\Delta U/|U|$ as a function of density ratio and eccentricity. At places we have used D and ND to respectively denote disruption and non-disruption. A bold line is drawn across the table to indicate the boundary between disruption and non-disruption. It can be seen from this table that increasing the density ratio ρ_h/ρ_R decreases the tidal effects and for a constant density ratio, increasing the eccentricity decreases the tidal effects. If we compare, for example, the tidal effects in the parabolic and circular cases, we find that the ratio $(\Delta U/|U|)_{parabolic}/(\Delta U/|U|)_{circular}$ decreases with increasing ρ_h/ρ_R whereas IA does not suggest this. This is in agreement with the suggestion made by Alladin et al. (1985) from a comparison of the results from impulse approximation and adiabatic approximation that for large density of the satellite, the parabolic case would give greater energy transfer than the circular case. Although the tendency of our results is in this direction, we find that this limit has not been reached until $\Delta U/|U| \approx 0.01$. It remains to be confirmed numerically whether this would happen at still lower values of

Table 9. Values of $\Delta U/|U|$ as a function of ρ_h/ρ_R and e

ρ_h/ρ_R \ e	0	0.5	1	2
0.75	D	14.095	6.023	2.080
1.50	D	13.222	5.357	1.260
2.67	D	10.236	4.100	0.986
5.34	D	8.711	2.297	0.514
10.68	D	3.774	0.970	ND
21.36	11.470	1.035	0.449	ND
42.71	1.610	0.396	0.066	ND
85.41	0.553	0.167	0.051	ND
341.63	0.032	0.026	0.003	ND

$\Delta U / |U|$.

Alladin et al. (1985) have also shown that there would be a sharp decrease in the disruption rate at $\rho_h \approx \rho_R$. The numerical work does not support this. On the contrary we find that the variation of $\Delta U / |U|$ with ρ_h / ρ_R is smooth over a wide range in density ratios which includes $\rho_h / \rho_R = 1$.

The formula derived by King (1962) for the tidal radius R_t

$$R_t = p \left[\frac{M}{M_1 (3 + e)} \right]^{1/3} \quad , \quad (8)$$

suggests that tidal effects depends weakly on e and increases with e if p and the masses of the galaxies are kept constant. But our numerical work shows that the tidal effects decrease with increasing e and depend on e if density ratio and distance of closest approach are kept constant.

Dekel et al. (1980) considered slow hyperbolic encounters and used a dimensionless parameter ν in the tidal limit to be

$$\nu = \left[(\Delta U / |U|)_{Sp} \right]^{1/2} \quad . \quad (9)$$

They used two models A and B in which model A consisted of elongated stellar orbits while in model B, the stellar orbits were less elongated. They observed that mass loss and energy change scaled linearly with collision parameter ν in model A whereas the scaling was found to be quadratic in model B. Our results for H models show a linear dependence of $\Delta U / |U|$ on ν

128

in agreement with the above work. The other models, however, do not show this type of linear dependence.

25. Dependence of $\Delta M/M$ on collision parameters

We have already noted that disruption occurs when mass loss is greater than 40 % which agrees with Miller's (1986) result. Further we see that for a constant pericentric distance, the mass loss increases as the relative eccentricity of the orbit decreases. In figure 61 we plot the fractional mass loss with $\Delta U_B/|U|$. This figure shows that the dependence can be expressed in the form

$$\frac{\Delta U_B}{|U|} \approx \alpha \frac{\Delta M}{M} \quad . \quad (10)$$

The value of $\alpha = 1.75$, 1.31, 1.27, and 1.14 for $e = 2$, 1, 0.5, and 0 respectively. These values are obtained by a least square fit to each set of models. Roos & Norman (1979) have shown that in head-on collisions where $p > 3 R_h$, $(\Delta M/M)/(\Delta U/|U|) \approx 0.7 \pm 0.4$ which is in agreement with our results. Dekel et al. (1980) noted a dependence of $(\Delta M/M)/(\Delta U_B/|U|) \approx 1$. Rao (1985) also obtained similar results. All these are in good agreement with our results.
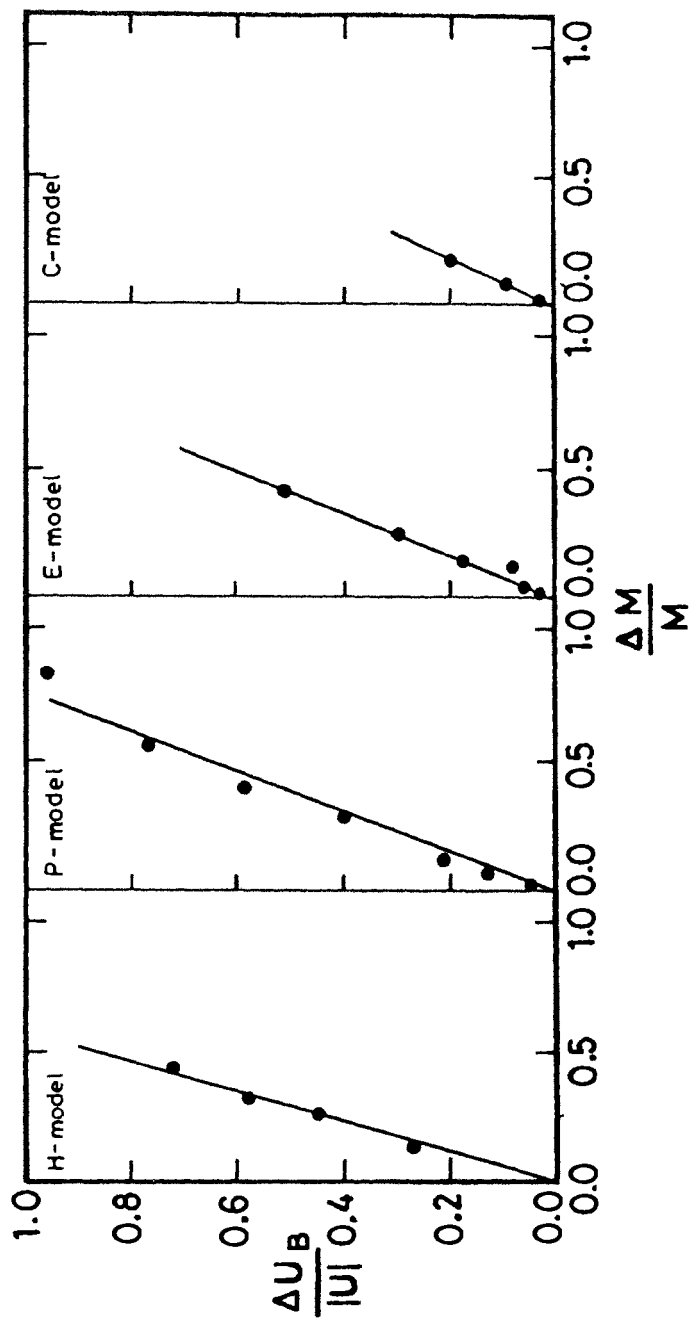
Figure   61.   Dependence   of $\Delta U_B/|U|$ vs. $\Delta M/M$ for   the   four

specific models.

26. Dependence of angular momentum transfer on collision parameters

Analytical work on interaction of spherical galaxies showed that angular momentum can not be transferred if any two principal directions of the test galaxy are parallel to the orbital plane (Peebles,1969; Wesson,1982). Som Sunder et al. (1989) used tensor virial equations within the framework of impulse approximation and obtained analytical formula for the angular momentum transfer as

$$\Delta J = \frac{1}{5} \frac{G M M_1}{p^2 V_p} a_1^2 \, y \, \sin 2\theta \quad , \quad (11)$$

where a_1 is the semi-major axis of the test galaxy; $y = 1 - (a_3/a_1)^2$; and θ is the angle between the Z-axis and orbital plane of the pair. It is clear that when $\theta = 0$ or $\pi/2$, no angular momentum transfer takes place. Our simulations indicate that angular momentum is transferred to the test galaxy during an encounter. This is due to the fact that as the encounter proceeds, considerable distortion of the test galaxy results whereas the earlier investigators assumed the shape of the galaxy to remain unchanged during interactions. It is probable that processes associated with distortion are responsible for the gain in the angular momentum. Even though the test galaxy gains angular momentum, 90 - 99 % of it is carried away by the escaping material. We also note that the angular momentum gained by the bound part is more in H models

than the corresponding quantity in other models.

It is interesting to note that the angular momentum transfer varies inversely as the eccentricity of the relative orbit. In the case of binary spiral galaxies, a similar result has been obtained by Osterloo (1988) from a study of a large sample of galaxies. His values of Λ nearly corresponds to J_{orb} / J_T of the present study. Thus we find that tidal interaction enable isolated pairs of galaxies to acquire spin. It remains to be seen whether the acquired spin is sufficient to induce rotation in such systems.

27. Relative orbits of the galaxies

As the perturber moves in a relative orbit of energy e, there is a transfer of orbital energy to the internal energy of the test galaxy. Consequently the galaxies are expected to revolve around each other with mean separation that will continuously decrease in time and finally form a single system. This effect is called the *tidal friction* (Lin & Tremaine, 1983). The strength of tidal friction falls rapidly with increasing orbital radius and depends strongly on the mass distribution in the outer parts of the victim galaxy. The separation between the two galaxies as a function of time is presented in figures 62 - 67 for all models. In all simulations we have set the value of the closest approach distance at p = 100 units except in model ES in which case p = 72 units. Our numerical results show that the variation in

132

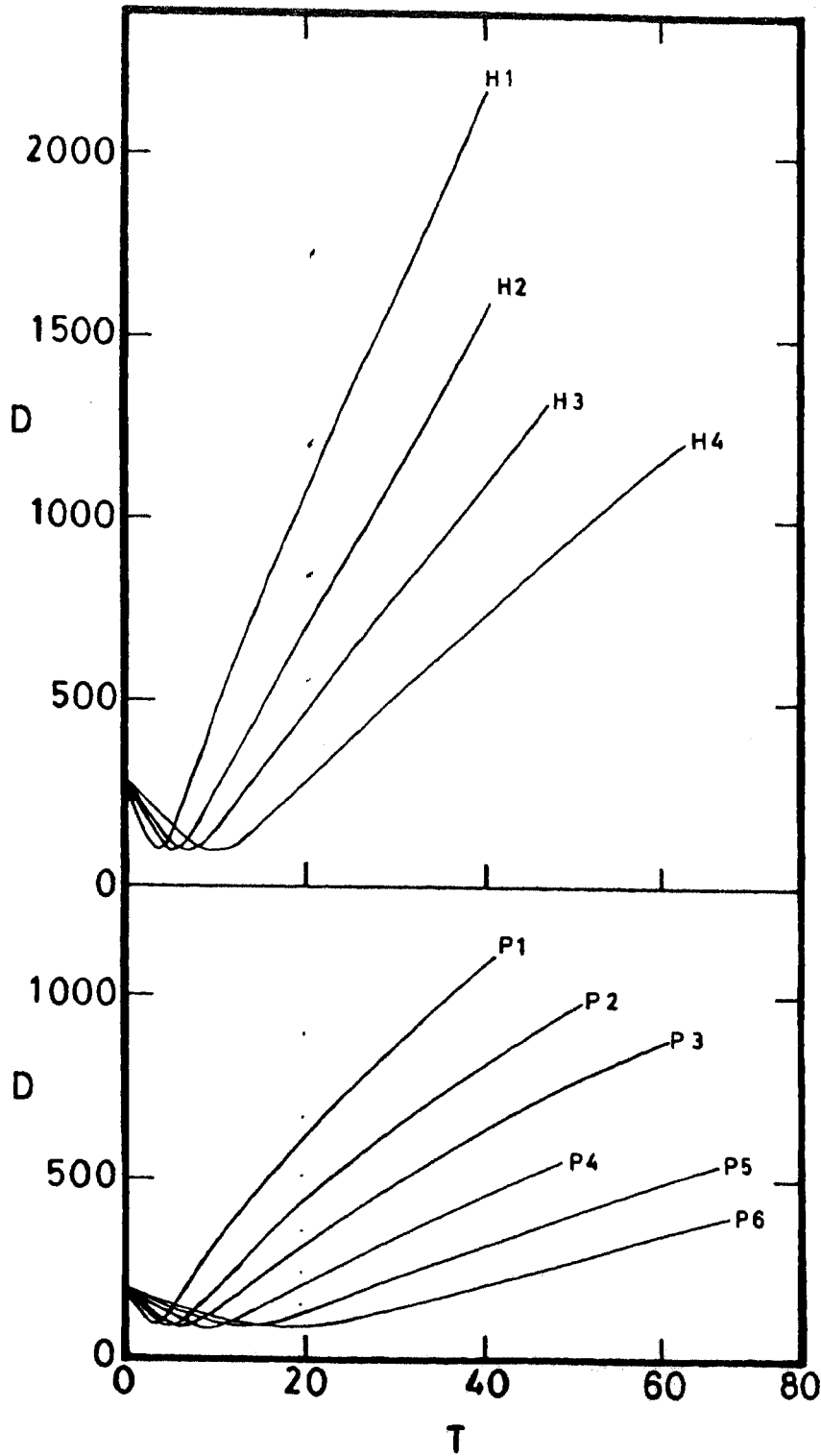Figure 62. The separation between the two galaxies as a function of time for models H and also for P1 - P6.
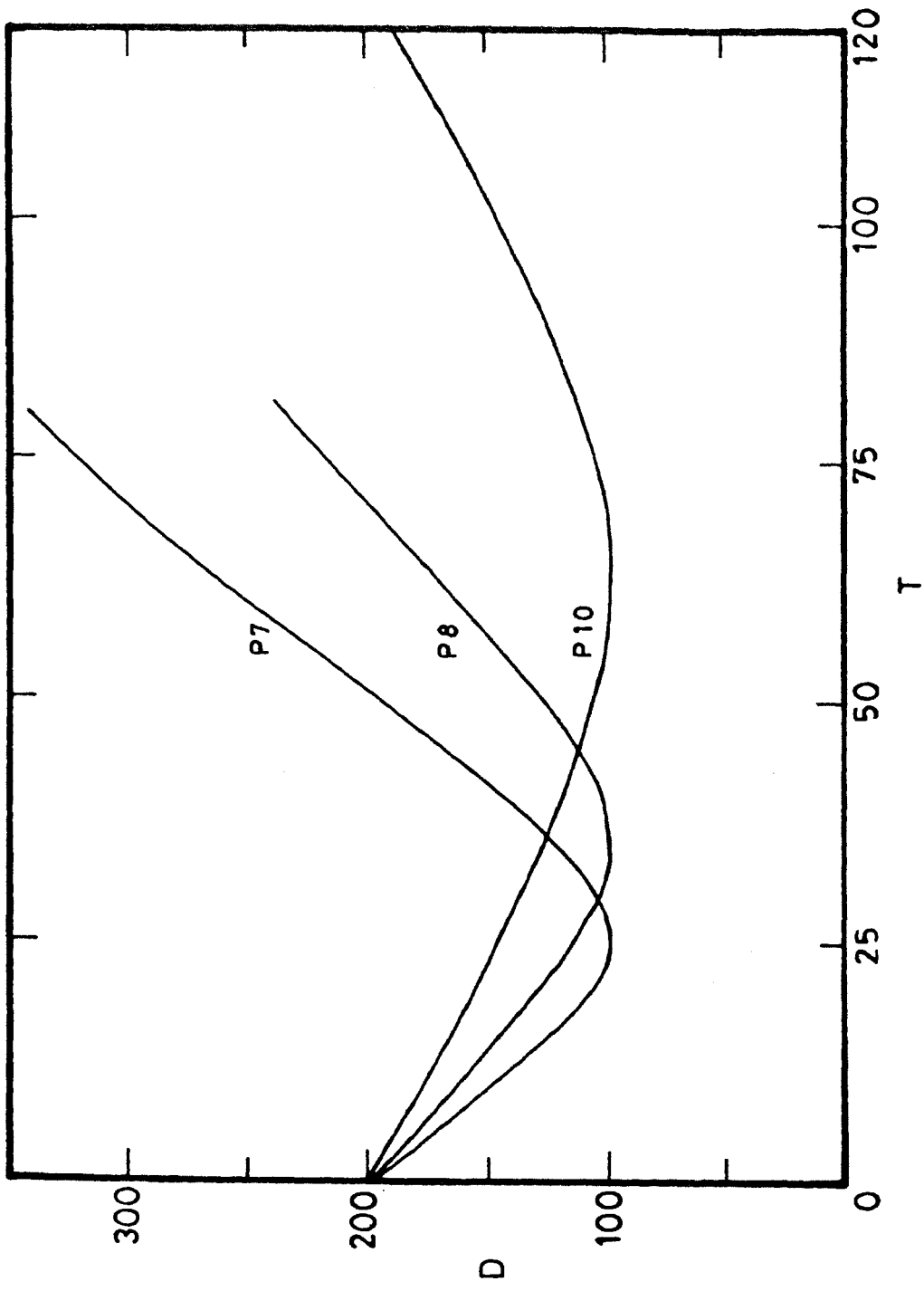
133

Figure 63. Same as figure 61, but for models P7, P8, and P10.
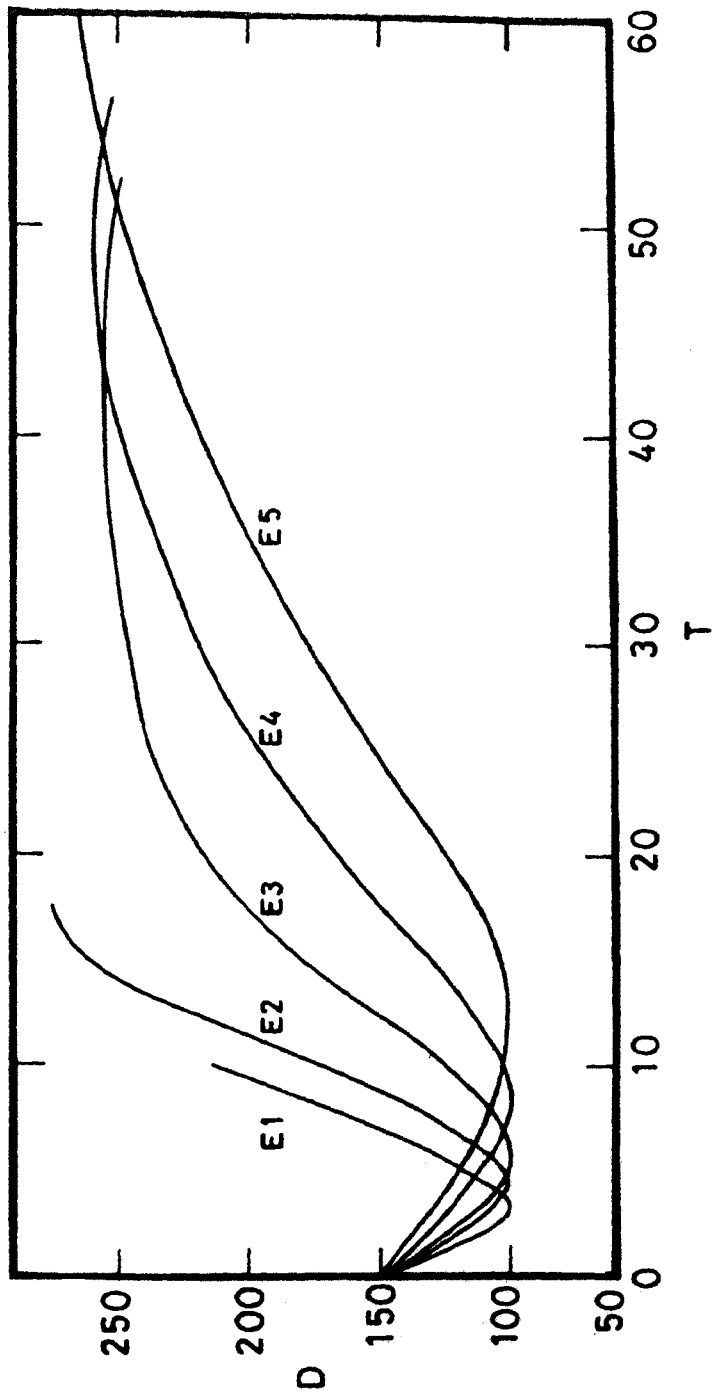
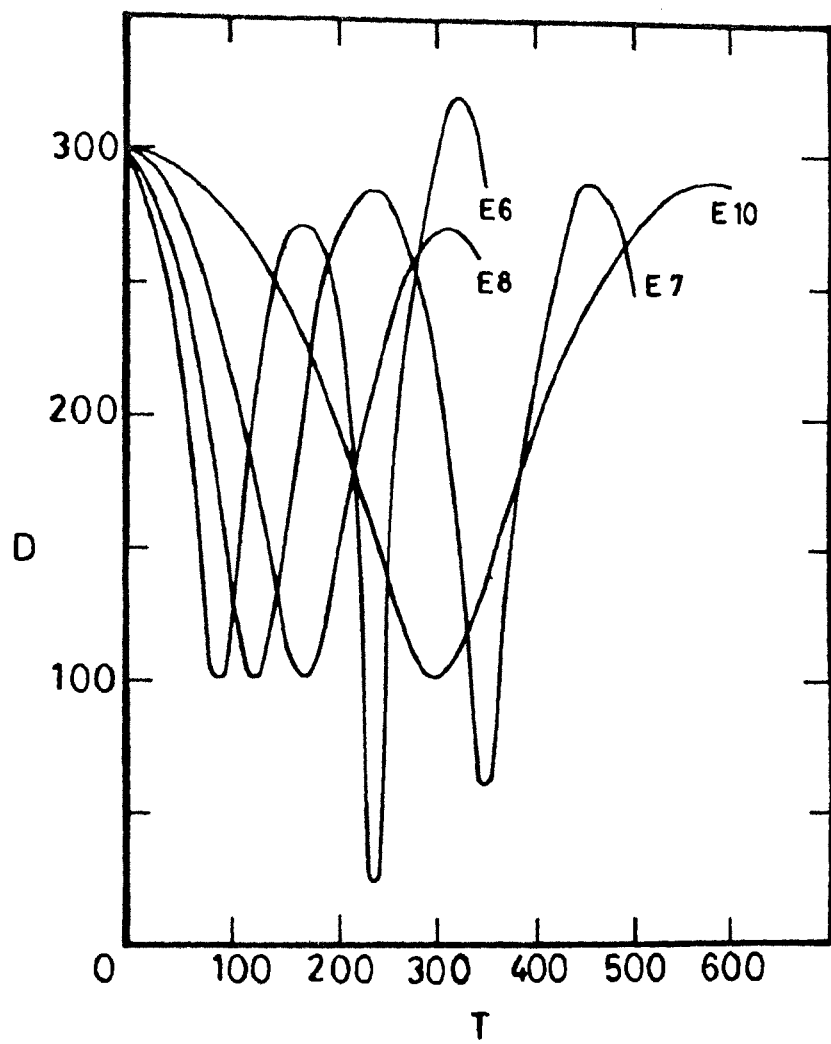Figure 64. Same as figure 61, but for models E1 - E5.

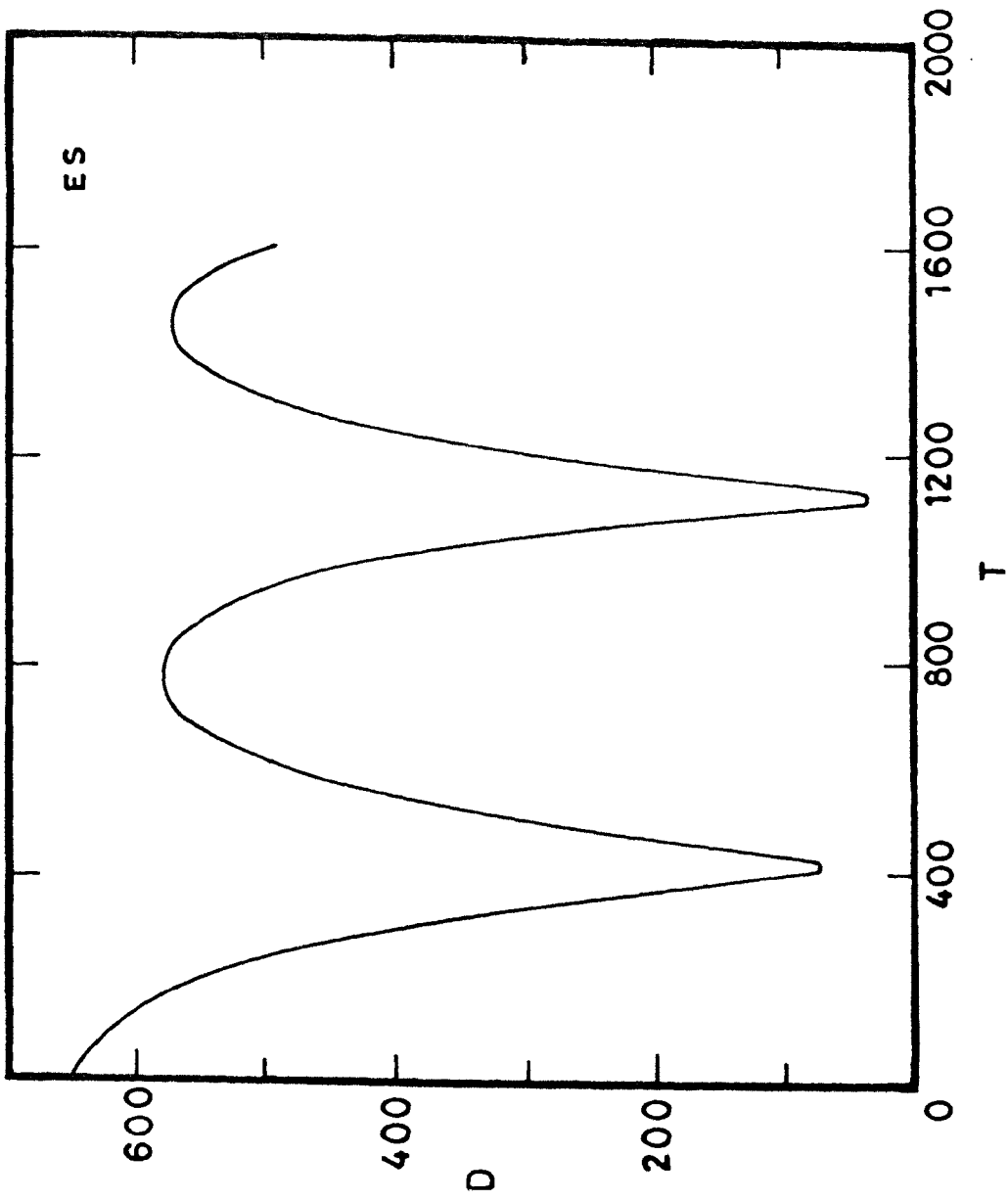Figure 65. Same as figure 61, but for models E6, E7, E8, and E10.

136

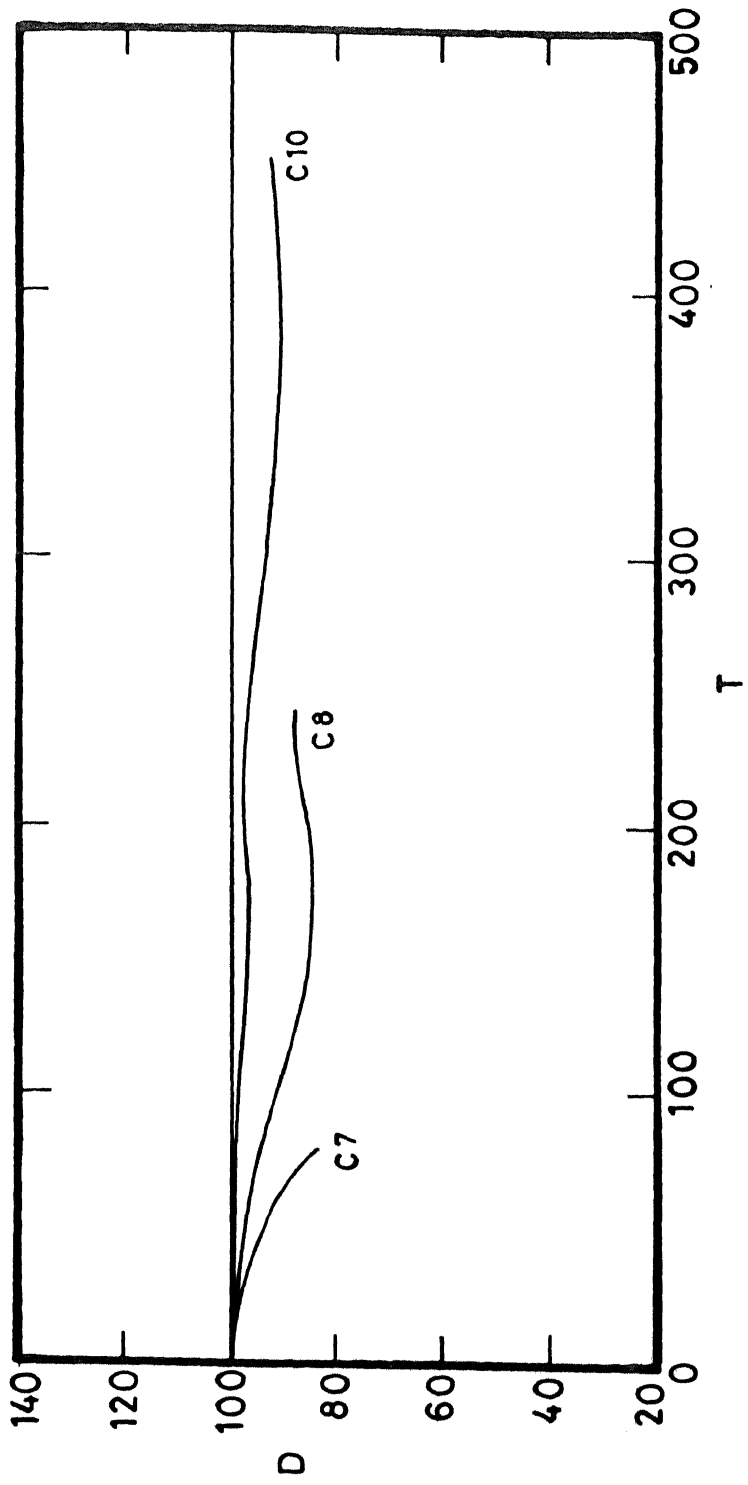Figure 66. Same as figure 61, but for models ES.

Figure 67. Same as figure 61, but for models C7, C8, and C10.

the value of p is less than two percent in models H, P, and E
which is well within the errors of our computation. The
numerical orbit did not deviate significantly from theoretical
orbit. Repeated collisions are effective in producing decay of
the satellite orbit. This can be seen in models E6, E7, and
ES.

There is considerable decay of the satellite orbit
in model C. In these models the tidal friction decreases as
the mass ratio decreases. We, therefore, conclude that the
orbit decay process is not sensitive in H and P models. This
is also true in elliptic models where the duration of the
encounter is less than one orbital period. Successive
encounters produce considerable tidal friction and decay of
satellite orbit.

28. Tidal disruption

The degree of disruption caused to the test galaxy
can be quantitatively described by knowing the fractional
change in the energy and the mass loss. The important
consequences of the disruptive effects are that the galaxy
becomes loosened and extended in size. Analytical work
suggests that disruption occurs when $\Delta U/|U| > 1$ (Alladin and
Narasimhan, 1982). Our numerical work, however, shows that a
galaxy may considered as disrupted if it looses more than 40 %
of its mass, and in such cases, the fractional change in the
energy turns out to be $\Delta U/|U| > 2$. This was shown to be the

appropriate condition for disruption by Miller (1986). Our study describes the disruption of a galaxy in terms of the density ratios of the two systems. The wide range of density ratios used in our simulations enable us identify the transition from disruption to non-disruption. Significant disruption is expected if $\rho_h / \rho_R < 4$ and for $\rho_h / \rho_R > 4$, the disruption is considered negligible. Further we also note that if a galaxy is going to be disrupted, it should occur during the first orbital period. This can be seen in our models E6, E7, and ES. In these models, the mass loss reaches a maximum during the first close contact and remains nearly constant afterwards.

29. Comparison of changes in shape in various models

The expansion parameters given in table 6 give us an idea of the size of the system after an encounter. For H and P models, the total system and the remnant bound system show larger expansion in the Y-direction than in the other two directions. This direction is roughly parallel to the direction of motion of the perturber and consequently the test system looses particles in a direction towards and away from the perturber. For models E and C, the total system shows larger expansion in the Y-direction whereas the bound system shows almost equal expansion in the X and Y directions. The expansion in the Z-direction is much less than the corresponding values for the X and Y directions. In general,

140

therefore, the expansion is greater in the equatorial plane than in the perpendicular direction. A larger amount of expansion is observed in models E and C than in models H and P. From a study of merging galaxies, White (1978) showed that expansion occurs mainly in two conical regions surrounding the axis of symmetry of collision. Miller (1986) found that a galaxy is stretched in some direction and compressed in the others by the mean cluster force field as a result of which tidal bulges are formed. All our models are flattened towards the orbital plane. The values of flattening parameter for models E and C are larger than those for models H and P.

We have already seen that the bound system acquires very little spin due to tidal interaction. The remnant of bound orbit encounter is shown to be oblate and rotating (Binney and Tremaine, 1987). Observations of low rotation velocities in elliptical galaxies suggest that they are oblate spheroids whose flattening is not due to rotation alone. However the remnant's flattening is only partly caused by rotation. Binney (1977) showed that elliptical galaxies are prolate or oblate and most of their ellipticities results from anistropic internal velocity dispersion. Our numerical results show that the remnant bound system closely resembles an oblate galaxy. It will be interesting to investigate how long the bound system could retain its form after an encounter.

CHAPTER SIX

CONCLUDING REMARKS

30. Three-body treatment

The tidal effects on a model spiral galaxy due to a point-mass perturber have been studied using restricted three-body treatment and N-body simulation technique. The restricted three-body method was used to study the formation of bridges and tails on the outer parts of a test galaxy due to the passage of a point mass perturber. The test galaxy was modelled as a thin disk consisting of a point-mass at its centre and mass less test particles distributed in its outer parts. The sense of rotation of the perturber is the same as that of the rotation of the disk. Various collision parameters like the mass ratio and impact parameter have been used. The main results of this study are summarised below:

i. The formation of bridges and tails are favoured when the mass ratio of the galaxies is of the order of unity. Tails last longer than the bridges.

ii. The tail is broad and long when the mass ratio is close to unity and becomes thinner and shorter as the mass ratio decreases.

iii. The test galaxy remains unaffected by an encounter if the mass of the perturber is much less than that of the test galaxy.

iv. Increasing the mass of the perturber leads to greater disruption of the test galaxy.

v. The formation of similar bridges and tails can be obtained by using the same *collision parameter* ν which is a function of the masses of the galaxies, their separation, and eccentricity of the relative orbit.

vi. Formation of well developed bridges and tails is possible for values of ν lying between 0.1 and 0.7. If $\nu < 0.1$, essentially no damage is done to the test galaxy while for $\nu > 0.7$, the test galaxy suffers appreciable disruption.

31. N-body simulations

In N-body simulations, we have attempted to study the tidal effects of an initially spherical galaxy due to a massive perturber considered as a point-mass. Aarseth's N-body 2 is used in the simulations. The collisions are non penetrating and distant. Results are obtained over a wide range in density ratios and eccentrisities of the relative orbit. A total of 27 simulations have been performed in which the initial relative orbit of the perturber is hyperbolic in

four cases; parabolic in nine cases; elliptic in ten cases; and circular in four cases. Several of the bound orbit encounters have been followed for two orbital periods. The important conclusions are summarised below:

i. Disruption of a satellite galaxy occurs if the value of $\Delta U/|U|$ is greater than two and in this case the satellite loses more than 40 % of its mass and the density ratio $\rho_h/\rho_R < 4$.

ii. Most of the change in $\Delta U/|U|$ occurs after the perturber passes the closest approach point. The change in the energy during the second half is nearly twice the corresponding change in the first half.

iii. The impulse approximation estimates of $\Delta U/|U|$ as given by equations (1) and (2) of Chapter five agree within a factor of two with the numerical results for all eccentricities in the range $0.1 < \Delta U/|U| < 2$. For $\Delta U/|U| < 0.1$ these formulae overestimate the energy transfer due to the neglect of stellar motions and for $\Delta U/|U| > 2$, they underestimate the same due to the neglect of the loosening of the satellite.

iv. Even though the test galaxy acquires angular momentum, 90 - 99 % of it is carried away by the escaping particles leaving the remnant bound system with very little spin. The gain in the angular momentum varies inversely as the

144

eccentricity of the relative orbit.

v. The energy and angular momentum changes of the satellite galaxy are continuous in hyperbolic and parabolic encounters whereas they show irregular variation in elliptic and circular encounters. This is due to the partial reversal of the direction of tidal acceleration during a part of the orbit in the latter case.

vi. The tidal effects increase with decreasing eccentricity of the relative orbit for constant density ratio ρ_h/ρ_R and distance of closest approach p. It remains to be investigated whether the opposite holds for values of ρ_h/ρ_R larger than those we have used.

vii. The variation of $\Delta U/|U|$ with ρ_h/ρ_R is smooth over a wide range in density ratio including $\rho_h/\rho_R \approx 1$. This is contrary to the result that there would be a sharp decrease in the disruption rate at $\rho_h \approx \rho_R$ obtained by Alladin et al. (1985) using adiabatic approximation.

viii. For constant pericentric distance, the mass loss increases as the eccentricity of the relative orbit decreases. The dependence of the change in the energy of the bound part $\Delta U_B/|U|$ on the mass loss $\Delta M/M$ follows the linear relation

$$\frac{\Delta U_B}{|U|} = \alpha \frac{\Delta M}{M}$$

where the slope of the line decreases as we decrease the eccentricity of the relative orbit.

ix. The process of decay of satellite orbit due to tidal friction is not significant for all the types of simulations reported except in the circular case. In circular models and also in repeated collisions of elliptic models, the effect of tidal friction is observed to be important.

x. If a galaxy is going to be disrupted, it happens during the first orbital period. Subsequent collisions are not found to be effective in producing appreciable disruption.

xi. After an encounter, the original spherical galaxy becomes elongated in the orbital plane and compressed in the direction perpendicular to it. The remnant bound system shows the characteristics of an oblate galaxy ($E_x \approx E_y > E_z$).

xii. The half-mass radius of the remnant bound system remains about the same as that of the initial test galaxy to within 20 %. Considerable expansion is observed in the region containing 90 - 100 % of the mass which supports the fact that mild encounters produce a distension in the victim's envelope.

We have introduced the concept of the density of the satellite in terms of the Roche density which helps us to determine the transition from disruption to non-disruption in interacting galaxies. We have also compared our numerical results with those of analytical ones and pointed out the relative importance of numerical simulations in cases where analytical work fails to give satisfactory results.

The number of particles used to represent a stellar system is small in our simulations. Nevertheless a comparison of our numerical results with those obtained by earlier investigators shows fairly good agreement. We, therefore, believe that many useful results can be obtained from numerical simulations using few particles and the discrepancies in the results are well within statistical fluctuations.

We have considered the galaxy to have only one component - the stellar component. The inclusion of a gaseous component makes the behaviour of the system very different. In observed galaxies most of the gas is in the form of dense clouds and their collisions may lead to formations of regions where star formation is likely to take place. The importance of star formation in colliding and merging galaxies increased remarkably since the Infrared Astronomical Satellite (IRAS) began its survey in 1983. The star formation rates in interacting galaxies is about three times the normal rate. A careful study of interacting galaxies consisting of the two components - gas and star - is expected to give us an idea

regarding star formation rates in interacting galaxies.

Although the light profiles of massive elliptical galaxies can approximately be represented by the $r^{1/4}$ law, considerable deviation from this law has been observed in the case of compact ellipticals. These galaxies which have very small size and very high surface brightness are always found to be associated with massive galaxies. The compactness was first thought to result from tidal truncation (Faber, 1973). The fact that there exists tight correlation between surface brightness and luminosity in ellipticals led Michard (1979) to classify them into three sequences SI, SII, and SIII in decreasing order of the degree of correlation. Recent investigations by Prugniel et al. (1989) suggest that SII galaxies evolve toward SI galaxies as a result of gravitational interactions. Gravitational encounters result in an exchange and redistribution of energy, angular momentum and mass. Escaping material carries away a substantial fraction of angular momentum as a result of which the remnant bound system has very little spin. The low rotational velocities observed in compact elliptical galaxies support this suggestion and point out the importance of studying gravitational interactions of pairs of galaxies having unequal masses. The environment clearly has, therefore, an important role in shaping elliptical galaxies and the study of these systems is crucial to the understanding of the origin and evolution of galaxies.

We have so far considered only initially spherical test galaxies. It is proposed to consider the important general case where the test galaxy is spheroidal, supported by rotation and / or velocity anisotropy. Another outstanding problem that we plan to do in future is to investigate the alignment of the initial orbital angular momentum vector and the internal spin of the test galaxy after an encounter.

References

Aarseth, S.J. (1963) M.N.R.A.S. **123**, 223.

Aarseth, S.J. & Fall, S. M. (1980) Ap. J. **236**, 43.

Aguilar, L.A. & White, S.D.M. (1985) Ap. J. **295**, 374.

Ahmed, A. & Cohen, L. (1973) J. Comp. Phys. **12**, 389.

Alladin, S.M. & Narasimhan, K.S.V.S. (1982) Phys. Rep. **92**, 339.

Alladin, S.M. (1965) Ap. J. **141**, 768.

Alladin, S.M., Ramamani, N. & Meinya Singh, T. (1985) J. Ap. Astr. **6**, 5.

Arp, H. (1962) Ap. J. **136**, 1148.

Arp, H. (1966) Atlas of Interacting Galaxies, California Inst. Tech.

Avner, E.S. & King, I.R. (1967) Astr. J. **72**, 650.

Barnes, J.E. (1988) Ap. J. **331**, 699.

Biermann, P. (1976) Astr. Ap. **48**, 295.

Binney, J. (1977) M.N.R.A.S. **181**, 735.

Binney, J. & Tremaine, S. (1987) Galactic Dynamics, Princeton University Press.

Borne, K. D. (1984) Ap. J. **287**, 503.

Byrd, G. G., Sarinen, S. & Valtonen, M.J. (1986) M.N.R.A.S. **220**, 619.

Clutton-Brock, M. (1972) Ap. Space Sci. **17**, 292.

Curtis, H.D. (1921) Bull. Nat. Res. Council Washington No. **2**, Pt 3, 171.

Dekel, A., Lecar, M. & Shaham, J. (1980) Ap. J. **241**, 946.

Eneev, T.M., Kozlov, N.N. & Sunyaev, R.A. (1973) Astr. Ap. **22**, 41.

Faber, S.M. (1973) Ap. J. **179**, 423.

Farouki, R.T. & Shapiro, S.L. (1982) Ap. J. **259**, 103.

Gallagher, J.S. & Ostriker, J.P. (1972) Ap. J. **77**, 288.

Gerhard, O.E. (1981) M.N.R.A.S. **197**, 179.

Gutowski Jr., W.J. & Larson, R.B. (1976) Publ. Astr. Soc. Pacific **88**, 374.

Holmberg, E. (1937) Ann. Obs. Lund. No. 6.

Holmberg, E. (1940) Ap. J. **92**, 200.

Hubble, E.P. (1936) The Realm of Nebulae, Yale University Press.

King, I.R. (1962) Astr. J. **67**, 41.

Kormandy, J. (1977) Ap. J. **218**, 333.

Lauberts, A. (1974) Astr. Ap. **33**, 231.

Lee, H. M. & Ostriker, J.P. (1987) Ap. J. **322**, 123.

Lin, D.N.C. & Tremaine, S. (1983) Ap. J. **264**, 364.

Lundmark, K. (1926) Cited by Zwicky, 1959.

Michard, R. (1979) Astr. Ap. **74**, 206.

Miller, R.H. & Smith, B.F. (1980) Ap. J. **235**, 421.

Miller, R.H. (1986) Astr. Ap. **167**, 41.

Namboodiri, P.M.S. & Kochhar, R.K. (1985) Bull. Astr. Soc India, **13**, 363.

Namboodiri, P.M.S., Kochhar, R.K. & Alladin, S.M. (1987a) Bull. Astr. Soc India, **15**, 186.

Namboodiri, P.M.S., Kochhar, R.K. & Alladin, S.M. (1987b) in
The Few Body Problem (Ed:Valtonen,M.J.) Kluwer p. 401.

Namboodiri, P.M.S. & Kochhar, R.K. (1990) M.N.R.A.S. in press.

Narasimhan, K.S.V.S. & Alladin, S.M. (1983) Bull. Astr. Soc.
India 11, 221.

Navarro, J.F. & Masconi, M.B. (1989) Ap. J. 336, 669.

Negroponte, J. & White, S.D.M. (1983) M.N.R.A.S. 205, 1009.

Osterloo, T. (1988) Angular momentum in binary spiral
galaxies, Ph.D. Thesis, Groningen, The Netherlands.

Ostriker, J.P. (1977) Evolution of Galaxies and Stellar
Populations, (Eds: Tinsley, B.M. & Larson, R.B.) Yale
University Press, p. 369.

Palmer, P.L. & Papaloizou, J. (1982) M.N.R.A.S. 199, 869.

Pease, F.G. (1917) Ap. J. 46, 24.

Peebles, P.J.E. (1969) Ap. J. 155, 393.

Pfleiderer, J. (1963) Z. Ap. 58, 12.

Prugniel, P., Davoust, E and Nieto, J. L. (1989) Astr. Ap.
222, 5.

Rao, P.D. (1985) N-body Simulations of Tidal Encounters
Between Stellar Systems, Ph.D. Thesis, Osmania
University, Hyderabad.

Rao, P.D., Ramamani, N. & Alladin, S.M. (1987) J. Ap. Astr.
8, 17.

Richstone, D.O. (1975) Ap. J. 200, 535.

Roos, N. & Norman, C.A. (1979) Astr. Ap. 76, 75.

Sastry, K.S. & Alladin, S.M. (1970) Ap. Space Sci. 7. 261.

Schweizer, F. (1978) IAU Symp. No.77, p. 279.

Som Sunder, G., Kochhar, R.K. & Alladin, S.M. (1989)
    M.N.R.A.S. (submitted).

Spitzer, L. (1958) Ap. J. **127**, 17.

Spitzer, L. & Hart, M.H. (1971) Ap. J. **164**, 399.

Stewart, P. (1981) *Investigating the Universe*
    (Ed: F.D. Kahn), Reidel, p. 385.

Stockton, A. (1974a) Ap. J. **187**, 219.

Stockton, A. (1974b) Ap. J. (Lett) **190**, L47.

Tashpulatov, N. (1970) Soviet Astr. **13**, 968.

Toomre, A. & Toomre, J. (1972) Ap. J. **178**, 623.

van Albada, T.S. & van Gorkom, J.H. (1977) Astr. Ap. **54**, 121.

Villumsen, J.V. (1982) M.N.R.A.S. **199**, 493.

von Horner, S. (1960) Z. Ap. **50**, 184.

von Horner, S. (1963) Z. Ap. **57**, 47.

Vorontsev-Velyaminov, B.A. (1959) Atlas and Catalogue of
    Interacting Galaxies, Pt. 1. Moscow University.

Vorontsev-Velyaminov, B. A. (1961) Problems of Extra-Galactic
    Research, IAU Symp. No. 15. (Ed: Mc Vittie, G.C.) p. 194.

Weilen, R. (1967) *Veroeff. Astron. Rechen. Inst.* Heidelberg,
    No. 19, p. 1-43.

Wesson, P.S. (1982) Vistas Astr. **26**, 225.

White, S.D.M. (1978) M.N.R.A.S. **184**, 185.

White, S.D.M. (1979) M.N.R.A.S. **189**, 831.

White, S.D.M. (1982) Morphology and Dynamics of Galaxies,
    (Eds: Martinet, L. & Mayor M.) p. 289.

Wright, A.E. (1972) M.N.R.A.S. **157**, 309.

Yabushita, S. (1977) M.N.R.A.S. **178**, 289.

Zwicky, F. (1952) Publ. Astr. Soc. Pacific, **64**, 242.

Zwicky, F. (1959) Handbuch der Physik Band LIII Springer
     Verlag.

PUBLICATIONS

1.Chandrasekhara,B.C.,Namboodiri,P.M.S. & Hanumanthappa,A.R.
(1984) Warme und Stoffubertragung, **18**, 17. *Similarity
solutions of buoyancy induced flows in a saturated porous
medium.*

2.Chandrasekhara,B.C.,Namboodiri,P.M.S. & Hanumanthappa A.R.
(1983) In Proc. 12th Nat. Conf. Fluid Dynamics and Fluid
Power, I. I. T. Delhi, 8-10 December, 1983, p. 322. *Mixed
convection in a saturated porous medium.*

3.Chandrasekhara,B.C. & Namboodiri,P.M.S. (1985) Int. J. Heat
Mass Transfer, **28**, 199 - 206 (1985). *Influence of variable
permeability on convection.*

4.Namboodiri,P.M.S. & Kochhar,R.K. (1985) Bull. Astr. Soc.
India, **13**, 363. *On the formation of tails and bridges in
interacting galaxies.*

5.Namboodiri,P.M.S. & Kochhar,R.K. (1985) In Proc. Space
Dynamics and Cel. Mech., Delhi, 14 - 16, November,1985, p. 229
(Ed: K. B. Bhatnagar) Reidel. *Numerical experiment on the
formation of tails and bridges in galaxies.*

6.Namboodiri,P.M.S., Kochhar,R.K. & Alladin,S.M. (1987) Bull. Astr. Soc. India, **15**, 186. *On the formation of bridges and tails in interacting galaxies II.*

7.Namboodiri,P.M.S., Kochhar,R.K. & Alladin,S.M. (1987) In Proc. IAU Colloq. No. 96 (Ed: Valtonen,M.J.) Kluwer, p. 401. *Formation of bridges and tails in interacting galaxies.*

8.Namboodiri,P.M.S. & Kochhar,R.K. (1989) Ap. Sp. Sci., **152**, 319. *Energy exchange during collision of a pair of disc-sphere galaxies.*

9.Namboodiri,P.M.S. & Kochhar,R.K. (1990) M.N.R.A.S. (in press). *Tidal change in the energy of a spherical galaxy.*

Name	P..M.Sankaranarayanan Namboodiri
Date of birth	12 July 1947

Academic Qualification

B.Sc.	Kerala University (1967)	First Class
M.Sc.	Kerala University (1969)	First Class

Positions held

Associate Lecturer	1972-1973	Regional Engineering College Calicut
Research Assistant	1973-1978	Indian Institute of Astrophysics Kodaikanal
Sr. Research Assistant	1978-1983	Indian Institute of Astrophysics Bangalore
Research Associate	1983-1989	Indian Institute of Astrophysics Bangalore
Scientific Officer	1989-	Indian Institute of Astrophysics Bangalore

Membership of professional

societies   Member Astronomical
                             Society of India

***